USING THE DEM TO RELATE DROP BALL TESTS TO SEMI-AUTOGENOUS GRINDING.

Shwarzkopf Oliver Samukute

A dissertation submitted to the Faculty of Engineering and Built Environment, University of the Witwatersrand, Johannesburg, in fulfilment of the requirements for the degree of Master of Science.

Johannesburg, 2019.

DECLARATION

I declare that this dissertation is my own, unaided work. It is being submitted for the Degree of Master of Science at the University of the Witwatersrand, Johannesburg. It has not been submitted before for any degree or examination at any other University.

____

(Signature of candidate)

_________day of _________________20____________at_____________

ABSTRACT

The Drop Ball Test (DBT) is a common quality control procedure used in many grinding media-manufacturing units to evaluate the quality of manufactured balls by subjecting a sample to an impact fracture test. Whilst DBTs have provided reasonable data over many years, the quantitative comparison of the energy that the balls are subjected to during the DBT and in high impact loading environments such as Semi-Autogenous Grinding (SAG) mills remains a grey area. The Discrete Element Method (DEM) is a numerical technique that can provide a much more detailed description of the grinding media collision behaviour in both DBTs and SAG mills.

The DEM allows simulation of the collision behaviour in various systems that involve interaction of many particles. The DEM model applied in this work uses a spring-slider-dashpot to calculate contact forces and the net resultant is used to compute acceleration, velocity and distance moved by the particles by applying Newton's laws of motion.

The objective of this work was to quantify the energy that grinding balls are exposed in both the DBT and SAG environments. Using the DEM, simulations where conducted in both environments to evaluate extent of ball impact loading. The impact energy spectra obtained from the DEM simulation of various ball sizes in the DBT was used to quantify the energy the balls are subjected to. The data showed that larger 125mm steel balls are exposed to relatively higher energy levels and have higher probability of fracture than smaller 115mm and 100mm balls. From the SAG mill simulations, ball trajectories were evaluated to determine the energy that the grinding media is exposed to. Increasing ore:ball ratios showed the extent of ore cushioning and reduction in energy that the balls are exposed to.

Using the DBT data and DEM impact energy spectra obtained from both the DBT and SAG simulations, empirical models were developed that attempt to predict ball fracture in the DBT and try to relate ball fracture in the DBT to ball endurance in the SAG environment.

A reasonable estimation of the energy that the balls are exposed in both the DBT and SAG mill was achieved. However, establishment of simulation parameters that specifically apply to the material of ball construction is recommended for future studies. From the results analysed, it was concluded that a more accurate determination of simulation parameters of the specific material of construction has the prospect of achieving improved ball fracture predictions.

DEDICATION

This dissertation is dedicated to my parents, Mr T Samukute and Mrs C Samukute for nursing me with love, support, mental strength and devotion to my personal growth and development. To my sibling brothers and sister, let this dissertation present a challenge for you to achieve more. May God bless you all to live a long and happy life.

ACKNOWLEDGEMENTS

I have pleasure in acknowledging and thanking the following for their input in this work either directly or indirectly:

I am very grateful to my MSc supervisor, **Dr M.M Bwalya**, for his encouragement and guidance throughout this work. Thank you for all the times we stayed after hours discussing and challenging our own thinking, your ingenuity in creating new programs and your patience as we tested various scenarios.

My co-supervisor, **Mr Clive Jones**, thank you for your belief in my abilities, taking me under your wing and showing me how to use technical research as a competitive edge in industry. I will forever be indebted to your mentorship, friendship, kindness and patience.

Thank you to the wonderful team that I worked with including, **Moses Mothibi**, **Ray Abrahams, Livhu Magidimisa, Mike Couch**, **Wayne Barlow-Jones** and **Sandile Hlatshwayo** for your belief in my ideas, critical thinking and continuous support.

I am also indebted to **Wits Enterprises** for funding this research work and providing a platform that stimulates critical thinking, professionalism, career growth and fun.

Finally, I wish to thank my fellow research group mates and special friends, Tatenda Chingosho, Karabo Masiu, Koketso Mamogale, Tshepo Mojela, Bright Mutandwa, Nondumiso Dlamini, Pembelani Mphaphathi, Godfrey Mawire, Chama Chama and Lisa Shambare for the work we completed together and the wonderful memories we shared!

Ndinokutendai uye Mwari wenyasha ave nemi mose.*

Shona for: I thank you and may our graceful Lord be with you all.*

Contents

LIST OF FIGURES

Chapter 2

Chapter 3

Chapter 4

Chapter 5

Appendices

LIST OF TABLES

Chapter 3

Chapter 4

CHAPTER 1

INTRODUCTION

1.0. BACKGROUND

In mineral processing, grinding is a process in which ore is reduced in size by a combination of impact, attrition and abrasion forces inside a grinding mill. Grinding mills are tubular vessels charged with loose crushing bodies (the grinding media) which freely move inside the mill, causing disintegration of the ore particles, (Wills and Napier-Munn, 2006).

Semi-Autogenous-Grinding (SAG) mills are types of grinding mills used in the primary stages of grinding. These machines are characterized by their diameter to length ratio of around two. With this high aspect ratio, SAG mills generate both thrown (cataracting) and cascading load motion that disintegrate the rocks. Hence, the mechanical environment in SAG mills provides both high impact loading to crush the rocks and abrasive wear that finely tear-off the ore, (Royston, 2007). However, the forces responsible for ore fracture also subject grinding balls to stress, causing wear and consequently requiring the replenishment of the grinding balls during the SAG process.

The construction of large SAG mills with diameters reaching over 12m has compelled the use of large grinding balls, up to 150mm in diameter. The high stressing conditions resulting thereof has necessitated the use of grinding media with significant fracture toughness, such as forged low-alloy carbon steel balls as compared to wear resistant high-chrome-white-cast-iron balls. Hence, over the years more grinding media manufacturers have been researching into improving the fracture toughness of grinding media during production.

In many grinding media manufacturing units, the grinding balls undergo rigorous testing processes to ensure that good quality grinding media is despatched. Some of the quality control tests include microstructural analysis, hardness surveys, fracture toughness tests and the Drop Ball Test (DBT). The DBT is a quality control procedure used in typical grinding media manufacturing units to estimate the manufactured balls' response to fracture. The test involves repeatedly dropping the balls from a certain height onto a hardened platform for a specific number of drops and evaluating their response to fracture.

The DBT has long been considered a reliable estimate of the impact toughness of the manufactured balls and they have provided reasonable quantitative data over many years.

However, questions still rise such as; can the energy that the balls are exposed to in the DBT be quantified? Can fracture of the balls be predicated using statistical data from the DBT? Moreover, how does this data relate to high impact loading environments such as Semi-Autogenous Grinding (SAG) mills?

In an attempt to answer some of the above questions, a computer-based numerical modelling tool, the Discrete Element Method (DEM), can be used to model the collision behaviour of the balls in both DBT and SAG mills. Using the DEM approach, the possibility of quantifying the energy, forces or stresses subjected to the balls in high impact loading environments such as SAG mills or DBTs significantly rises. Modelling of such mechanical environments at micro-levels provides an interesting insight into energy transfer during ball collisions, extent of plastic and elastic deformations and interactions that can potentially fracture the balls.

1.1. PROBLEM STATEMENT

The advent of large SAG mills in recent years has necessitated studies to improve the impact toughness and wear resistance of grinding media. To manufacture grinding media that can survive in high impact loading SAG mills, a firm understanding of the process involved and estimating the mechanical status of the service environment are fundamental prerequisites. Scientists have successfully applied computer based tools to study particle collisions, load behaviour, power draw and impact energy distribution in grinding mills (Radziszewski and Tarasiewcz, 1993; Guerrero *et al.*, 2016; Salazar *et al.*, 2014). However to date, the use of the DEM to quantify the energy, stress and forces that grinding balls are exposed in Drop Ball Tests (DBTs) and SAG mills has not been studied in depth.

Most of the DEM mill research has focused on the effects of grinding variables such as speed of mill rotation, mill charge level and size distributions of both the ore and grinding media on output factors such as power draw, grinding rates and quality of product (Smith and Rangel, 1989; Sun *et al*., 2009; Deniz, 2011). The present study aims to apply the DEM to quantify the energy that grinding media are exposed to in both the DBT and SAG mills. This information will be used as a basis for comparison of the severity of the DBT to SAG mill environments. Moreover, from the grinding media manufacturers' perspective, understanding the mechanical environment under which the grinding media operates aids in evaluating the capabilities of the manufactured grinding media relative to its target service environment.

This information also helps us to adjust the production parameters accordingly to manufacture grinding media that can survive longer in a specific grinding environment.

This research provides a good insight into the mechanical environment, energy and stress levels that the grinding media is subjected to in both DBTs and SAG mills. This information will be useful in understanding the toughness requirements for the grinding media. Furthermore, developing the grinding media to improve its wear characteristics reduces the possibility and frequency of grinding media fracture during SAG operations, as well as improving SAG mill efficiency and product quality. This can also assist in advising mill operators on information that is most optimal for running SAG mills and factors that have the greatest influence in such milling environments.

1.2. RESEARCH OBJECTIVES

The overall aim of this research was to use the Discrete Element Method (DEM) to quantify the stress that the grinding balls are subjected to during both the Drop Ball Test (DBT) and SAG milling so as to have better understanding of conditions that are responsible for ball damage and fracture rate. In detail, the study entailed:

- Applying the DEM to characterize the energy, and stress that the grinding media experience during the Drop Ball Test and in SAG mill.
- Physical calculations of the impact energy and stresses subjected to the grinding media during the Drop Ball Test.
- Relating the severity of the Drop Ball Test to that of the SAG mills in which the balls operate.

1.3. DISSERTATION LAYOUT

This dissertation is divided into six main chapters including this introduction. The following briefly describes the content of each chapter:

- **Chapter 2** reviews literature related to Semi-Autogenous Grinding (SAG) technology. The mechanical loading environment in SAG mills is also described as well as literature on the Discrete Element Modelling of the SAG process. Grinding media usage in SAG mills, various types of grinding media and their unique applications are further discussed. Finally, research on quality control procedures during SAG mill grinding media manufacturing specifically the Drop Ball Test (DBT) is reviewed.

- **Chapter 3** describes the equipment and experimental test work that was performed to characterize the material of construction of the grinding balls under study. Tests that were conducted include: chemical analysis, microstructural analysis, hardness tests and Drop Ball Tests. This chapter also introduces the Discrete Element Method Particle Flow Code 3D (DEM – PFC 3D) program, its basis, calculations, results integration and possible sources of errors. The SAG mill and DBT simulation work are also described in this chapter.
- **Chapter 4** analyses the results of the experimental work described in Chapter 3. This includes the chemical composition, metallography results, hardness tests and analysis and modelling of the DBT results. Results of the DBT simulation work are also analysed and discussed in this chapter.
- **Chapter 5** describes the SAG mill simulation work. The mill set up, actual simulation and results are described. The energy levels that the balls are subjected to during the SAG mill simulation is compared to the energy experienced by the balls during the DBT simulation. An empirical comparison is made between the two processes to evaluate the severity of each process.
- **Chapter 6** draws the main conclusions and lists the recommendations for future work that emanated from this study.

CHAPTER 2

LITERATURE REVIEW

2.0. INTRODUCTION

Semi-Autogenous-Grinding Mills (SAG Mills) are currently the technology of choice in hard-rock comminution processes to reduce the Run-Of-Mine ore to hydro-metallurgical separation or secondary ball mill feed (Royston, 2007). In recent years, the construction of large SAG mills with diameters exceeding 12m has compelled the use of large grinding balls, up to 150mm in diameter. The high impact loading environments within large SAG mills has necessitated the use of grinding media with significant fracture toughness, such as forged low-alloy carbon steel balls as compared to wear resistant high-chrome-white-cast-iron balls.

Grinding media replenishment is the highest above-the-ground cost of operating SAG mills. Hence, operators are now closely monitoring and controlling the effects of grinding variables such as mill filling level, speed of rotation and size distributions on grinding media wear characteristics and usage in SAG mills. Likewise, there has been a proliferation of research studies to improve understanding of the high impact loading environments in SAG mills and quality control processes such as the Drop Ball Test (Muzinda *et al.*, 2013; Aldrich, 2013; Chenje, 2003). The availability of such information has gone a long way in improving the understanding of wear and toughness requirements of the grinding media. Furthermore, the information offers an opportunity to reduce the possibility and frequency of grinding media fracture during SAG operations, as well as improving SAG mill efficiency and product quality.

Development of numerical tools that can model the collision behaviour in particulate systems has aided SAG mill designers, operators and grinding media manufacturers to measure and control grinding media usage more precisely and accurately. By using modelling tools, the wear characteristics and stresses the grinding media are subjected to during SAG milling and drop ball tests can be evaluated.

In this literature survey, the general theory of SAG mills and Drop Ball Tests will be reviewed. Likewise, the numerical models available for modelling such particulate environments will be reviewed.

2.1. THEORY OF MILLING

Milling (grinding) can be described as a process in which coarse ore feed is converted into a finer product by a combination of impact and abrasion inside either a tumbling or stirred mill (Bwalya, 2005). Grinding is achieved in tumbling mills which are large cylindrical chambers that rotate about their central axis at some fraction of the speed required to centrifuge the particulate charge (Owen and Cleary, 2015). When a mill rotates, the mixture of ore, grinding media and water known as the mill charge is intimately mixed and rises against the shell of the mill in the direction of rotation. A certain point of dynamic equilibrium is reached when the media on the shell parts from the liner and falls freely to the bottom (toe) of the mill (cataracting). A large portion simply cascade over the rising portion but eventually moves in the direction of the mill rotation. Figure (2.1) shows the motion of charge inside a mill (Gupta and Yan, 2006).

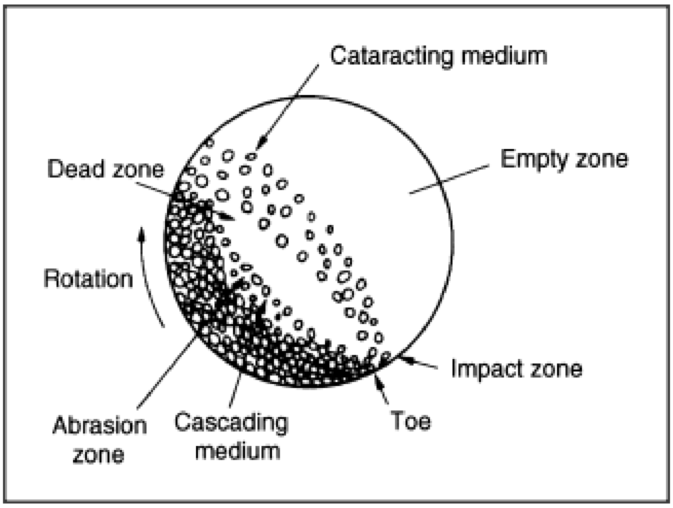

Figure 2. 1: *Charge Motion in a tumbling mill* (Wills and Napier-Munn, 2006)

While grinding within a tumbling mill is strongly influenced by the physical characteristics of the ore, the mill load behaviour is equally influential. The behaviour of the load within the mill is affected by factors such as mill geometry (diameter and length), lifter design, mill speed, ore feed size and ore competence. The behavior of the load can be described as any of the following:

a. **Cascading –** Occurs at mill speeds around 60% of the critical. This motion is characterized by the charge material rolling from the shoulder of the mill down to the toe. The ore particles break due to attrition and abrasion, (Kiangi, 2011).
b. **Cataracting –** Occurs at speeds higher than cascading speeds. The charge material is thrown from the mill shoulder and it lands either onto the mill toe or shell liner. The

higher the speed above the cascading speed, the higher the fraction of the charge landing onto the shell liners. Ball to shell liner impacts increase grinding media consumption, reduce the mill power draw and frequency of ore breakage contacts and the grinding efficiency suffers (Kiangi, 2011). Cataracting motion promotes breakage of large ore particles due to high-impact-energy collisions.

c. **Centrifuging –** Occurs at speeds ≥ 100% of the critical. The charge material forms a layer in contact with the mill shell. The fraction of the charge in contact with the mill shell becomes inactive, the effective mill diameter reduces and the grinding efficiency suffers (Kiangi, 2011). Centrifuging is mainly characterized by a reduction in power draw and significant drop in mill throughput.
d. **Surging –** This behavior occurs within a mill with worn out or smooth lifters. The lifting capacity of the mill will be reduced and part of the charge moves along the perimeter of the mill but slips back to the toe from a very low shoulder position. The charge will move in both the direction of the mill and the counter direction. Surging is promoted by smooth lifters and low ball filling within the mill (Kiangi, 2011).

The forces responsible for ore fracture also subject grinding balls to stress, causing wear and consequently requiring the replenishment of the grinding balls during the grinding process.

In the succeeding sections, the operational aspects and grinding media usage in Semi-Autogenous (SAG) mills are discussed.

2.2. SEMI-AUTOGENEOUS GRINDING MILLS

SAG mills are robustly constructed, heavy-duty grinding machines that are mainly characterised by their diameter-to-length ratio, which ranges from 1.5 to 3. With this high aspect ratio, SAG mills generate both high impact and shear forces in both cataracting and cascading motions respectively. These actions cause ore breakage and in some instances can cause ball breakage because of the severe impact loading. The factors discussed below have the greatest influence on survivability of steel grinding media in SAG mills.

Ore Feed Size: In SAG mills, the ore constitutes a significant fraction of the grinding media (all of it, in AG mills). Changes in ore feed size distribution will result in a change in grinding media size distribution, hence affecting grinding kinetics (Wills and Napier-Munn, 2006). However, changes in ore feed size also changes the frequency of ball-on-ball and ball-on-liner contacts. Large ore feed size cushion the balls from such aggressive contacts whilst small ore particles tend to promote severe ball-on-ball contacts that might cause ball damage.

Ore Hardness: In SAG mills, softer ores result in high mill throughput. This is because the steel balls can easily break the critical-size rocks. However the product size becomes coarser because once the critical size particles are broken, they escape the mill through the grates and will spend less time being torn off by abrasion and attrition (Napier-Munn *et al.*, 1999). This action might lead to ball-on-ball or ball-on-liner contacts if the mill feed rate is not sufficiently controlled.

Top-up Ball Size: The general principle is that the top ball size charged into the mill should be big enough to deliver a force that can break the largest and hardest fraction of ore. If too large balls are used, the frequency of ore breakage contacts will be reduced, excessive fines will be produced, grinding efficiency will suffer and the probability of ball damage will increase. If the balls are too small, the impact collision events will be too weak to deliver force which can cause ore fracture, grinding efficiency will suffer and the steel balls will have accelerated wear rates due to attrition and abrasion (Bond, 1961).

Ball Charge Volume: Presence of steel balls in SAG mills augments impact breakage of ore particles, increasing ball charges in SAG mills tends to increase the frequency of breakage collisions hence the breakage rate of large rocks increases. However, this action also exposes the balls to higher frequency of ball-on-ball and ball-on-liner collisions that might cause ball damage (Napier-Munn *et al.*, 1999).

Mill Speed: Increasing the mill speed increases the amount of lift imparted on the charge until a specific level is reached. Increased lift tends to promote cataracting action hence improving ore breakage rate as a result of impact. However, high impact loading increases stress level induced into the steel balls hence increasing their probability of fracture (Napier-Munn *et al.*, 1999).

2.3. STEEL GRINDING MEDIA USAGE IN SAG MILLS

The impact-loading environment in SAG mills compels the use of grinding balls with significant fracture toughness such as forged low-alloy carbon steel balls as compared to wear resistant high-chrome-white-cast-iron balls. The impact, abrasion and attrition forces responsible for ore breakage also subject grinding balls to stress, causing wear, breakage in some instances and consequently requiring the replenishment of the grinding balls during SAG processes.

In industrial practice, grinding media replenishment is the highest above-the-ground cost of operating SAG mills. Hence understanding the mechanics of ball depletion and failure in SAG mills due to the mill's operating regime is a key objective of this work. Grinding media's material of construction strongly influence its performance in grinding mills.

The selection of material of construction for grinding balls depends on application, properties of the ore, ore feed and product size, type and size of the mill, mill operating parameters (mill speed, lifter design etc.) and availability of suppliers (Powell *et al.,* 2006). The main factor that influences the choice of grinding media material selection is the abrasiveness of the ore but the material of choice should also balance conflicting characteristics such as high hardness – which maximizes resistance to wear and adequate impact toughness – to reduce the probability of ball fracture and spalling (Aldrich, 2013).

The alloys listed below summarise the materials of construction commonly in use today and does not represent an exhaustive list of all the materials available in literature.

2.3.1. FORGED LOW ALLOY STEEL

A significant proportion of commercial grinding media today is produced from forged martensitic low alloy steels. The main advantages of these products are their adaptability to most milling conditions and the favourable cost to wear ratios (Chenje *et al.,* 2004). Forged low-alloy steel grinding balls are mostly used in rough grinding operations where metallic contamination is not an objection (Aldrich, 2013). The carbon content in forged balls is usually kept between 0.7% and 0.8%. However, higher carbon content up to 1.0% is common for balls 30-80mm in diameter. The carbon content is the primary contributor to the balls hardness. Carbon content is proportional to the balls' hardness. However, a maximum range of 0.7-0.8% is maintained for large diameter balls (>100mm). Exceeding that range will lead to significant loss in impact toughness.

Forged alloy steel balls are mostly used in high impact environments such as SAG mills or large diameter ball mills. The hardness to impact toughness trade-off in forged alloy steel balls favours toughness in order that the balls can withstand the high frequency of high-energy impact collisions in these mills. The integrity of low alloy forged steel balls is such that they have significant impact toughness for application in these mills.

2.3.2. AUSTENITIC STAINLESS STEEL

Stainless steel balls are mainly defined by their low carbon content (<0.2%) and high chrome and nickel contents, up to typically 22% and 8% respectively. In hard rock grinding processes, the use of stainless steel balls is limited due to their high cost. However, stainless steel balls are used in special operations that require acid resistant and non-magnetic balls.

2.3.3. WHITE CAST IRON BALLS

While the world over has slowed down on the production of unalloyed white cast iron due to its rather average resistance to abrasion and insufficient impact toughness when used in modern large diameter mills, it remains the most popular type of grinding media in some countries (Chenje *et al.*, 2004). Over the years, development of High Chromium White Cast Irons (HCWCI) has led to its utilisation in grinding balls exposed to high corrosion and severe wear environments such as grinding mills (Muzambi, 2014). For grinding mill applications, not only the high wear resistance of the alloy is adequate but also high impact strength is essential. The application of HCWCI grinding balls is limited to mills in which cascading motion is most dominant. Such environments include fine grinding of cement and milling of dumps. As global mineral processing is moving towards the reclamation of metals from previously processed dumps due to depletion of natural metal deposits, the use of HCWCI grinding media in various operations is expected to rise.

2.4. GRINDING MEDIA PROPERTIES THAT INFLUENCE PERFORMANCE

Over the years, scientists have successfully researched on improvement of wear characteristics and life of grinding media (Pintaude et., 2001; Albertin and Sinatora, 2001; Moema *et al*., 2010; Muzinda *et al.*, 2013). Most of the researches concluded that wear and failure of grinding balls can be attributed to significant variation in chemical composition, hardness and microstructure of the balls. In the succeeding sections, the physical, chemical and microstructural characteristics of grinding balls that influence their performance are discussed.

2.4.1. EFFECT OF CHEMICAL COMPOSTION ON BALL WEAR

Grinding media is manufactured from a range of Iron/Carbon systems discussed in the previous sections. Of importance is that in all the alloys, an increase in the carbon content is associated with an improvement in hardness and wear resistance. High carbon content leads to a microstructure consisting of primary carbides (which are hard) instead of austenite or one of its transformation products (Moema *et al.*, 2009). Additionally, chromium addition to the alloy further improves the hardness. Alloying elements such as silicon, molybdenum and manganese additionally improve the uniformity of hardness within the ball. As addition of carbon improves hardness, further addition (>0.85) in forged alloy steel balls leads to embrittlement of the alloy, thus increasing the susceptibility of the ball to brittle fracture.

2.4.2. MICROSTRUCTURE OF THE BALLS

Several microstructures can develop in alloys used to manufacture steel balls. The microstructure depends on both the carbon content and heat treatment (Callister, 2007). Steel balls with purely pearlitic microstructure throughout their cross-section possess excellent impact toughness but with inferior hardness. However, their resistance to fracture is very good in high impact loading grinding environments such as SAG and large diameter ball mills (Moema *et al.*, 2009).

One of the major causes of accelerated ball wear rate or failure is the non-uniformity of the balls microstructure resulting from delayed austenite to martensite transformation (Moema *et al.*, 2009). The resultant microstructure might constitute of a mixture of martensite, bainite and retained austenite. This leads to the initiation of internal stresses within the ball. The harmful effect of retained austenite may be explained in terms of it reducing the hardness of the matrix thus decreasing the abrasion wear resistance of the ball (Moema *et al.*, 2010).

2.4.3. BALL HARDNESS AND IMPACT TOUGHNESS

Hardness of the grinding balls is defined as the measure of the ball’s resistance to localized plastic deformation (Callister, 2007). Hardenability describes the ability of a steel alloy to be hardened by formation of martensite because of a specific heat treatment procedure. As opposed to hardness which is a measure of the balls’ resistance to indentation, instead, hardenability is a quantitative measure of the rate at which hardness varies with depth into the interior of the ball as a result of diminishing uniformity of martensite (Callister, 2007).

Impact toughness is the ability of the grinding balls to resist crack propagation for a given discontinuity size. In SAG and large diameter ball mills, impact toughness is a very important property to prevent premature fracture of the balls.

2.4.4. EFFECT OF HYDROGEN

Hydrogen plays a pivotal role in the brittle fracture of large diameter (>125mm) low alloy steel balls. Hydrogen has various ways of manifesting its effect in steel balls viz. high temperature hydrogen attack, hydrogen induced cracking (hydrogen blistering) and hydrogen embrittlement. The mechanism of hydrogen damage is that atomic hydrogen reacts with the carbon content of the steel to form methane (Ahmad, 2006).

$$Fe_3C + 4H = 3Fe + CH_4 \qquad (2.1)$$

Loss of carbon from the metal matrix Equation (2.1) leads to loss of strength. Accumulation of the methane results in creation of fissures along the grain boundary or non-metallic inclusions (Ahmad, 2006). Neither molecular hydrogen nor methane has the capability of diffusing through the steel at ambient temperatures hence stresses will build-up within the ball in addition to loss of strength due to decarburization (Louthan, 2008).

2.5. QUALITY CONTROL DURING GRINDING MEDIA MANUFACTURE

In most grinding media manufacturing facilities world over, quality control procedures have been developed that ascertain that the grinding balls meet some sort of standard. The quality control procedures not only give an indication of the grinding media's performance in its target environment, but also provide comparisons to international standards and other competitors' products.

2.5.1. CHEMICAL ANALYSIS

Grinding balls are manufactured to international chemical composition standards. Testing methods such as Spark Emission Spectroscopy, X-Ray Fluorescence (XRF) and Atomic Absorption Spectroscopy are typically used to measure the chemical composition of the alloy during the metal melting process. It is desirable to control the chemical composition of the alloy because it has direct implications on the microstructure obtained during heat treatment. The resultant microstructure determines the mechanical properties and performance of the grinding media.

2.5.2. PIN-ON-BELT (HIGH STRESS ABRASION WEAR TEST)

The purpose of the Pin-On-Belt (POB) test is to determine the resistance of the manufactured balls to wear against a material with superior hardness to the material under test. The particles of the abrasive material are bonded onto a platform that provides adequate mechanical support for the particles subjected to the abrasive test. Figure (2.8) shows a schematic of a POB test. Common materials used for abrasives include silicon carbide, quartz and garnet. A plot for continuous weight loss against time determines the high stress wear rate of the balls.

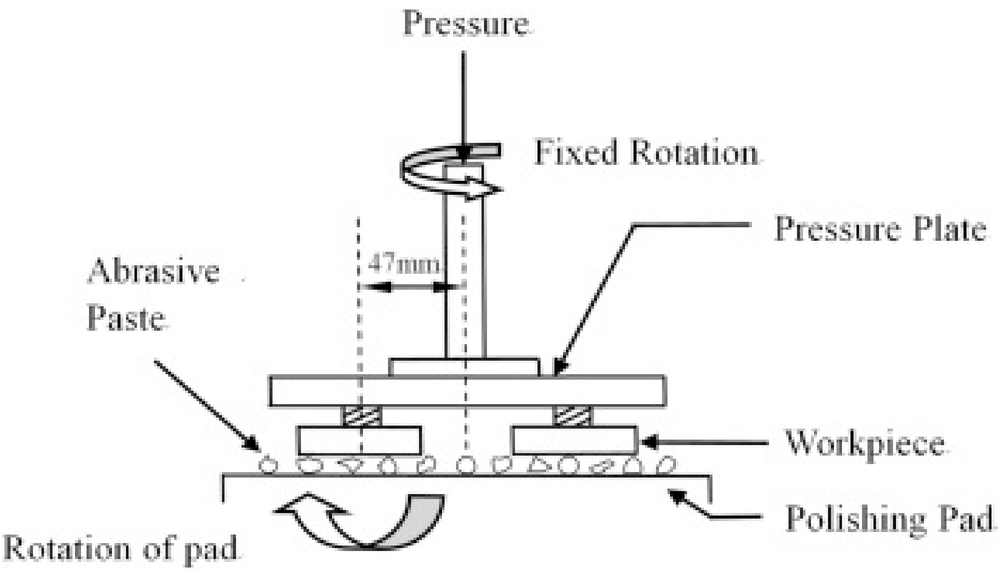

Figure 2. 2: *Schematic representation for High Stress Pin-On-Belt*

2.5.3. DRY RUBBER WHEEL ABRASION TEST

The Dry Rubber Wheel Abrasion Test is used to evaluate the abrasive wear behaviour of the manufactured grinding media under three-body conditions. A schematic representation of the apparatus set up is shown in Figure (2.9). During the test, a plane specimen is loaded against the rim of a rotating rubber wheel; sand is fed into the gap between the wheel and specimen, is carried past the specimen, and thus abrades it. Contrary to the high stress POB abrasion test, the DRAWT is a low stress scratching-abrasion test, which closely relates to the attrition or cascading regions within grinding mills (Stevenson and Hutchings, 1996).

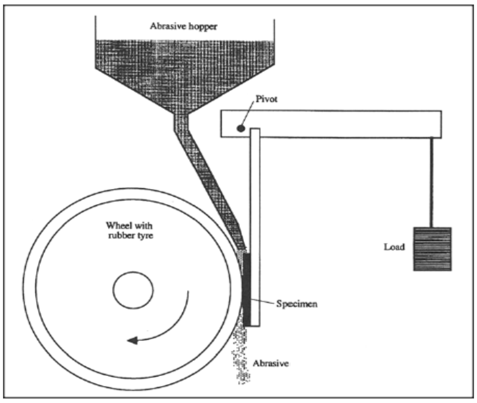

Figure 2. 3: *Schematic representation of the DRWAT* (Stevenson and Hutchings, 1996).

2.5.4.THE DROP BALL TEST

The Drop Ball Test (DBT) is a quality control procedure used in typical grinding media manufacturing units. The purpose of the DBT is to estimate the fracture toughness of the manufactured balls. Figure (2.10) shows a schematic cross-section through a Drop Ball

Testing machine. The machine consists of a long vertical tube connected to a curved tube section. Typically, a known number of balls sit in the curved tube section. A ball is dropped from the top end of the vertical tube and impacts onto the ball sitting on top of the curved section. The impact energy resulting from the collision is transferred throughout the balls such that the last ball sitting in the curved section is projected out. The projected ball rolls down a channel and is hoisted back to the top end of the vertical section where it is dropped off again. The test pass/failure criteria is set depending on the ball size and material of construction.

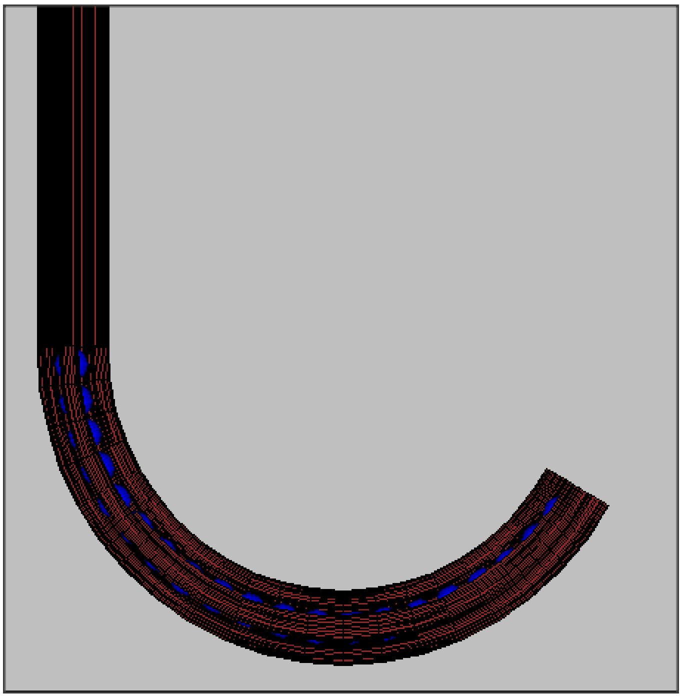

Figure 2. 4: *Schematic cross section of a Drop Ball Test*

The energy (E) (in J/kg) provided by the ball on impact can be described by the potential energy that the ball possesses before it is dropped from the top of the vertical section of the DBT machine, Equation (2.2).

$$E = mgh \qquad (2.2)$$

Where m is the mass of the ball (in kg), g is the acceleration due to gravity ($9.81 ms^{-2}$) and h is the vertical height through which the ball falls (in m).

World over, DBTs are widely used in grinding media production units and laboratory facilities and they have provided reasonable qualitative data over the years. However, questions still arise such as: How accurately the DBT represents actual high impact loading environments such as SAG mills in terms of the energy that the balls are exposed to? Can the energy that the balls are exposed to during the DBT be characterised? The above questions constitute a significant portion of this study.

2.6. MODELLING OF GRINDING MILLS AND PARTICULATE SYSTEMS

Global trends of metallic resources have compelled primary metal producers to install or retrofit large diameter grinding mills to handle huge volumes of material than in previous years. The introduction of robustly built grinding machines such as SAG mills that can handle huge volumes has also brought with it a new set of challenges. Challenges such as improved control, performance optimization and grinding media usage have arisen because of the use and complex nature of SAG mills. However, the ability to model comminution and particulate processes has been a key breakthrough in handling some of the challenges.

Models form the basis of simulation of complex particulate systems such as DBTs and SAG mills. The evolution of numerical modelling and its fundamental concepts are summarised in the succeeding sections.

2.6.1. MODELLING

A model is an established relationship which seeks to link causes and effects (Tönshoff *et al.*, 1992). In order to develop a model, a sound grasp of the process involved and the likely effects of the operational changes are fundamental prerequisites. A study of the system both quantitatively and qualitatively results in the establishment of a model that relates input to output quantities in order to describe the dynamic as well as the static performance of the process. The model can then be used to predict the results of a process or initial conditions required to produce certain results. Using this approach, it is possible to vary setup variables of the process in a purposeful manner (Tönshoff *et al.*, 1992).

Models are broadly divided into physical and empirical depending on how they are developed. Physical models are derived from first principles. With certain objectives in mind, physical variables are selected using experience and knowledge of the process and a model is established which conforms to some mathematical and physical laws (Tönshoff *et al.*, 1992).

On the contrary, empirical models are established on the basis of a vast suite of data gathered over many years for a specific operation with various ores and the semi-empirical models that have evolved through a combination of practice, observation, research and model-fitting of the data (Weerasekara *et al.*, 2013). According to the objectives, tests are carried out, and all input and output quantities have to be recorded. After evaluating the results, a criteria of modelling is chosen, the coefficients are determined and then the empirical model can be verified in further tests (Tönshoff *et al.*, 1992).

2.6.2. SIMULATION

Simulation is the mimicking of a system or process based on some developed mathematical model. Simulation allows for a clear definition of the state of a process at any moment (Tönshoff *et al.*, 1992). Hence, users can understand and give advice on process control, optimization or design based on the simulation results. The quality of results obtained from a simulation process depends on the accuracy of the model.

Today, automatic control of grinding circuits is the most advanced and most successful area of the application of models and simulation in the minerals industry today (Wills and Napier-Munn, 2006). While technological studies are being carried out regularly within the field, important challenges remain for the future and some of the questions that arise are; can the simulation tools accurately quantify the stresses induced into the grinding balls during grinding? Can simulation models such as the Discrete Element Method (DEM) clearly define to what extent the quality control procedures such as Drop Ball Test emulate actual grinding environments?

2.6.3. THE DISCRETE ELEMENT METHOD

The Discrete Element Method (DEM) is a numerical tool for modelling the behaviour of discontinuous and particulate systems. DEM has become widely accepted as an effective method of addressing engineering problems in granular and discontinuous materials, especially in granular flows, powder mechanics, rock mechanics, and comminution. Hence by its very nature, the DEM is suitable for most grinding mill problems (Weerasekara *et al.*, 2013). The advent of affordable high speed computers made simulation of complex systems feasible, and hence increased interest shown by the mining industry to simulate various applications (Powell, 1991).

When applied to grinding, the DEM can be used to predict mill output factors such as grinding rates, power draw and impact energy spectra provided basic inputs about the material properties, mill geometry and operating conditions are available thus giving an opportunity to improve design and optimization of several variables of grinding in detail.

Fundamentally, the DEM solves Newton's equations of motion to resolve particle motion and uses a contact law to resolve inter-particle contacts. Forces are typically integrated explicitly in time to predict the time history response of the material using an appropriate quadrature method. The DEM includes a family of techniques that use radically different treatments for the element geometry and the form of the contact forces (Weerasekara *et al.*, 2013). A fully integrated DEM code consists of a contact model, bonding model and energy logging model. These are further discussed below.

CONTACT MODEL

The DEM codes used for comminution modelling generally use a linear spring and dashpot model in both the normal and tangential direction with a frictional slider in the tangential direction, or a variation thereof, Figure (2.12). Due to its simplicity, this form of model is suited to tracking the motion and gross kinetics of a large number of particles. The energy dissipated in collisions is captured in the dashpot, allowing it to be accounted for and recoded for later analysis in the comminution models. However, the idealised nature of the contact model does not allow for the detailed analysis of the contact event, indeed the outputs should not be over-interpreted in terms of physical significance. Rather the outputs should be utilised in a pragmatic manner to provide the rates and frequencies, distributions and energies of collision events (Weerasekara *et al.*, 2013).

BONDING MODEL

Modern DEM codes incorporate the Bonded-Particle Model (BPM), which directly mimics the rock behaving like a cemented granular material of complex-shaped grains in which both the grains and the cement are deformable and may break. Conceptually the BPM, in principle, can explain all aspects of the particle’s mechanical behaviour. This system exhibits a rich set of emergent behaviours that correspond well with those of real rock. It provides the ability for the DEM to investigate the micro-mechanisms that combine to produce complex macroscopic behaviours and predict these macroscopic behaviours, (Weerasekara *et al.*, 2013). In general, the BPM is characterised by the grain density, grain shape, grain size distribution, grain packing and grain-cement micro-properties. Each of these items influence the model behaviour (Weerasekara *et al.*, 2013).

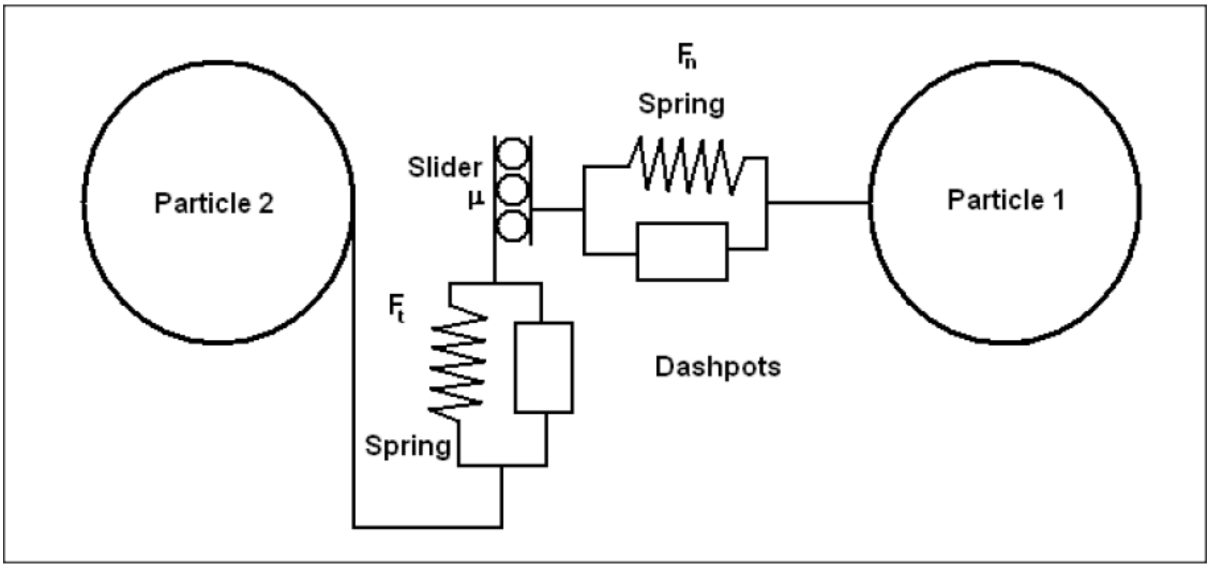

Figure 2. 5: *Spring-slider-dashpot for modelling particle contacts* (Kiangi, 2011).

ENERGY LOGGING

As particles interact, they exchange energy. The DEM contact law calculates the total energy dissipated from particle collisions. The energy calculations incorporates the normal and tangential components and the results obtained are dependent upon the law that is utilised and the simplifications that are applied (Weerasekara *et al.*, 2013). The energy losses from all the individual collision events are collected to form frequency distributions of these energy losses, both in the normal and tangential (shear) directions. Energy spectra can then be calculated for each type of collision event and for each ball and rock size class. These collision energy spectra provide the opportunity to better understand the various contributions to the overall energy dissipation within the mill and how the energy supplied by the mill to the particles is consumed (Weerasekara *et al.*, 2013).

A DEM simulation for a typical mill section with several thousand particles generates massive amounts of output data, running to several gigabytes. Even with good sampling techniques, this generates files of close to or bigger than a gigabyte in size. Although some DEM software provides an interface based data analysis environment, their techniques either require a considerable amount of processing capacity or are not capable of delivering the required inputs for a fully mechanistic comminution model. Therefore, a data logging system is required to fulfil the following objectives: provide flexibility in handling huge data sets generated by typical DEM codes; extract particle collision information from the DEM output database and summarise data to provide data that is more useful for further comminution modelling processes. To this end, considerable effort has been directed towards data extraction and analysis dedicated to providing the outputs required for comminution modelling (Weerasekara *et al.*, 2013).

The attractiveness of the DEM is its reliance on fundamental laws of physics to predict the behaviour of particulate systems. In particular, inter-particle forces and energy dissipations are predicted which are important variables used in the description of particle fracture (Bwalya, 2005). The major limitation of the DEM is its high computational demand. However, advances in mathematical algorithms and computer power have resulted in the implementation of practical models for milling.

2.7. FAILURE MODELLING OF MATERIALS UNDER FATIGUE

Fatigue is a failure mode exhibited by materials under cyclic, repeated or alternating loading. Fatigue manifests as progressive brittle fracture that emanates from nucleation and propagation of a crack that finally leads to rapture of the material. Steel grinding balls in SAG mills or Drop Ball Test (DBT) are subjected to repeated impact loading that might lead to fatigue failure. Such impact-loading initiates or results in nucleation of cracks that grow until they reach a critical crack size leading to fracture. During impact loading in SAG mills and DBT, the magnitude of the stress induced into a ball in a single drop or cycle is insufficient to cause fracture. However, the number of cycles required to cause ball fracture vary from a few thousands to tens of thousands. This variation could be a result of pre-existing imperfections or cracks that act as points of high-stress concentration from which rapture propagates. New cracks can also nucleate during cyclic loading. This fatigue crack nucleation occurs at stress levels far below tensile strength of the material (Bhat and Patibandla, 2011)

Karl, (2012), discussed that fatigue fracture is influenced by various types of factors (scatters). These scatters include; material of construction, nature of loading environment, extent of stress in one cycle, existence of imperfections and consistency of the cyclic loading. The environmental factors that affect fatigue include operating temperature, aqueous or corrosive environments and nature of the impact loading. Nature of the impact loading refers to either low stress elastic deformation that requires high number of cycles to cause fracture or high stress plastic deformation that requires less number of drops to cause fracture.

The inherent mechanical properties of the material of construction also influence fatigue fracture. Microstructure of the material influences the particle movements within the crystalline microstructure. Size of the grains and phase transformations occurring during loading also influence the material's fatigue life.

Manufacturing processes such as extrusion, drawing or forging influence fatigue life. Processes such as cold rolling, peeling or heat treatment or hardening procedures relieve stress in the material thus reducing chances of crack initiation and induce fatigue strength. Rough surfaces that appear after manufacturing (forging laps, extrusion scratches etc.) act as points of high stress concentration from which cracks initiate. Geometry of the component influences fatigue strength. Solid spherical components are likely to have high fatigue tolerance than materials with sharp edges such as cubic, rectangular and cylindrical components (Bhat and Patibandla, 2011).

For over a century, fatigue life prediction has been based on Wohler's S-N curves. The S-N curves concept is a rotating-bending fatigue test that estimates fatigue life and endurance or fatigue limit of metal. Figure (2.13) shows S-N curves that indicate the fatigue limit of various metals.

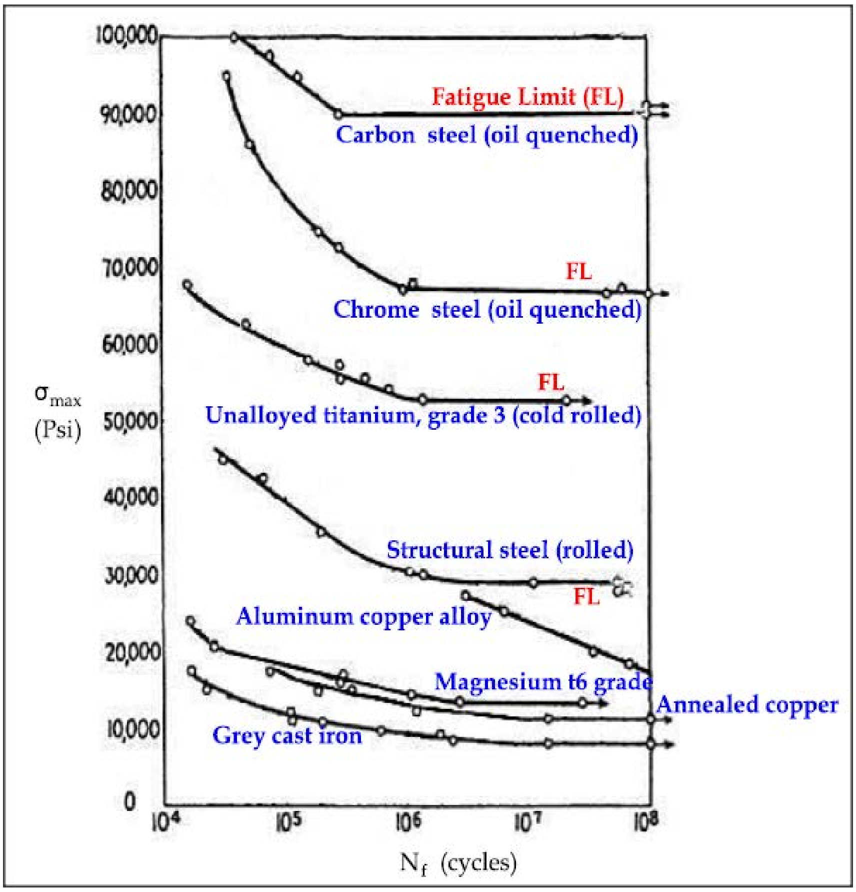

Figure 2. 6: *S-N curves for various metals* (Bhat and Patibandla, 2011)**.**

Where, N_f is the number of cycles, σ_{max} is the maximum stress required for fracture and σ_a is the stress amplitude (stress induced in the component in one cycle).

However, S-N curves have some limitations when predicting fatigue fracture of a material. Firstly, they only estimate fatigue life without an indication of specific number of cycles required to cause crack initiation and growth. Secondly, they do not take into account size and geometry of the component. Consequently, S-N curves do not impart sufficient confidence in predicting fatigue failure of components.

Basquin, (2010) introduced the Linear Damage Rule (LDR) in an attempt to develop a stress-based law of predicting fatigue failure:

$$\sigma_a = \sigma_f \left(2N_f\right)^b \qquad (2.3)$$

where, $\sigma_a$is the stress amplitude, σ_f is the fatigue strength coefficient, N_f is number of cycles and b is a fatigue strength component.

Equation (2.3) is the basis of most fatigue failure models developed over the years. Karl, (2012) developed a fatigue failure model that takes into account both defects in the component and the stress that it experiences, Equation (2.4):

$$P_{f,total} = 1 - \left(1 - P_{f,D}\right)\left(1 - P_{f,S}\right) \qquad (2.4)$$

where, $P_{f,total}$ is the probability of fatigue failure, $P_{f,D}$ and $P_{f,S}$ are failure probability according to defects in the component and stress that the component is subjected to respectively. $P_{f,D}$ and $P_{f,S}$ are defined in the equations below:

$$P_{f,D} = 1 - \exp\left(-\int_V \left(\frac{\sigma_{eff} - \sigma_{th}}{\sigma_u}\right)^m \frac{dV}{V_{ref}} \qquad (2.5)$$

$$P_{f,S} = \int_{-\infty}^{\sigma_{eff}} \frac{1}{\sigma_{std}\sqrt{2\pi}}\, exp\left(-\frac{\left(\sigma_{eff} - \sigma_{mean}\right)^2}{2\sigma_{std}^2}\right) \qquad (2.6)$$

where, σ_{eff} is the point-vice stress measure in the component, σ_{mean} is the mean stress value, σ_{std} is the standard deviation, V is volume of the material and σ_{th}, σ_u and m are material parameters associated with arbitrary reference volume, V_{ref}.

A common feature of the models discussed above is that they all do not take into consideration the shape of the material. This is an important parameter for example, two components, one spherical and the other rectangular can have the same volume and flaw distribution but the rectangular shape might fail under less number of drops than the spherical shape because of existence of sharp edges that act as points of high stress concentration.

2.8. MODELLING OF THE DROP BALL TEST

The Drop Ball Test (DBT) is a particulate system in which steel balls interact with each other. The fundamental difference to other particulate systems such as grinding mills is that the ball collisions within the DBT are controlled and predictable as opposed to random particle collisions in grinding mills. However, DEM simulation model for the DBT has been set up to study energy transfer, kinetic energy behaviour and to estimate the stresses induced into the grinding media during the DBT.

The DEM is an attractive tool for simulating the DBT. Using the DEM, the elastic, kinetic and potential energy behaviour of the balls can be evaluated. Furthermore, using the DEM gives an opportunity to develop a method to predict the stress that the steel grinding balls are exposed to. Characterising the DBT at such a microscopic level allows room for comparisons of the DBT to high impact loading environments such as SAG mills.

2.9. CONCLUSION

The popularity of SAG mills has increased as the machines of choice in most primary grinding operations. The attractiveness of SAG mills lies in their ability to handle huge tonnages and their ability to reduce many size reduction steps into one. Hence as more mineral processing operations are moving towards treatment of more competent ores, most new plant designs incorporate SAG mills whilst most existing operations are retrofitting them.

SAG mills rely on impact energy provided by the cataracting fraction of the charge for most of the ore breakage. This type of charge motion demands use of grinding balls that have improved fracture toughness to avoid catastrophic failure of grinding balls during operation. When grinding balls fail, the failure is attributed to both the physical metallurgy of the balls and the operational aspects related to the mill. Usually the grinding media manufacturer has a firm grip on the quality of the balls. The mill aspects are strongly influenced by the mill design, optimization and operation.

The continuous popularity of SAG mills has resulted in an increase in demands for techniques to predict performance, optimize ball consumption and predict grinding kinetics and ball failure from mill operators. Likewise, grinding media manufacturers are required to rigorously test their products and provide data on the maximum stress that the grinding media can be exposed to. In order to achieve these tasks, traditional sampling methods and test works are being used in typical mineral processing plants and grinding media manufacturing units and these have provided reasonable data over the years. However, the development of numerical techniques such as the DEM has provided a platform for better mill control to yield improved product quality and mill performance. Furthermore, there is an opportunity for grinding media manufacturers to use the DEM to understand the energy that the balls are exposed to in quality control procedures such as the Drop Ball Test. This information will be very useful in further developing the mechanical properties of the grinding media.

The scope of the present study is to apply the DEM as a tool to understand the influence of load behaviour in SAG mills on stresses induced into the grinding balls during operation, characterizing the energy exposed to the balls in the DBT and comparing the severity of the DBT to a SAG environment in terms of the energy that the balls are exposed to. This information will be useful in further developing the toughness and hardness requirements of the balls for high impact loading SAG mill environments.

CHAPTER 3

MATERIAL CHARACTERIZATION TESTS AND SIMULATIONS SET UP

3.0. INTRODUCTION

Over the years, significant research has been conducted on applying the Discrete Element Method (DEM) to simulate various particulate systems, (Sun *et al.*, 2009; Jonsen *et al*., 2012; Weerasekera *et al.*, 2013; Cleary and Sinnott, 2015). However, to the present day, the use of the DEM to model the stress induced into the grinding media because of certain load behaviour remains a grey area. Furthermore, using the DEM to model collision behaviour in Drop Ball Tests is a new and exciting prospect that has the potential of further enlightening threshold stress within the manufactured grinding balls.

This chapter describes the DEM simulations that were conducted to generate the data that is discussed in the succeeding chapters. The parameters involved in each simulation were adopted from industrial mills with well-known operating parameters. The Drop Ball Test (DBT) simulations were based on parameters adopted from an operating Drop Ball Tester. Furthermore, this chapter also describes material characterization test-equipment and procedures that were performed to evaluate the physical and chemical properties of the type of grinding media under study.

3.1. BALL DESCRIPTION AND MATERIAL CHARACTERIZATION

The purpose of the material characterization tests were to establish a consistent set of physical and chemical properties of the material under study. The type of grinding media used for the Drop Ball Tests (DBT), SAG mill and DBT simulation was forged steel grinding media of varying size diameters. The succeeding sections describe the physical tests that were conducted to characterize the material.

3.1.1. CHEMICAL COMPOSITION

The spark emission spectrometer was used to perform chemical composition tests. The spark emission spectrometer is a device used to analyse the elemental content of metallic samples using the principle of Optical Emission Spectroscopy (OES). Figure (3.1) describes the principle of operation of OES that involves exciting of the atoms and ions contained in a metallic sample by an arc spark discharge. Once excited, the atoms and ions emit radiations that have characteristic wavelengths and intensities.

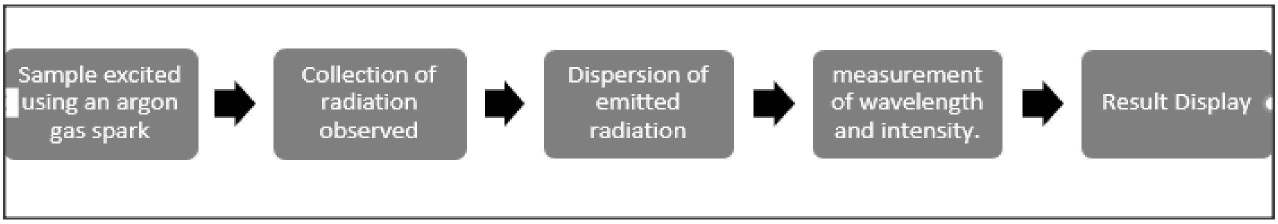

Figure 3. 1: *OES principle*

The wavelength gives the identity of the element and the intensity is proportional to the elemental concentration. Figure (3.2) shows a generic wavelength-intensity graph of an analysed sample. The chemical composition results show the percentage weight of each element present in the sample.

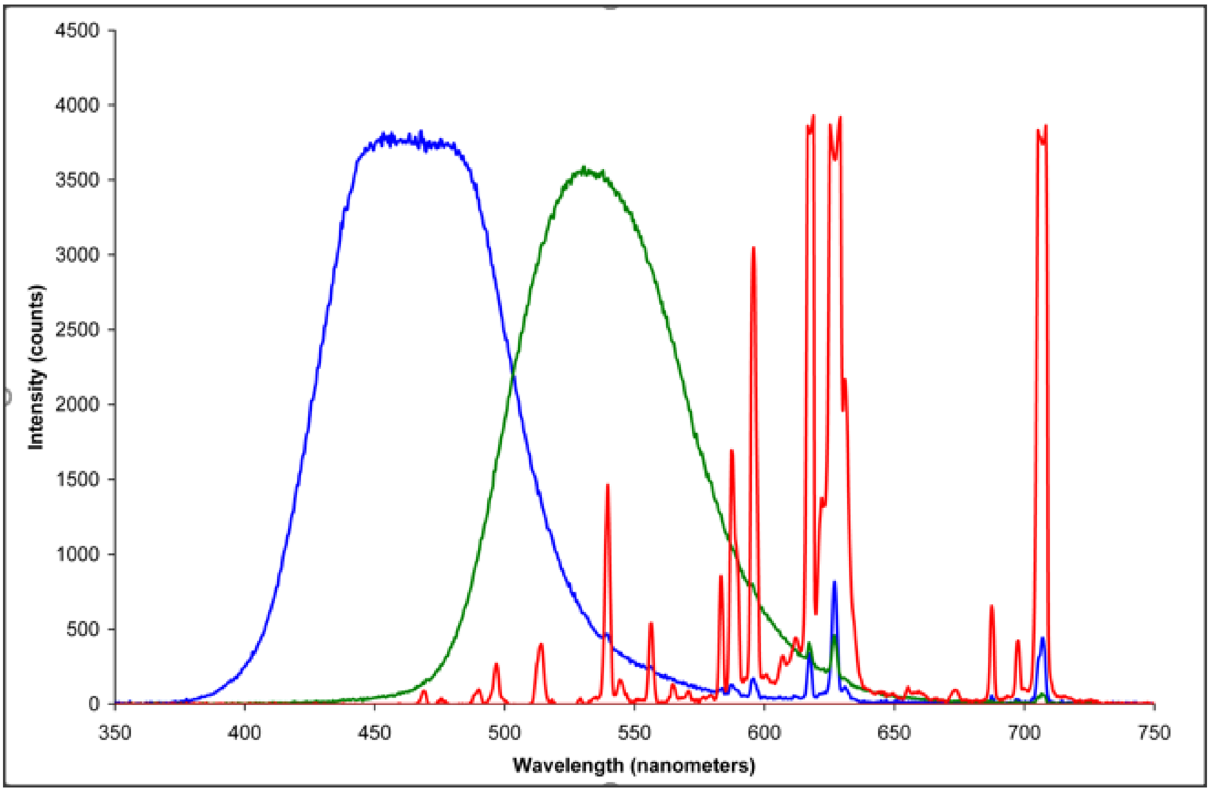

Figure 3. 2: *Sample wavelength vs intensity elemental analysis of OEM*

3.1.2. MATERIAL HARDNESS

Hardness is characteristic of a material. It is a physical property defined as the resistance to indentation, and is determined by measuring the permanent depth of an indentation. The Rockwell Hardness Testing (RHT) machine shown in Figure (3.3) was used to measure the hardness of the balls. The machine utilises a fixed force (load) and an indenter. The smaller the indentation, the harder the material.

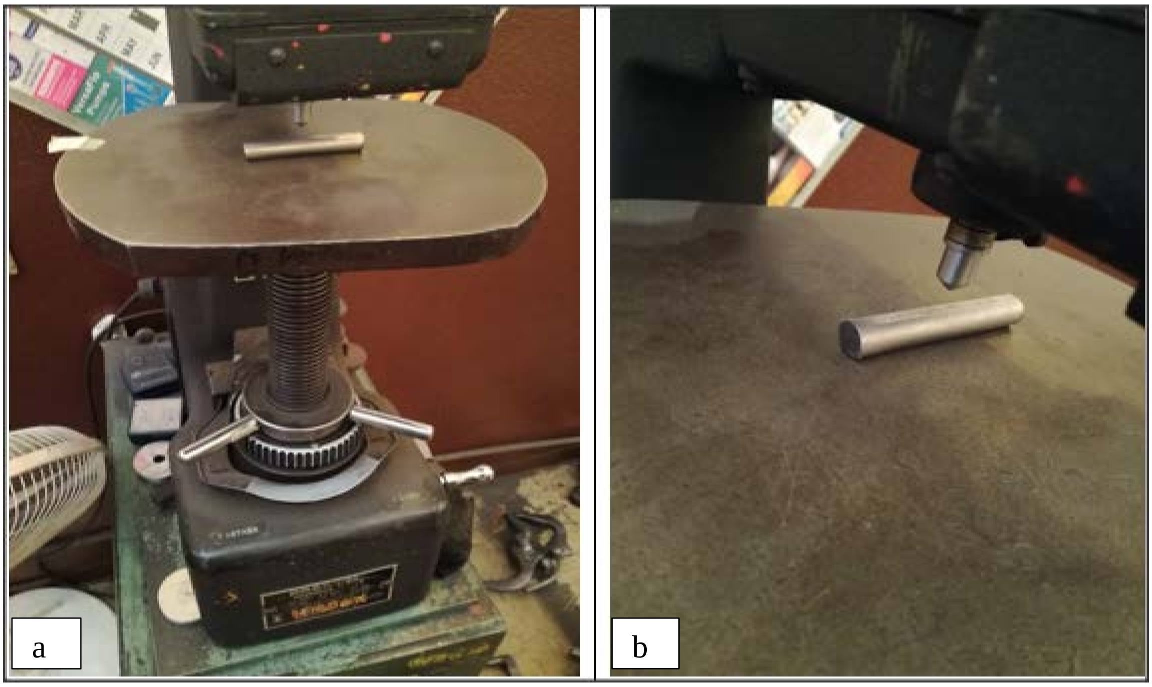

Figure 3. 3: *Rockwell Hardness Testing Machine (a) Machine set-up (b) RHT machine indenter*

Figure (3.4) shows the principle of operation of the RHT that involves, firstly, a preliminary test force (preload or minor load) applied to a sample using a diamond or ball indenter. This preload breaks through the surface to reduce the effects of surface finish. After holding the preliminary test force for a specified dwell time, the baseline depth of indentation is measured. After the preload, an additional load (major load) is added to reach the required total test load. This force is held for a predetermined amount of time (dwell time) to allow for elastic recovery. This major load is then released, returning to the preliminary load. After holding the preliminary test force for a specified dwell time, the final depth of indentation is measured. The Rockwell hardness value is derived from the difference between the baseline and final depth measurements. This distance is converted to a hardness number (Newage Testing Instruments, 2010).

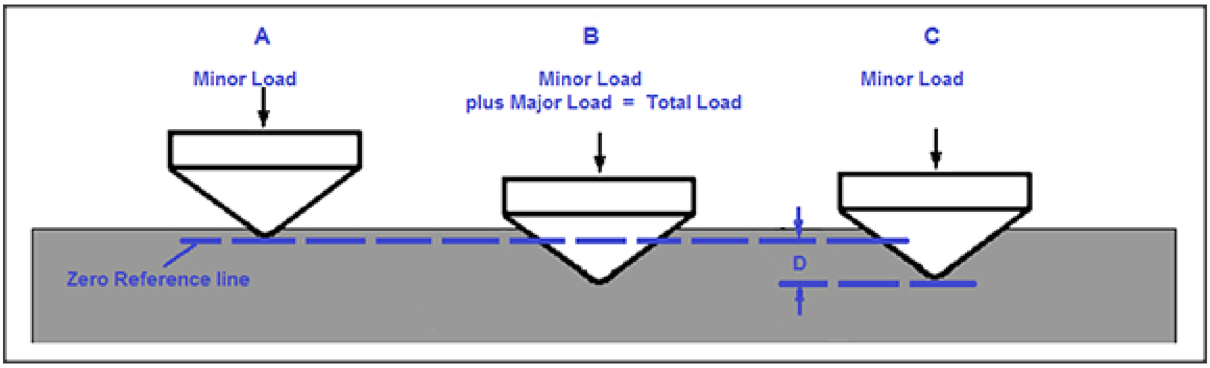

Figure 3. 4: *Hardness Rockwell testing principle* (Newage Testing Instruments, 2010)

Figure (3.4) Test Method Illustration:

- A - Depth reached by indenter after application of preload (minor load)
- B - Position of indenter during Total load, Minor plus Major loads
- C - Final position reached by indenter after elastic recovery of sample material
- D - Distance measurement taken representing difference between preload and major load position. This distance is used to calculate the Rockwell Hardness Number (Newage Testing Instruments, 2010).

The Rockwell Hardness Scale ranges 0 – 66 HRc. A lower hardness number indicates that the material is softer while a higher number denotes a hard material. The hardness values of various types of steels ranges between 45 – 66 HRc.

Samples were extracted along the diameter of the ball to measure the hardness profile of the grinding ball from its surface to the core.

3.1.3. MICROSTRUCTURE ANALYSIS

The purpose of the metallography analysis was to determine the predominant microstructure of the grinding balls. An Eclipse – MA100 optical microscope was used to perform this task. The Eclipse – MA100 optical microscope's principle of operation involves using a system of lenses and visible light for image magnification. The microscope was fitted with a Nikon photosensitive camera that captures images to generate the micrographs. Figure (3.5) shows a picture of the Eclipse – MA100 optical microscope that was used for the metallography work.

Figure 3. 5: *Eclipse MA100 Optical Microscope*

The metallography samples were ground and polished to produce a clean surface free from dirt and prints. This ensured that the micrographs obtained were clear and reliable. To enhance handling, the samples were mounted in an acrylic based resin, Figure (3.6).

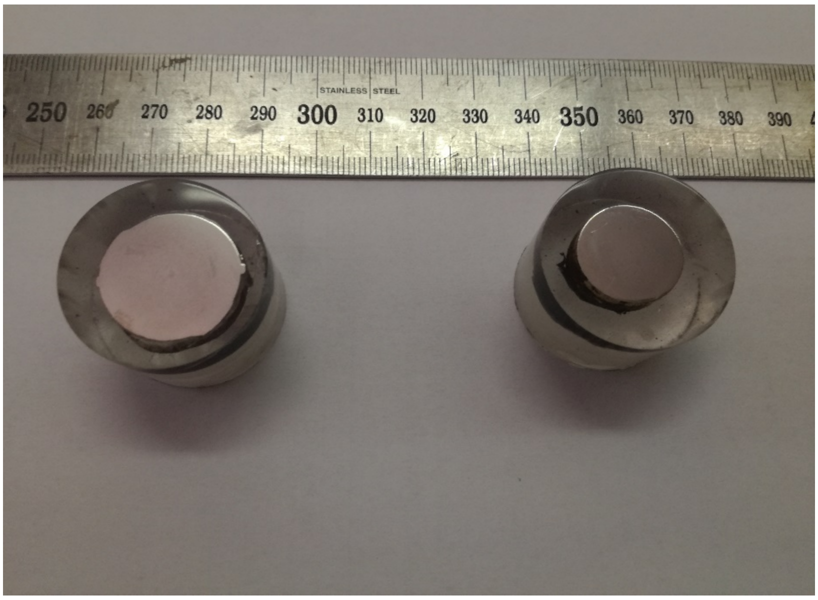

Figure 3. 6: *Resin mounted metallography samples*

3.1.4. DROP BALL TEST

The purpose of the Drop Ball Test (DBT) was to establish a physical and quantitative pattern of the balls' response to fracture under severe impact loading conditions. To perform this task, a DBT machine shown in Figure (3.7) was used.

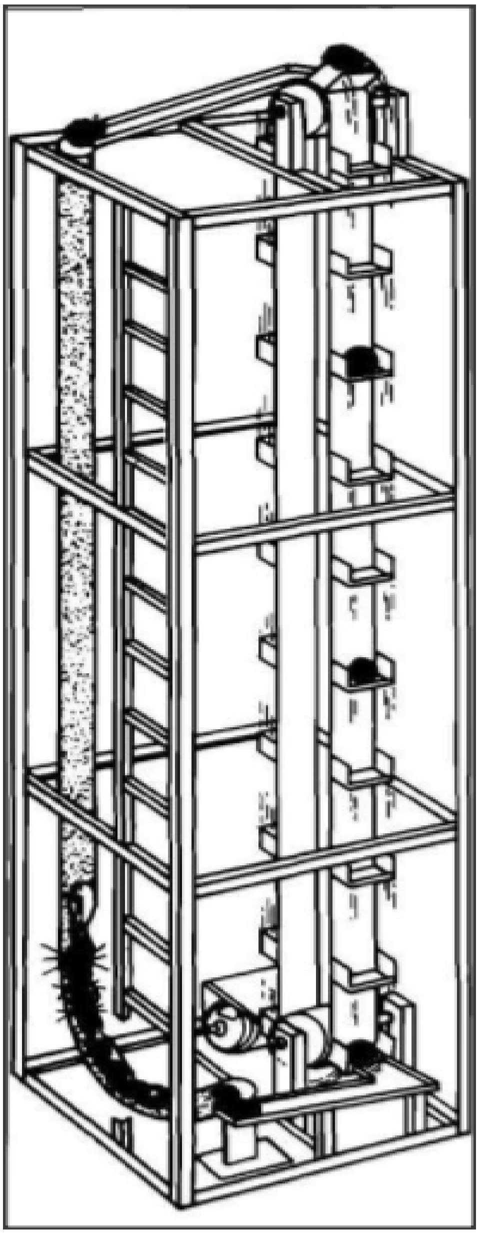

Figure 3. 7: *Sketch of the DBT* (Tylczak, 1989)

The DBT constitutes of forty (40) same-sized balls in circulation during a single test. During the test, a ball was dropped from a 10m height onto a line of 20 balls arranged in a curved section. The shockwave resulting from the impact energy of the ball coming from free-flight and the ball sitting on top in the curved was transferred throughout all the balls until the last balls sitting in the curved section was projected out. The impact energy decayed gradually from the first to the last ball in the curved section. An anvil guided the projected ball into a channel through which the ball rolled past an electronic counter then it was carried by a chain system back to the top of the device where it was dropped off again (Tylczak, 1989).

This process was repeated continuously and after every 1000 drops, the balls were inspected for breakage or spalling. The test was stopped after a total of 10000 drops and the breakage and spalling results were summarised.

3.2. DEVELOPMENT OF DEM PARTICLE FLOW CODE (PFC-3D) SIMULATORS

The development of an efficient DEM simulation code is an enormous task that can take long man-hours. Itasca Consulting Group developed a Particle Flow Code (PFC) which can be adapted to model particle-collision behaviour in many industrial systems (Bwalya, 2005). The PFC has an inbuilt programme, FISH, that allows users to write customized scripts to tackle many environments that involve particulate systems.

The DEM-PFC-3D program is controlled by commands that can be typed at the command line or coded by using its FISH programming language to write a structured code with functions, using any text editor. The program script is saved with the extension “Dat” in the same folder as the PFC program. To run the program, the command “call” is typed followed by the script name. All the functions and variables are loaded and compiled before running. It is possible to load many scripts in one session as long as the running simulations are not conflicting with each other. For example, it is possible to run one script and then load the next to use the data generated by the previous script (Bwalya, 2005).

3.2.1. DEVELOPMENT OF A PFC MILL SIMULATION PROGRAM

The mill simulator was modified from the variable and permanent scripts programmes developed by (Bwalya, 2005). The variable script can be generated according to user input and the permanent script reads the data from the variable script to convert these into instructions that drive the PFC software accordingly.

3.2.1.1. THE VARIABLE SCRIPT

Bwalya, (2005) developed a windows Graphic User Interface (GUI) program to allow users to draw the internal geometry of the mill and specify the distribution of different sized balls within the mill charge. A complete list of parameters specified by the user is shown below:

a. Mill Geometry

- Internal mill diameter and Length

- Number of Lifters
- Lifter Design (Height and lifter face angle)

b. Ball and Wall Contact Parameters

- Stiffness of ball and wall in both normal and shear directions
- Ball and wall coefficient of restitution
- Ball and Wall coefficient of friction

c. Simulation Parameters

- Mill Speed
- Mill Filling and ball voidage
- Number of revolutions before any sampling
- Number of data sampling revolutions
- Number of simulation frames to be collected for visualization of the simulation animation
- Scale of classifying the energy spectra (Bwalya, 2005).

3.2.1.2. THE PERMANENT SCRIPT

Once the variable script is loaded, the simulator executes a series of steps as described in the variable script. The series of procedures performed by the simulator are described in the flow diagram below:

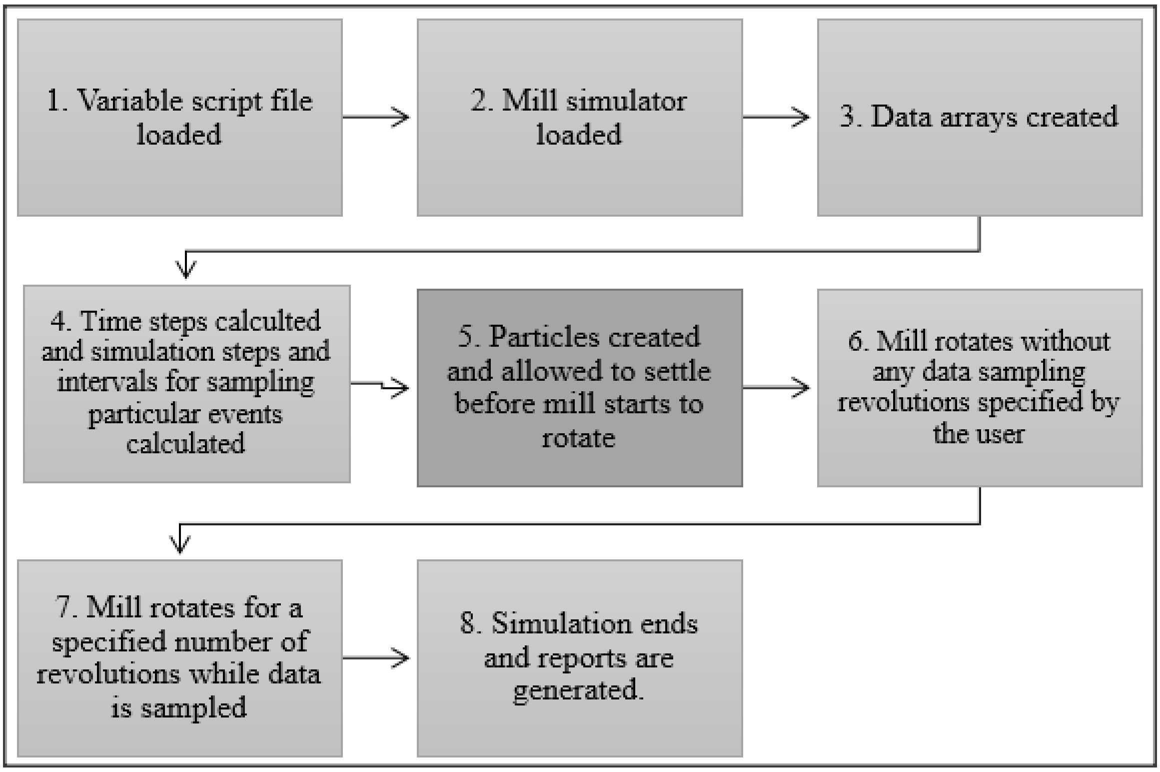

Figure 3. 8: *DEM Mill Simulator sequential tasks* (Bwalya, 2005)

Figure (3.8) is further clarified by the comments below:

- **Creation of data arrays (Step 3)**

The purpose of this step is to allocate enough memory storage space for anticipated simulation events. The major objective of this research was to understand the stress induced into the grinding balls as a result of the ball collisions within the mill and DBT. Hence the arrays were focused on capturing energy conversions during the collisions between various interacting elements. There were millions of collisions especially during the mill simulation and as a result, memory allocation was given first priority to data that was relevant to this study.

- **Time step calculation (Step 4)**

The stability of the numerical algorithm is very important to assure dependable and accurate results. In theory, the stability of the algorithm depends on the time step chosen. The simulation time step chosen ensured that at least twenty (20) time steps were involved in any contact event. The maximum time steps that can be used without creating an unstable simulation were derived by treating the interacting elements as springs at the points of contact (spring-dashpot contact model). Hence the linear elastic behaviour of the spring was adopted and the force involved in the collisions was assumed to be proportional to the relative velocity of the colliding bodies.

Generation of particles (Step 5)

The balls were generated and packed in a rectangular shape placed across the horizontal diameter of the mill. The program lowered the stiffness of the particles to accelerate the settling rate of particles into the rest position of the mill. The stiffness was then gradually restored to the normal value.

- **Mill rotation without any data sampling (Step 6)**

The simulation allowed a number of revolutions to be specified by the user before doing any data sampling. This ensured that the simulation data was only sampled after the mill reaches steady state. However, the power behaviour and impact energy show that there are never two revolutions that can ever be identical, even when the mill is operating under steady state conditions. Hence, time permitting, it is recommended to have a higher number of sampling revolutions for improved accuracy of the data to be analysed.

- **Mill rotation with data sampling (Step 7)**

This part of the simulation demands the longest computational time. It involves identification of each particle (element) interaction taking place during every time step, computing the required calculations and storing the output data. Figure (3.9) shows the sequence of computations at this stage.

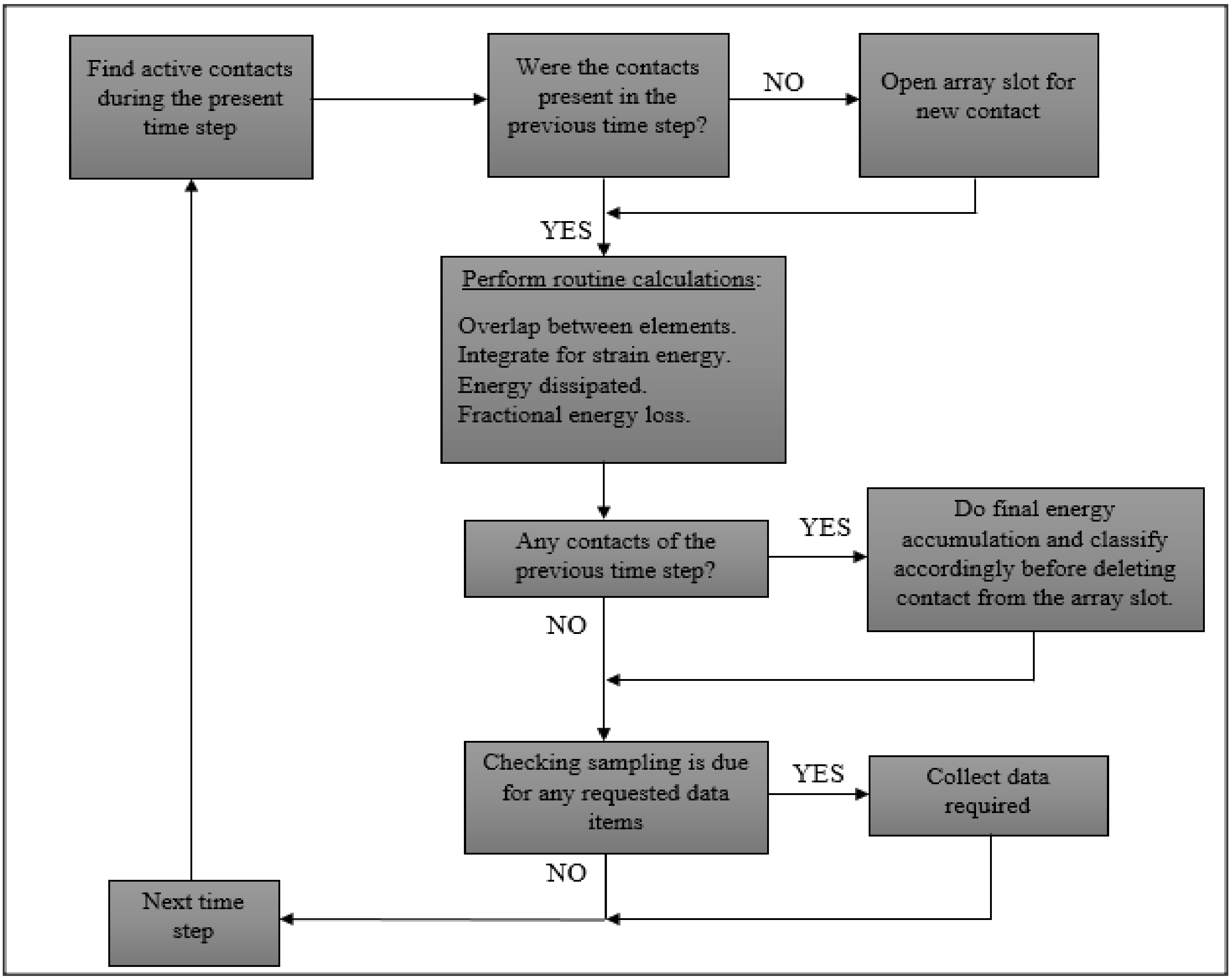

Figure 3. 9: *DEM simulator computational procedures* (Bwalya, 2005)

3.2.1.3. THE SIMULATION COMPUTATIONAL SCHEME OVERLAP CALCULATION

This procedure enables the calculation of interacting forces between two elements by resolving the extent of overlap occurring between them (Bwalya, 2005). The determination of the overlap is easiest when particles are represented as discs and spherical shapes but for more complex shapes, bounding spheres and circles are used for a quick check of possible contact before employing a more detailed analysis of the contact (Williams and O'Connor, 1995).

Figure (3.10) shows the calculation of forces in the simplest case involving discs. The procedure is also applicable to particles of arbitrary shape provided the directions of the tangential and the normal forces have been determined (Bwalya, 2005). The overlap distance (Δ_n) for the purpose of determining the normal force is calculated from equation (3.1):

$$\Delta_n = r_i + r_j - \sqrt{(x_j - x_i)^2 - (y_j - y_i)^2} \qquad (3.1)$$

Where r is the radii of the elements *i* and *j, x and y* are the coordinates of their centres.

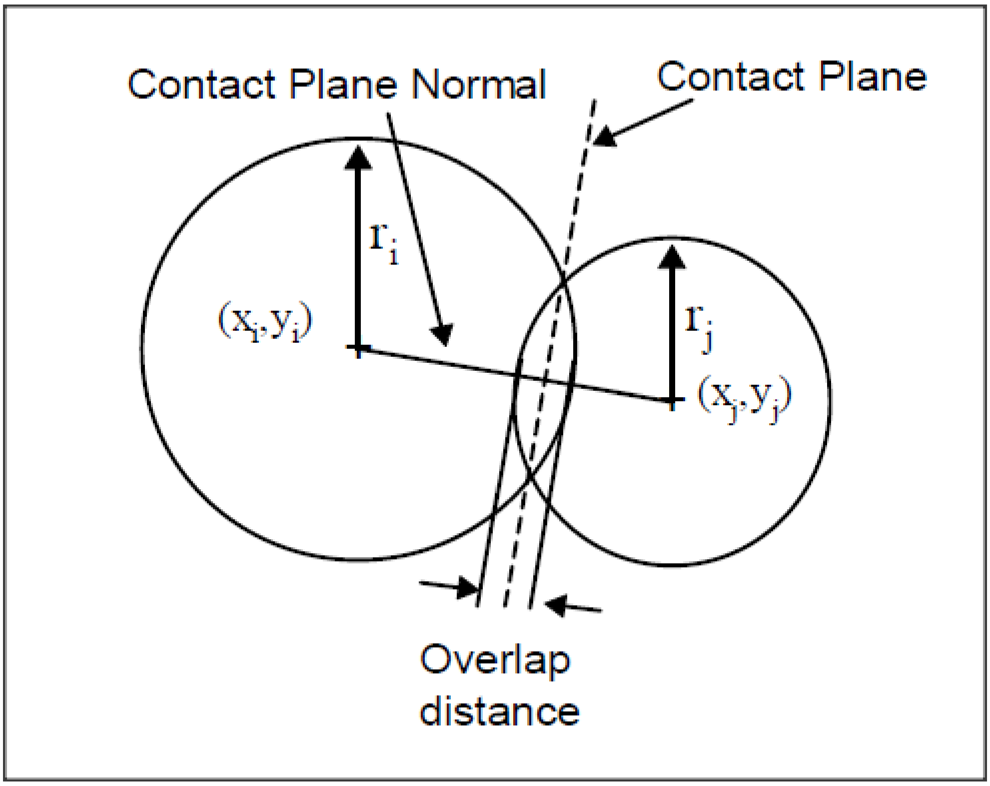

Figure 3. 10: *Ball on Ball contact mechanics* (Bwalya, 2005)

Determining the overlap between the discs and the wall is more challenging because the contact can occur with the edge or corner (end of the two walls) or the corner and the edge at the same time (Bwalya, 2005).

Once the overlap has been determined for two elements in contact, the prevailing forces (normal, shear and angular) at the point of contact can then be calculated. The normal force is modelled as visco-elastic, *i.e.* it consists of an elastic (spring) and a viscous damping (dashpot) component. The force in the tangential direction (shear), includes a slider in addition, to model friction (Bwalya, 2005). Equations (3.2) and (3.3) represent the contact forces.

$$F_n = K_n\Delta_n + CV_n \qquad (3.2)$$

$$F_s = K_s\Delta_s + CV_s \qquad (3.3)$$

Equation (3.3) is applicable when $F_s \leq \mu F_n$ (3.3b) otherwise sliding is implemented instead and $F_s = \mu F_n$

STRAIN ENERGY

The strain energy absorbed by a particle at a time interval i can be calculated by numerical integration from the contact forces given by the PFC, (Equation 3.4):

$$E_i = (F_i + F_{i-1})(\Delta_i - \Delta_{i-1}) \qquad (3.4)$$

Where E is the energy, F is the force and Δ is the overlap distance between the contacting elements. The extent of the overlap is inversely proportional to the material's resistance to indentation.

As the overlap increases, energy is continuously accumulated. The user selects the range of energy classes and the maximum energy strain energy attained at the end of each contact event is recorded into its energy class. At the end of the simulation run, an energy spectra is generated (Bwalya, 2005).

DISSIPATION ENERGY

The energy dissipated during contact at time step i is calculated using Equation (3.5) (Itasca Consulting Group, 2014):

$$E_i = \frac{2D(\Delta_i - \Delta_{i-1})}{\delta t}\sqrt{K_m} \qquad (3.5)$$

D is the Damping Ratio, K_m is the coefficient of stiffness for a particle of mass *m*, and other terms are as discussed earlier. To account for the dissipated energy, the dissipated energy values are accumulated and consolidated at the end of the contact event. The energy is represented in an energy spectra similar to that generated for the strain energy (Bwalya, 2005).

Bwalya, (2005) pointed out that to improve computational accuracy of the scheme, consideration must be taken both at the beginning and end of a contact to compensate for the uncertainty in the exact times when the contact ended or began. Figure (3.11) shows the analysis of issues that may affect calculations of contact velocity when using the Particle Flow Code (PFC).

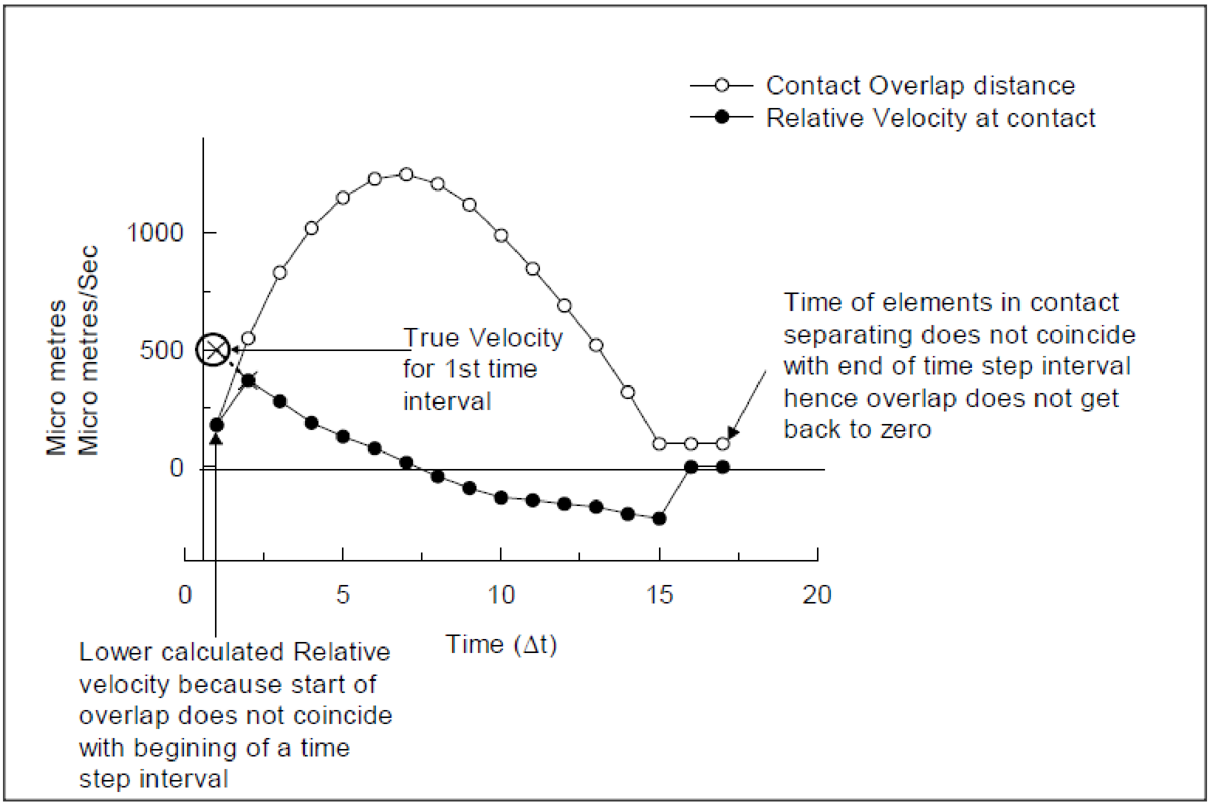

Figure 3. 11: *Factors affecting calculation of the contact velocity when using the PFC* (Bwalya, 2005)

FRICTIONAL ENERGY

During the simulation, particles move in parallel and perpendicular direction to each other, hence there will be frictional energy loss during contact. The frictional energy loss at a contact point for the current time step is available directly from the PFC program, Equation (3.5b) (Bwalya, 2005). The energy involved is calculated and an energy spectra is generated similar to the strain and dissipation energy above.

DATA SAMPLING

The mill simulator allows a variety of information to be collected throughout the simulation. After the pre-sampling revolutions, the mill reaches steady state and information such as power draw, impact energy, frictional energy and number of impact collisions are recorded. Below is a full list of data which can be generated from the simulation:

- Mill Power – recorded as instantaneous input power calculated from the torque due to the balls in direct contact to the wall. This is also referred to as input power. The user specifies the sampling time intervals e.g. every second or every tenth of a second.

- Frictional Loss – this is the energy lost due to friction between the elements in contact i.e. ball to ball or ball to wall.

- Simulation Frames – during the simulation, photographic frames of the mill contents are captured at regular intervals as specified by the user. At the end of the simulation, the frames are combined to produce an animation or video of the load motion throughout the simulation. The animation can be viewed as:

  a. Stills – which show the actual positions occupied by the balls at cross sectional view.

  b. Particle Paths – which show the path taken by each individual ball during mill rotation represented in a single diagram at cross sectional view.

  c. Position Density Plots (PDPs) – which show the areas most occupied by the balls across the mill diameter at cross sectional view.

- Spectral Energy Data – the simulator records all the collision events throughout the simulation and classifies them into different energy groups. The user specifies the energy range to be used during the simulation. There is also an option to record an impact energy spectra for a single size of particles within the load.

- Damping, Normal and Tangential Energy Losses – these are energy losses due to damping between colliding elements, normal and tangential losses.

Prior to the simulation, caution should be taken when selecting data that is required by the user. Excessive information will significantly slow down the simulation. For purposes of this research spectral energy, frictional loss and simulation frames were allowed to be collected from the simulations.

SIMULATION REPORT

At the end of each simulation a report is generated which summarizes the simulation data according to information specified by the user prior to the simulation e.g. power draw, simulation frames and energy spectra. A sample of the report is shown in Appendix A.

3.2.1.4. CRITERIA FOR CHOICE OF CONTACT MODEL AND SIMULATION PARAMETERS

Bwalya, (2005) discussed that the need to closely relate the simulation results to reality and simulation time are two conflicting factors. A wide data sample describes the simulated process more quantitatively and qualitatively but is more computationally and time demanding. The choice of contact models and simulation parameters depends on the following factors:

THE CONTACT MODEL

The DEM algorithm applies Newton's second law of motion to the particles in motion and the linear spring-dashpot model for particles during collisions. Newton's second law of motion gives the motion of the particles resulting from the forces acting on them (Mishra and Rajamani, 1992). The major drawback of Newton's second law is the resulting computational demand especially when many large particles are involved such as during the simulation of large diameter SAG mills.

At every contact between the elements (ball to ball or ball to wall), the forces developing due to the collisions are modelled using the linear spring-dashpot contact model discussed above. Bwalya, (2005) discussed that the major disadvantage of the linear spring-dashpot model is a direct consequence of equation (3.3). The model always produces a large instantaneous force at the beginning and a negative force before the colliding elements separate. Hence the overlap between two colliding elements does not come back to zero because the time when contact ceases does not necessary correspond with the time step interval i.e. the exact time when particles separate is never detected but is determined by extrapolation.

Crosley, (1975) suggested that the large initial force observed at the beginning can be avoided and the negative force occurring at the end more or less eliminated if equation (3.3) is modified to:

$$F = K\Delta + C'V\Delta \qquad (3.6)$$

Where C' is a modified damping constant and V is the relative velocity at the point of contact.

Equation (3.6) shows that the damping term is also dependent on the overlap and thus the behaviour of forces at the beginning and end of contact are better-behaved.

3.2.1.5. SIMULATION PARAMETERS

The linear spring-dashpot model deals with individual particle-to-particle contact hence it is necessary to choose realistic values for the contact parameters. These parameters are material stiffness, coefficient of restitution and coefficient of friction. The material stiffness is required to correctly establish the forces generated in the springs. The coefficient of restitution is a measure of the damping property of the material, and hence it determines the damping parameters that are applied in the dashpot. The coefficient of friction is used to check whether sliding occurs at any contact (Mishra and Rajamani, 1992). The main purpose of the work was to develop a method of quantifying the energy that the balls are exposed to during their residence time within both the SAG mill and the DBT. Hence, the coefficient of restitution and coefficient of friction values were adopted from work done by previous researchers, (Mishra and Rajamani, 1992; Bwalya, 2005; Polycarpou, 2005).

MATERIAL STIFFNESS

The material stiffness determines the force generated in the springs. This force determines the energy exchanged during ball collisions. The material stiffness can be determined in an apparatus known as the ultrafast load cell. It consists of a 5m long steel rod in which fast-responding strain gauges are embedded. These gauges record the strain waves when a steel ball strikes the rod. As soon as the ball strikes the rod, a primary wave is recorded, and as the wave reaches the bottom end of the rod, it is reflected. This wave is also caught by the strain gauges. From these recordings, the force versus displacement curve can be computed, which is the primary use to the ball motion study. Simply, the slope of the force versus displacement curve is what is required to determine material stiffness (Mishra and Rajamani, 1992).

The real stiffness of rock and steel material is in the order of 10^9 N/m and 10^{10} N/m, which would require a time-step of about 10^{-7} seconds, which is very slow. (Bwalya, 2005) suggested that increasing stiffness increases particle vibration without necessarily increasing the overall energy in the system. He also suggested that the collision events that can cause particle fracture at the lowest stiffness are more than double those at the highest stiffness. Thus, it is likely that breakage will be over-predicted when lower stiffness is specified. Further discussions on the modelling and measurement of contact parameters are also available in literature, (Polycarpou, 2005). For the purpose of this research, it was decided not to use stiffness values higher than the order of 10^7 N/m due to the time constraint.

COEFFICIENT OF RESTITUTION

By definition, the coefficient of restitution for colliding bodies is given by:

$$e = \frac{\int R\, dt}{\int P\, dt} \qquad (3.7)$$

Where, $\int R\, dt$ and $\int P\, dt$ are the deformation and restitution impulses, respectively. Using this definition, for two discs moving in the same direction before and after impact, the coefficient of restitution is given by:

$$e = \frac{(V_b)_2 - (V_a)_2}{(V_a)_1 - (V_b)_1} \qquad (3.8)$$

Where V_a and V_b are the velocities of discs a and b and 1 and 2 refer to the situation just before and after the impact, respectively.

However, it is known that the coefficient of restitution is a material property; it depends primarily on the hardness, size, shape, and impact velocities of the colliding bodies. For these reasons the coefficient of restitution must be measured under conditions that are known to exist in the mill, (Mishra and Rajamani, 1992). Depending on the nature of load behaviour within the mill, the ball collisions can be either cascading or cataracting (section 2.1). Cataracting balls are involved in high energy impact collisions and it is simple to determine the coefficient of restitution. However, it is difficult to determine the coefficient of restitution for the cascading balls because there is no impact.

Drop ball tests can be performed to experimentally determine the coefficient of restitution. A ball is dropped from a known height onto a steel anvil. The rebound height is also measured using advanced cameras. The coefficient of restitution is determined using equation (3.9).

$$e = \sqrt{\frac{h_1}{h_2}} \qquad (3.9)$$

Where h_1 is the bounce height and h_2 is the drop height.

For the purpose of this research, the coefficient of restitution used was in the range 0.4-0.6.

COEFFICIENT OF FRICTION

From the spring-dashpot model of ball collisions, the shear force due to the dashpot is limited by the maximum that can exist at the contact, which is given by equation (3.3b). If the absolute value of the force in the shear-spring and dashpot exceeds the value given by equation (3.3b), then slip is presumed to occur, (Mishra and Rajamani, 1992). (Bwalya, 2005) suggested that higher energy collision events (>800J) are less when the coefficient of friction is low and thus correct specification of the coefficient of friction is necessary for correct prediction of impact energy collisions. The higher energy events are less when friction is low due to the balls not being raised high enough. Very little change is observed in the trends when the coefficient exceeds 0.5, this behaviour is probably dependent on both the mill speed and lifter design. For the purpose of this research, coefficient of friction used was in the range (0.4-0.6).

PARTICLE SHAPE

Spheres were preferred for particles. Both the ball and media fraction of the ore during SAG mill simulation were regarded as spherical particles. However, the PFC program allows the creation of ellipsoids but the study of the effects of different particle shapes is beyond the scope of this work.

3.2.2. SAG MILL SIMULATION SET-UP FOR THE PRESENT STUDY

The purpose of the SAG mill simulation work was not to study the SAG kinetics per se but to understand how the SAG mill load behaviour influences the stress induced into the grinding media. The energy that the grinding balls are exposed to in the SAG mill was compared to that of the DBT.

The Particle Flow Code – Discrete Element Method 3D (PFC-DEM 3D) was applied to perform the SAG mill simulations. The SAG mill simulations that were performed were adopted from a practical industrial SAG mill and engineering system.

The physical operating parameters of the SAG mill used for the simulation are described in Table (3.1). The average number of interacting particles in a full-mill simulation was about 160000. Hence, the amount of computational time required to complete such a simulation would have exceeded 5600 person-hours. To reduce the computational time whilst still retaining important simulation data, a slice of the mill was considered. This significantly reduced the number of interacting particles to an average of 14500. Likewise, the required computational time significantly reduced to an average of 504 person-hours.

Table 3. 1: *SAG mill dimensional and operational parameters*

PARAMETER	VALUE	UNITS
Diameter	11.6	M
Length	0.5	M
Speed	72	% N_c
Total Filling	24	%
Lifters	Hi-Lo, 25^0 face angle	
Number of Lifters	36	

All the simulations were performed under the same operating parameters as given in Table (3.1). The lifter design was uniform for all the simulations. Figure (3.12) shows the lifter design that was applied.

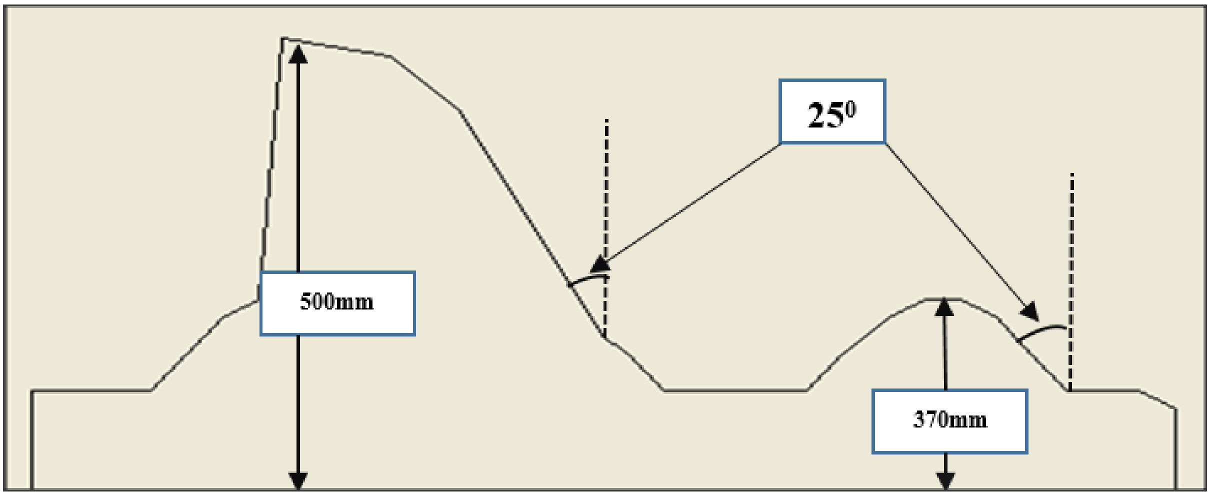

Figure 3. 12: *SAG mill lifter design applied for the mill simulations*

Only the ball:ore ratio (by % mill filling degree) was varied as this provided the basis for comparison. The purpose of varying the ball:ore ratio was to understand and quantify the impact energy cushioning provided by the ore particles to the grinding balls. Hence, the different SAG mill simulations were compared based on the energy exposed to the grinding balls as a result of the different ball:ore ratios.

Ball:ore ratio is a very important process parameter during SAG operation. If the ratio favours grinding balls, the resulting effects are increased ore grinding rates and power draw. However, the probability of steel on steel contact increases (ball on ball or ball on liner) and this reduces the ore cushioning effect hence, the energy and stress that the balls are exposed to increases. On the other hand, if the ratio favours the ore, grinding rates and power draw will drop. Grinding rates will drop because of the decreased number of hard (steel) surfaces that provide much needed high-energy breakage collisions. The resulting effects on the grinding balls are less energy and stress induced into the grinding balls though the ball wear rate might increase.

Table (3.2) shows the various ball:ore ratio in the respective simulation identities (IDs).

Table 3. 2: *Ball:Ore ratios and ore feed distribution in the various mill simulations*

SIM ID	**TOTAL MILL FILLING (% v/v)**	**BALL FILLING (% v/v)**	**ORE FILLING (%v/v)**	**ORE PARTICLE FRACTIONS (%v/v)**				
				150mm	**120mm**	**90mm**	**60mm**	**30mm**
Sim1	24	24	0	0	0	0	0	0
Sim2	24	13	11	2	2	3	2	2
Sim3	24	10	14	2	3	4	3	2
Sim4	24	8	16	2	3.5	5	3.5	2
Sim5	24	6	18	2	4	6	4	2

*(% v/v) – Percentage of total mill volume.

The SAG mill simulation parameters were similar to the DBT simulation parameters. These provided a basis for comparison of the energy that the balls are exposed in both the SAG mill and DBT. A full study of the effect of simulation parameters on the results remains a recommendation for future work. Table (3.3) shows the SAG mill simulation parameters.

Table 3. 3: *SAG mill simulation and load parameters*

PROPERTY	VALUE		UNITS
	Steel Balls	**Ore**	
Coefficient of restitution	0.6	0.6	
Coefficient of friction	0.4	0.6	
Normal Stiffness	400	200	kN/m
Shear Stiffness	300	150	kN/m
Density	7750	2900	Kg/m^3
Power sampling time interval	0.1	0.1	Sec
Energy scale	5.0	5.0	J
Ball Size	125	Refer to Table (3.2)	Mm

3.2.3. CONCLUSION

From the discussion, it is observed that simulation parameters have significant effects on the quality of the simulation data generated. Optimizing simulation parameters is a considerable task that takes long person-hours.

3.3. DEVELOPMENT OF A PFC DROP BALL TEST SIMULATION PROGRAM

A code was developed based on the Particle Flow Code (PFC) that simulates the collision behaviour of balls in the Drop Ball Test. Unlike the PFC Mill Simulator that was generated from both the variable and permanent scripts, the DBT Simulator was generated from only the permanent script because the process is predictable and the collisions are well known unlike SAG mill collisions that are random. Figure (3.13) shows the 2D drawing of the Drop Ball Test machine.

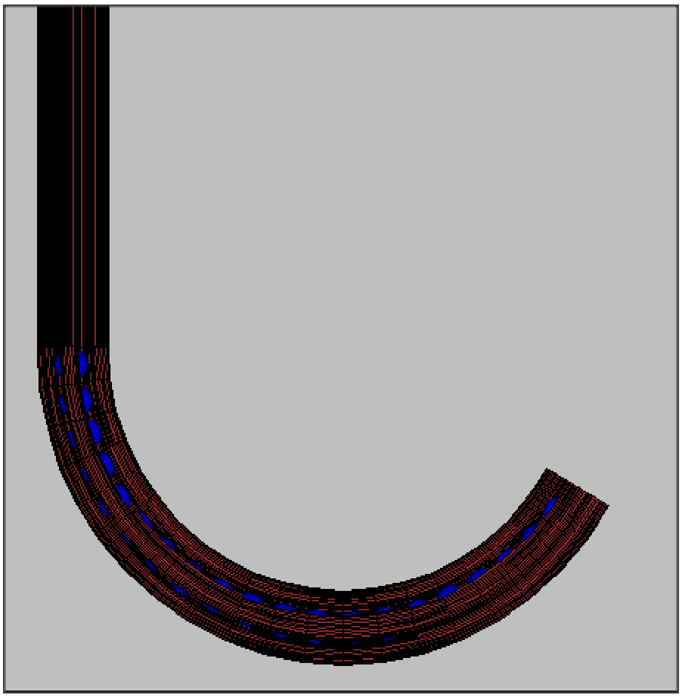

Figure 3. 13: *Schematic 2D representation of the DBT*

3.3.1. THE DBT PERMANENT SCRIPT

The permanent script was developed from a code based on the Particle Flow Code (PFC). Once the permanent script is saved, the simulator executes a series of procedures described in Figure (3.14). The computational procedures are similar to the mill simulator procedures described in the previous sections. The major difference is the memory allocation of the DBT simulator which requires less memory space compared to the mill simulator.

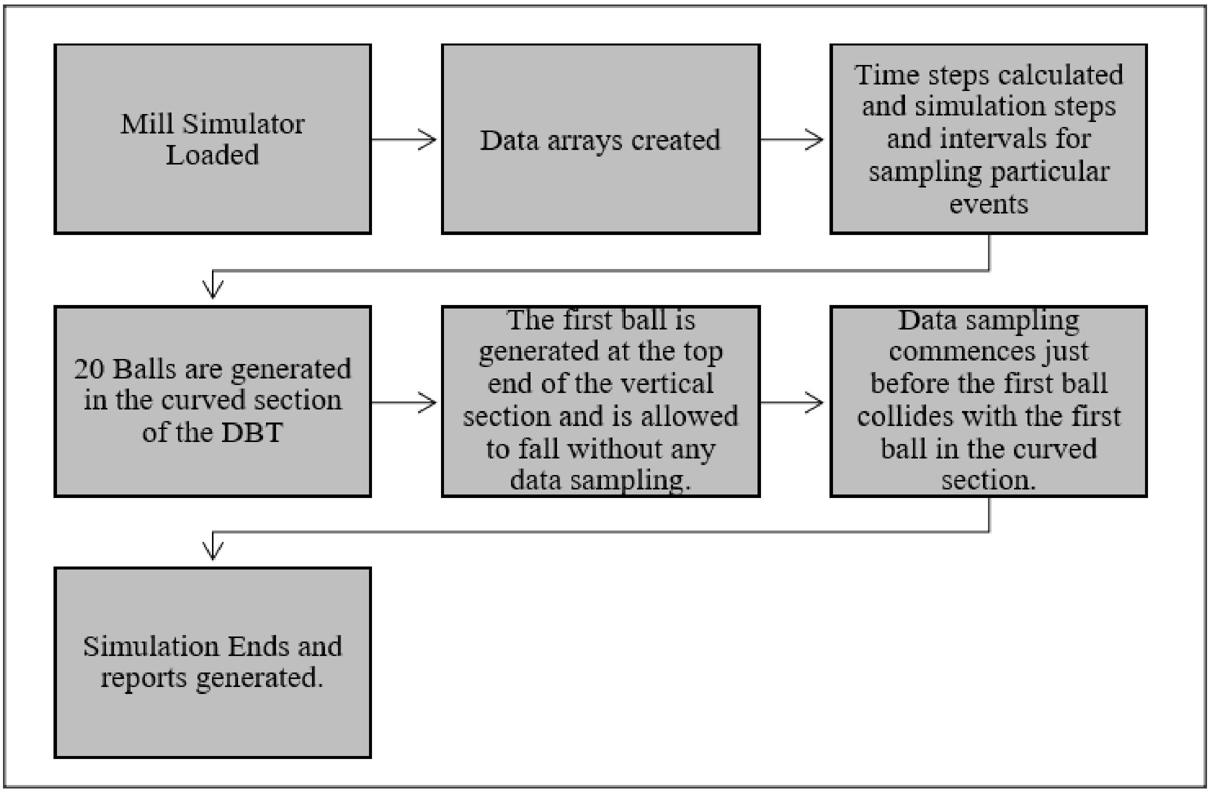

Figure 3. 14: *DBT computational scheme*

The DBT simulation follows a series of collision events that are very similar to each other. Balls are created and twenty (20) balls are allowed to settle within the curved section. One (1) ball sits on top of the vertical section. This ball is dropped and the energy involved during its collision with the ball sitting on top of those in the curved section is recorded. Equation (3.10) was used to calculate the required free flight time from the drop-off to the impact time:

$$S = ut + \frac{1}{2}at^2 \qquad (3.10)$$

Where *s* is the free flight height, *u* is the initial velocity, *a* is the acceleration and *t* is the free flight time.

The ball was dropped from rest hence, u = 0. The acceleration was due to gravity hence, Equation (3.10) can be rewritten as:

$$t = \sqrt{\frac{2s}{g}} \qquad (3.11)$$

The energy from the impact collision between the free-falling ball and the ball sitting in the first position within the curved section is transferred throughout all the balls sitting in the curved section until the last ball sitting in the curved section is projected out. There is energy transfer from ball to ball in the curved section because of the impact collision is recorded. The simulations ends when the last ball sitting in the curved section is projected out.

As opposed to the mill simulation which is characterized by random collisions of different energy levels, the collisions within the DBT are well controlled and predictable. Hence, much effort was directed towards capturing high resolution data on the energy transfer throughout the simulation.

3.3.2. THE SIMULATION COMPUTATIONAL SCHEME

The DBT simulator computational scheme is similar to the mill simulator computational scheme Figure (3.9). The distance overlap calculation, strain energy and dissipation energy are calculated using Equations (3.1), (3.4) and (3.5) respectively.

3.3.3. CONTACT MODELS AND SIMULATION PARAMETERS

The Spring-Dashpot Model was used to model collisions during the simulation. Similar to the mill simulator, the DBT adopted the same simulation parameters. To maintain consistent and reliable comparisons, the coefficient of restitution, coefficient of friction and material stiffness used for the mill simulator were adopted for the DBT simulator. These are described in Chapter 4.

3.3.4. SIMULATION REPORT

At the end of the simulation, a report was generated which shows the impact energy distributions, damping loss and frictional loss. Furthermore, elastic, potential and kinetic energies of all the balls were recorded throughout the simulation. A sample of the report is shown in Appendix B.

3.3.5. DROP BALL TEST SIMULATION SET-UP FOR THE PRESENT STUDY

The purpose of the Drop Ball Test (DBT) simulations was to quantify the energy that the balls are exposed to during their residence time in the DBT. An attempt was made to understand the ball stress mechanism. The simulation program used to perform this task was the DEM-PFC-3D described in the previous sections. The dimensions of the DBT that were used for the simulation work are given in Table (3.4):

Table 3. 4: *DBT geometrical dimensions for the simulations*

PROPERTY	VALUE	UNITS
Vertical Height	10	M
Curved section	975	Mm
Number of balls in curved section	20	
Ball diameter	125	Mm
Ball density	8000	Kgm^{-3}

The DEM simulation parameters for the DBT were adopted from work done by other researchers, (Mishra and Rajamani, 1992; Bwalya, 2005; Polycarpou, 2005). However, it was important that material parameters such as stiffness, coefficient of restitution and friction be the same as for the SAG mill simulations so that a basis for comparisons can be established. The DBT simulation parameters are listed in Table (3.5):

Table 3. 5: *DBT parameters applied for the simulations*

PROPERTY	VALUE	UNITS
Ball coefficient of restitution	0.6	
Wall coefficient of restitution	0.6	
Ball coefficient of friction	0.4	
Wall coefficient of friction	0.4	
Energy sampling time interval	0.02	sec
Energy scale	0.5	J
Time Step	1.43×10^{-4}	sec
Number of cycles	11500	

The number of cycles is the simulation cycles required up to the time just after collision as calculated from Equation (3.12):

$$n = \frac{t_f}{\delta t} \qquad (3.12)$$

Where n is the number of cycles, t_f is the free flight time calculated from Equation (3.10) and δt is the time step calculated from Equation (3.3 – 3.4).

If the number of cycles selected are not enough, the simulation will end before impact occurs hence, there will be no useful data recorded. The selected number of cycles ensured that the data recording exceeded the impact time since the most important data was from the point of impact onwards.

The time sampling interval refers to the regularity of data recording. The sampling rate used was 0.02 seconds. This means that data was recorded every 0.02 seconds and impact occurred after 1.42 seconds, which would be between the 71st and 72nd intervals.

The positions that the balls occupy within the DBT are described below:

Ball 1 (B1) is the ball dropped off from the top end of the vertical section.

Ball 2 (B2) is the ball sitting on top in the curved section.

Ball 3 – Ball 20 are the balls occupying positions below B2 in the curved section.

Ball 21 (B21) is the last ball sitting in the curved section. This is the ball that will be projected out after the impact between Ball 1 and Ball 2.

3.4. CONCLUSSION

The Discrete Element Method (DEM) is an effective and reliable tool that can be applied to study the collision behaviour of steel balls in both the Drop Ball Test (DBT) and SAG mill. The main purpose of this study was to understand the collision behaviour and develop a method to predict energy transfer and the stress induced in the grinding balls during their residence time within both the DBT and SAG mills. Hence, although it was important to clearly establish the material stiffness, coefficient of restitution and friction for the material under study it became apparent during the research that such a task will take considerable man-hours and will constrain the research budget hence the parameters used were adopted from work done by other researchers. However, such tasks are strongly recommended for future work.

Among the data that is fundamental in developing a method to predict the stress induced into the grinding balls are kinetic, potential and elastic energy during collisions, the forces that the balls are exposed to, mill power draw and the distribution of the impact energy.

CHAPTER 4

MATERIAL CHARACTERIZATION RESULTS AND DBT SIMULATION WORK

4.0. INTRODUCTION

This chapter describes the various sets of material properties and physical Drop Ball Test (DBT) results that were evaluated from the experimental set-up described in the previous chapter. The results from the Discrete Element Method Particle Flow Code 3D (DEM-PFC-3D) simulation work on the DBT are also discussed in this chapter.

4.1. MATERIAL CHARACTERIZATION

4.1.1. VISUAL EXAMINATION

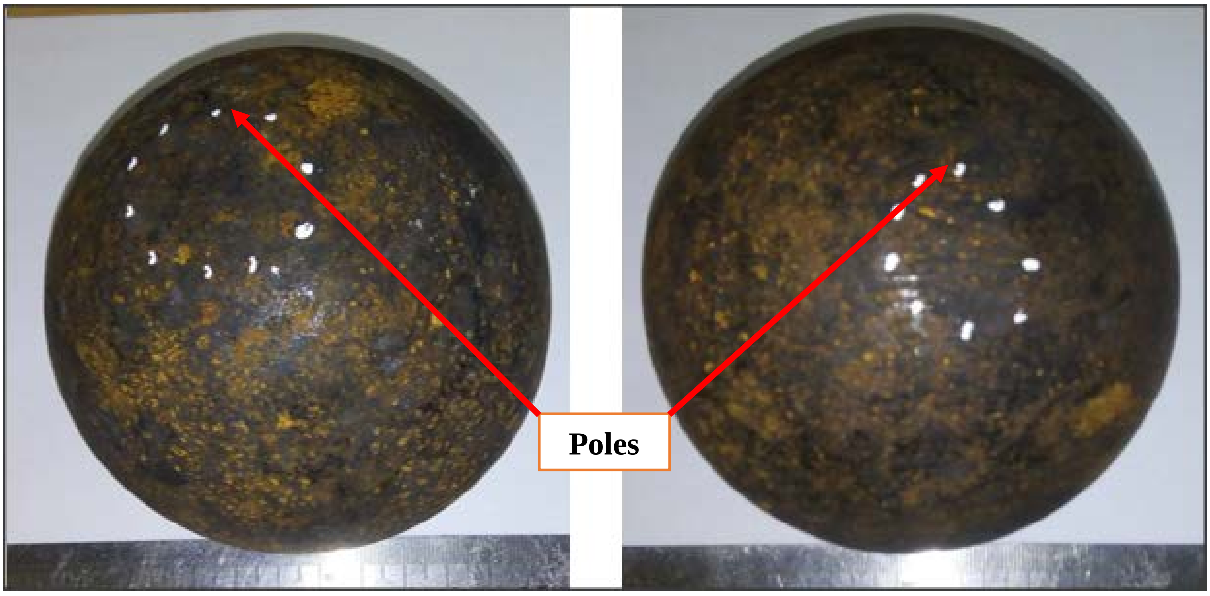

Figure 4. 1: *125mm forged steel balls showing the forging flat spots (poles)*

Figure (4.1) shows the visual examination of the grinding balls before any tests were conducted. The balls are 125mm in diameter and are characterized by two flat spots at opposite ends (poles). The balls were manufactured from a forging process in which round bars were upset forged into a ball. The flat poles are a result of the upset forging process. Hence, the polar diameter and the diameter measured perpendicular to the poles (equatorial) diameter differ by several millimetres. Table (4.1) shows the average polar and equatorial diameters of 20 balls that were sampled from 10 different production batches.

Table 4. 1: *125mm ball dimensions*

Pole-to-Pole Diameter	Equatorial Diameter	Diagonal Diameter	Diameter of Pole
118-122mm	122-131mm	122-126mm	35-37mm

The balls did not show any surface imperfections such as scratches and dents. These were the same balls used for the tests discussed in the succeeding sections.

4.1.2. CHEMICAL COMPOSITION

The chemical composition results summarized in this section are an average of results gathered across 10 production batches of 100mm, 115mm and 125mm forged steel balls. The material of construction and manufacturing process of the three ball sizes was the same. Table (4.2) shows the chemical composition of the balls. The elemental analysis shows that the alloy is high-carbon steel. The presence of chromium and nickel improves the tensile strength and impact toughness of the balls respectively. Manganese increases hardenability and tensile strength of the alloy, but to a lesser extent than carbon. It is also able to decrease the critical cooling rate during heat treatment, thus using this alloy hardenability can be achieved most efficiently. Silicon and molybdenum also improve hardenability of the balls.

The chemical composition in Table (4.2) ensures that the grinding balls manifest a reasonable trade-off between hardness (wear resistance) and impact toughness

Table 4. 2: *Ball elemental analysis*

Element	**C**	**Si**	**Mn**	**S**	**P**	**Cr**	**Ni**	**Mo**	**Cu**	**V**	**Sn**	**Al**	**Nb**	**Ti**
% Weight	0.76	0.30	1.0	0.02	0.015	0.93	0.25	0.03	0.25	0.005	0.03	0.005	0.025	0.020

**Difference is %wt of Iron (Fe)*

4.1.3. BALL HARDNESS

The hardness values discussed in this section were measured using the Rockwell Hardness Testing machine described in Chapter 3. A sample was extracted along the pole diameter of the ball. Figure (4.2) shows the extracted sample with dents resulting from the hardness testing.

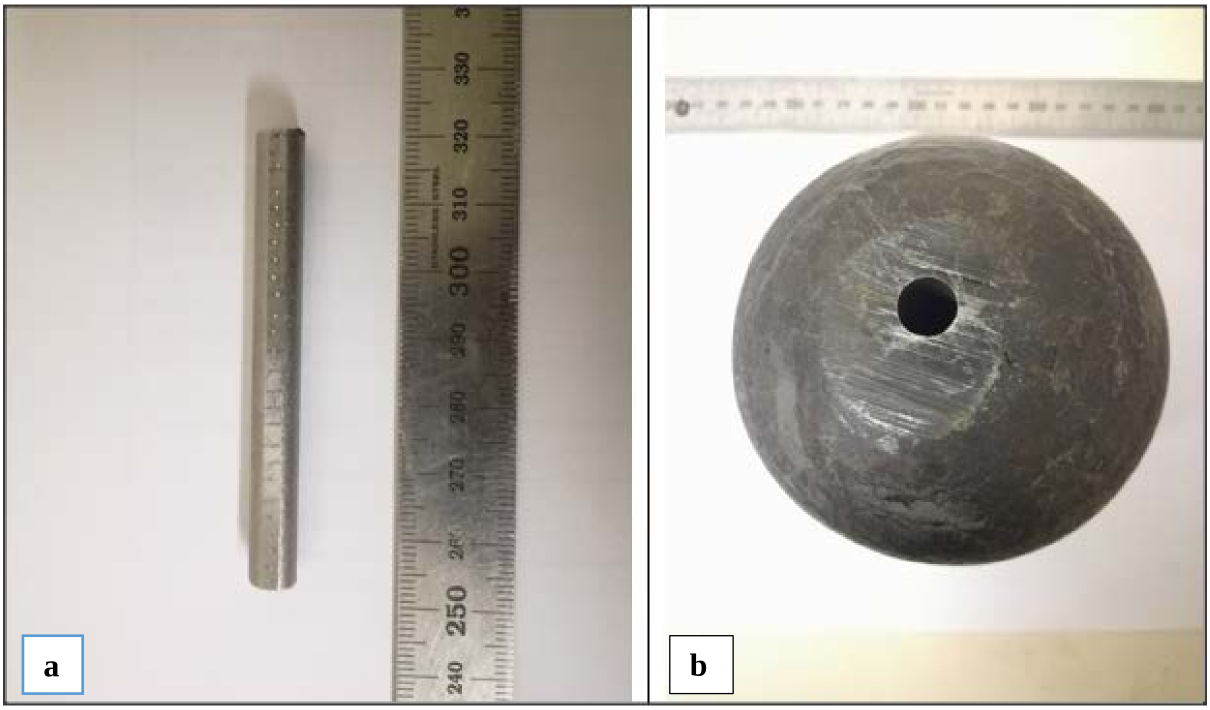

Figure 4. 2: *a. Hardness profile sample b. Position on the ball from which the sample was extracted.*

The wide ends of the sample represent the surface of the ball on both polar ends. The central part of the sample represents the core of the ball. Figure (4.3) shows the scatter plot of hardness profiles of 100mm, 115mm and 125mm balls from the surface to the core. The profiles show a trend that the hardness varies inversely with the depth towards the core. This observation is a direct result of the heat treatment process during grinding media production. The formation of a hard martensitic microstructure depends on the rate of heat extraction from the ball structure during quenching after heat treatment. Rate of heat extraction is lower in the core region of the ball than it is on the surface, hence from the ball surface towards the centre, the probability of hard martensite formation reduces and ball hardness follows the same trend.

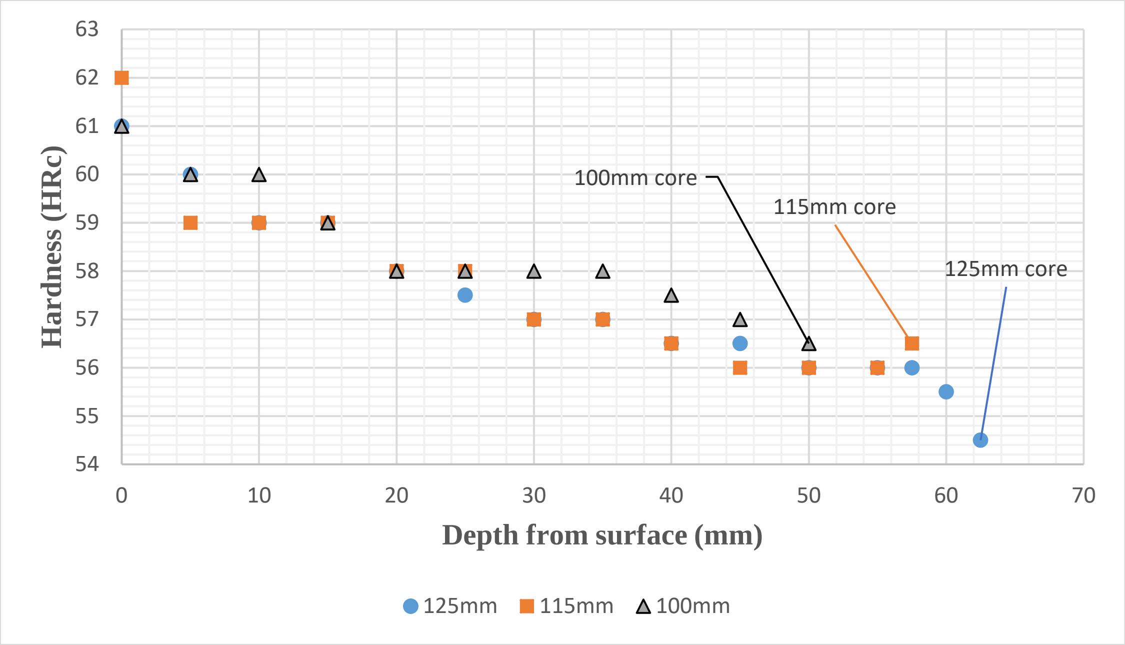

Figure 4. 3: *Hardness profile of various ball sizes*

4.1.4. METALLOGRAPHY ANALYSIS

The microstructural analysis was performed according to the procedure described in the previous chapter. Figure (4.4) shows the micrographs that were observed on surface, mid radius and core of the ball under *100X* magnification.

The surface and mid-radius of the balls show a fully tempered microstructure. A mixture of tempered martensite and bainite were observed on the core of the ball. The formation of martensite is dependent on the rate of heat extraction during quenching after heat treatment. In the quenching medium, the rate of heat extraction is higher at the surface than it is at the core of the ball. Hence, the surface and mid-radius sections of the ball have higher probability of forming martensite than the core. At the core, a minimum amount of martensite was observed but bainite was also observed. Bainite is transformation microstructure that results from slow cooling during quenching after heat treatment.

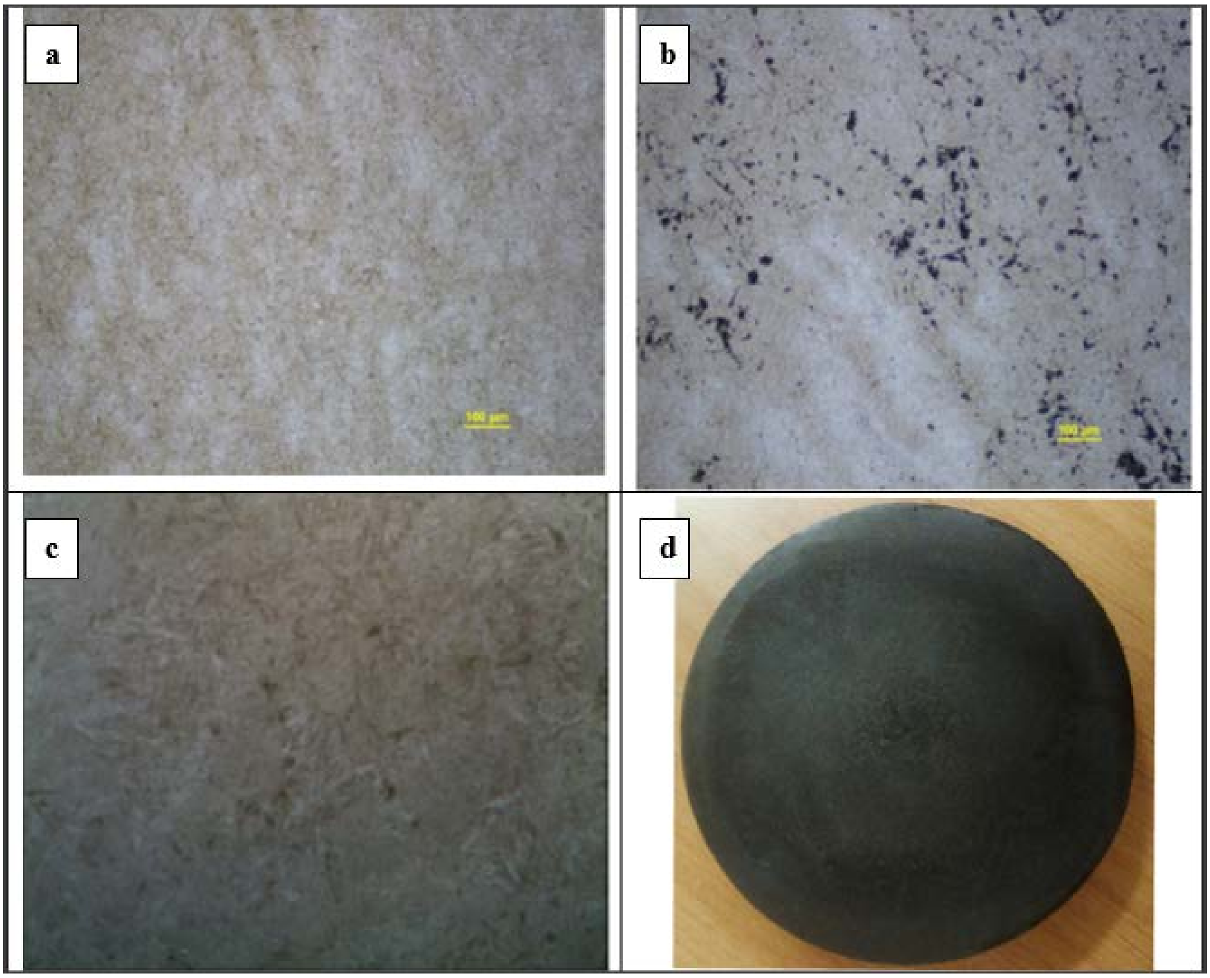

Figure 4. 4: *Micrographs of the various balls sections. A. Surface b. Core c. Mid-radius. D. shows the sectioned ball after grinding*

4.1.5. DROP BALL TESTS

The Drop Ball Test (DBT) results from the equipment set-up discussed in Chapter 3 are discussed in this section, and these were gathered over a period of twelve (12) months. The three main sizes under study were 100mm, 115mm and 125mm forged steel balls with the mechanical properties described in the previous sections.

The ball failures were described as either total fracture or spalling. Total fracture is a mode of failure in which the ball breaks into two semi-spheres across either its polar or equatorial diameter. Spalling is described as chipping-off of the ball’s outer surface exposing the inner part of the ball. After spalling, the ball sometimes retains its shape but with a loss in mass. Table (4.3) shows a summary of the statistical ball failure results gathered.

Table 4. 3: *Raw DBT fracture data of various ball sizes*

Number of Drops	1000	2000	3000	4000	5000	6000	7000	8000	9000	10000	11000
Failures (125mm)	0	2	9	17	29	8	7	3	6	3	1
Failures (115mm)	0	1	7	2	1	3	4	17	9	7	3
Failures (100mm)	1	1	6	1	3	5	9	11	21	9	2

Table (4.3) shows the number of ball failures that occurred between each thousand ball drops. The raw data recorded was not cumulative. For example, of all the tests recorded, 17 balls that were 125mm in diameter failed during the 3000 to 4000 drops interval. Likewise, two balls that were 115mm and 1 ball 100mm in diameter failed during the same interval.

Figure (4.5) shows the graphical representation of the data shown in Table (4.3).

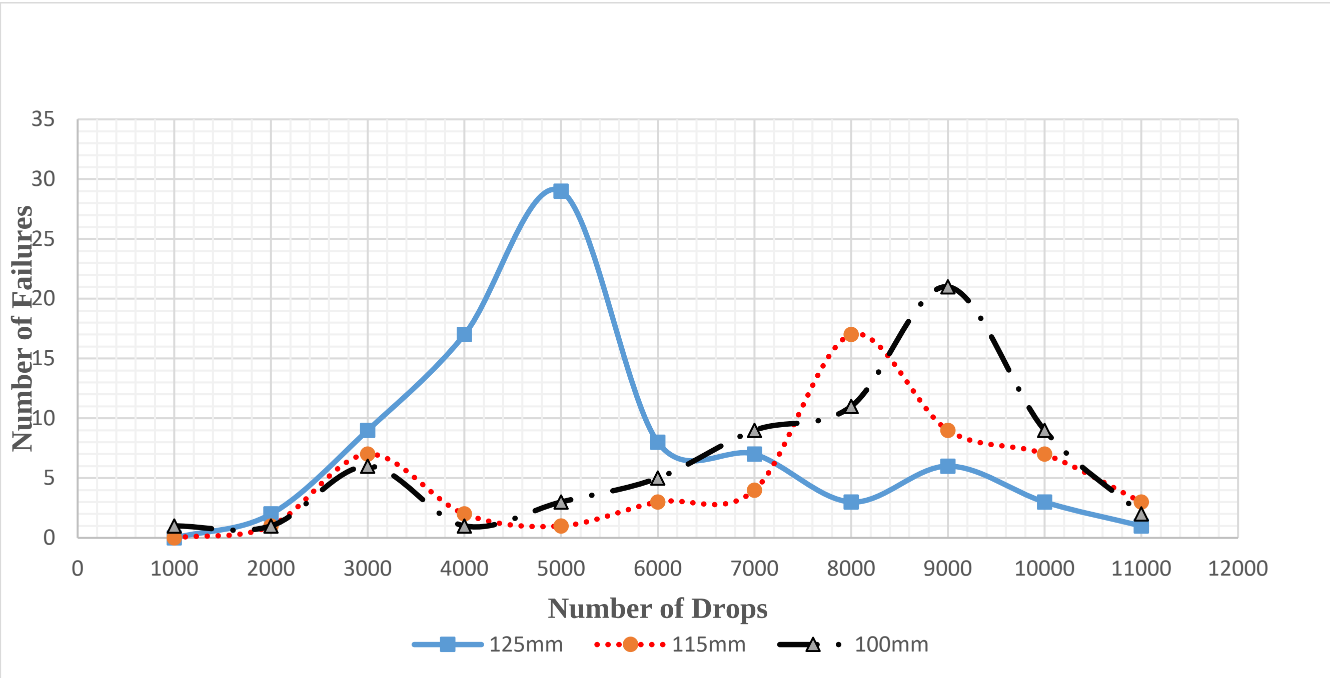

Figure 4. 5: *DBT failure trends, different ball sizes*

Figure (4.5) shows a trend that the larger the ball size, the more failures are observed earlier during the tests. 125mm failure trend line peaks at 5000 drops while 115mm and 100mm trends peak at 8000 and 9000 drops respectively.

The balls were manufactured from the same material hence the difference in the failure behaviour can be explained from the factors discussed below:

a. During collision, the large balls are exposed to higher energy than smaller balls. This is a direct consequence of Equation (4.1):

$$E = mgh \qquad (4.1)$$

Furthermore, the impact force is high for large balls than small balls. This is explained by Hertzian contact stress theory, Equation (4.2):

$$d = \sqrt[3]{\frac{9F^2}{16RE^2}} \qquad (4.2)$$

where *d* is the depth of indentation, *F* is the impact force, *R* is the radius of the ball and *E* is the modulus of elasticity, (Zhu, 2012).

The depth of indentation (damage to the ball) is proportional to the force exerted and the magnitude of the force depends on the size of the ball.

b. Hinde *et al.*, 2001 discussed that the stress distribution in a particle is a function of the energy that the particle is exposed to. This concept can be applied to the steel balls under discussion. That is, the maximum stress induced into the ball from the contact point and along the line of contact is given by Equation (4.3) derived from Hertzian contact stress theory:

$$p_{max} = \frac{2F}{\pi a} \qquad (4.3)$$

The force, *F*, applied gives rise to a pressure (stress) distribution in the ball (p_{max}) along a line at the centre of the area of contact, *a*. Hence, the stress distribution is more pronounced in large balls than in small balls, (Etter, 2012).

c. Presence of imperfections in the manufactured balls also aid to the ball fracture. The balls were manufactured from the same material and process, the large balls have more imperfections per unit volume than small balls. The imperfections vary differently including quench cracks, foreign inclusions and scratches that act as points of high stress concentration.

To improve the understanding of the frequency distribution of the failures and effect of the cumulative stress on the balls during the DBT, cumulative frequency curves were plotted, Figure (4.6).

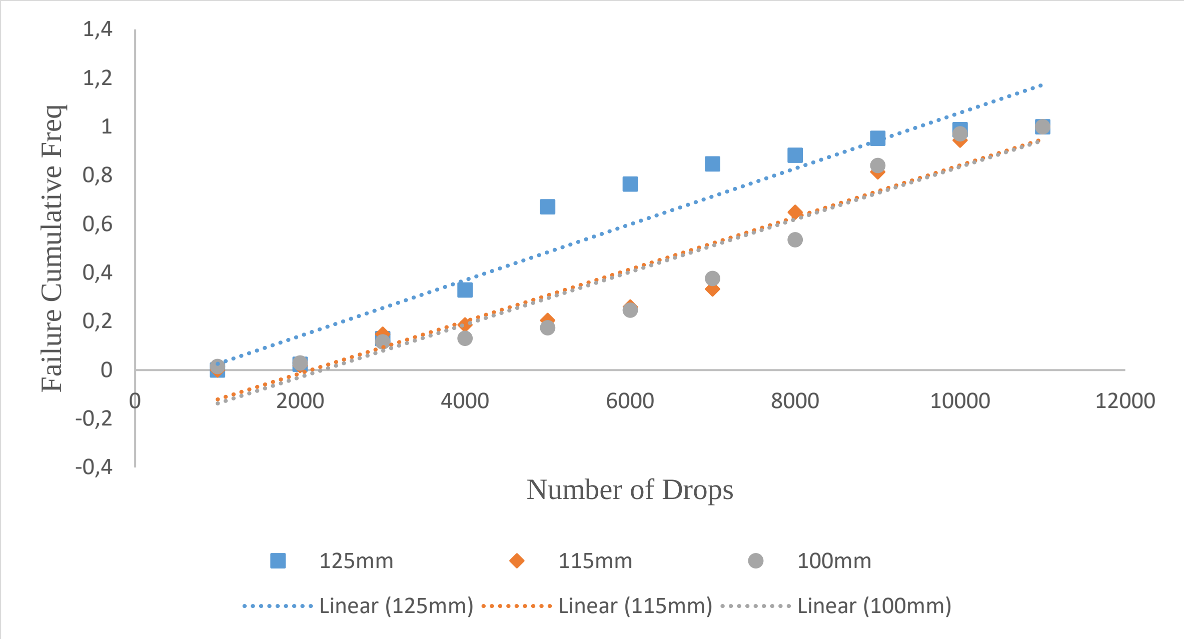

Figure 4. 6: *Ball failure cumulative frequency*

Figure (4.6) shows that the 125mm curve rises earlier than the 115mm and 100mm curves. This means that although initial ball breakages within the first 4000 drops might have been caused by contact surface area and higher energy that the balls are exposed to, the effect of cumulative energy/stress is more pronounced on the larger 125mm balls than it is on the 115mm and 100mm balls. Thus, 125mm balls are more likely to fail than 115mm and 100mm as the DBT exceeds 4000 drops.

An attempt was made to develop a model that describe the failure behaviour of the balls within the DBT. The Rosin-Rammler equation was used as a foundation from which the model was developed. The Rosin-Rammler distribution is a common statistical method used in various applications such as mineral processing, particle sorting and rock mechanics to develop models that best describe cumulative frequency behaviour of a set of raw data, Equation (4.4).

$$Y = 1 - \exp\left(\frac{-x}{x_0}\right)^n \qquad (4.4)$$

where Y is the ball failure cumulative fraction, x is the number of drops, x_0 is the model characteristic failure and n is a uniformity constant.

However, a more definitive model was developed from work done by (Bwalya, 2018) on predicting ore particle breakage probability in the Drop-Weight Test.

$$P_b = 1 - exp\left[-an^b\left(\frac{E - E_{xo}}{E_{xo}}\right)\right] \qquad (4.5)$$

where, P_b is the probability of ball fracture, *E* is the impact energy as given in Equation (4.1), *n* is the number of drops and a and b are model fit constants. E_{xo} is the minimal energy required to cause ball fracture given by:

$$E_{xo} = cx^d \qquad (4.6)$$

Solver on Microsoft Excel was used to find the most suitable *a, b, c, d* and E_{xo} values. The *a, b, c and d* values obtained for 125mm balls were 3.18 x 10^{-8}, 2.5, 4.92 and 2.44 respectively. The E_{xo} value for 125mm balls was as high as the energy involved in a single drop collision of each ball size, Table (4.4):

Table 4. 4: $\boldsymbol{E_{xo}}$ *calculated and collision energy recorded during simulation*

	Ball Size		
	125mm	115mm	100mm
E_{xo} - (J)	778.61	606.90	399.71
Collision Energy (*mgh*) - (J)	782.51	609.33	400.65
% E_{xo} of Collision Energy - (J)	99.5	99.6	99.7

Although the E_{xo} values are very high, this is justified by the number of impact attempts required to break the ball which are in thousands. This makes the minimum energy required to cause damage as high as the energy involved in a single drop. This observation can further be explained by the fracture theory discussed in Chapter 2 that spherical components tend to equally distribute stress than sharp shaped components; hence, the spherical balls require thousands of drops to fracture.

Figure (4.7) – (4.9) show the failure cumulative frequency plotted with the probability of fracture model against number of drops.

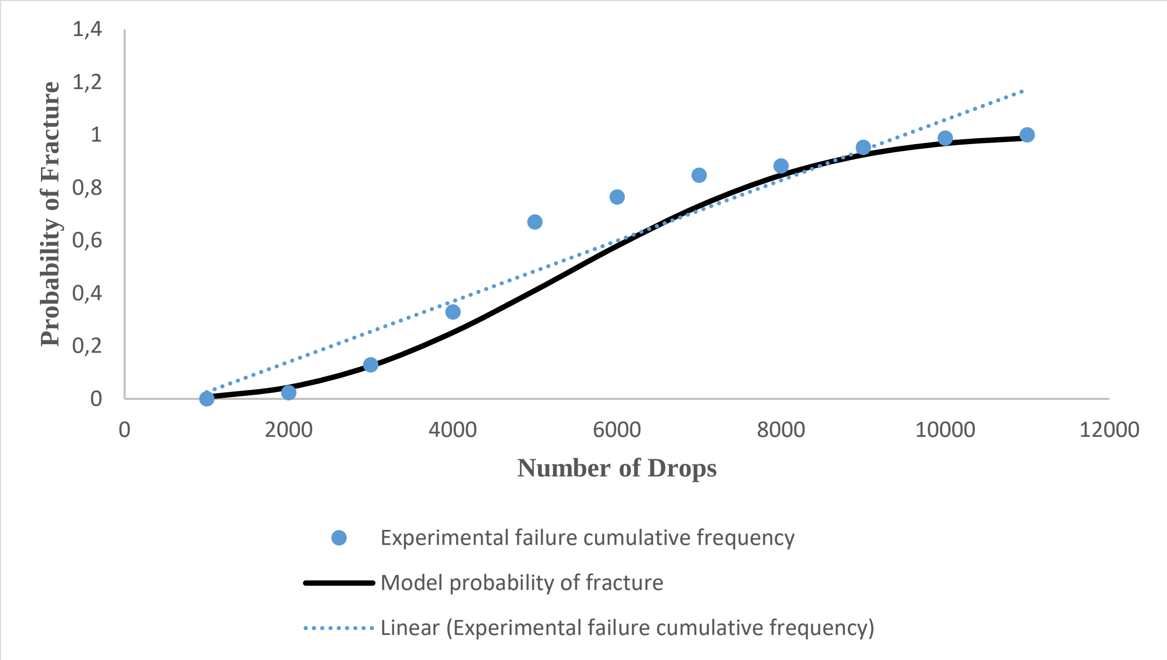

Figure 4. 7: *Failure cumulative frequency and failure model for 125mm balls*

Failure prediction for 125mm balls is accurate in the first 3000 – 4000 drops and beyond 8000 drops. Ball fractures below 4000 drops indicate poor ball quality that could be a manifestation of existence of imperfections or pre-existing defaults within the ball. Beyond 8000 drops, ball failure is mostly attributed to the energy that the ball is exposed to and the quantity of stress that the ball has absorbed. The middle number of drops fractures (4000 – 8000) are not as accurately predicated because fracture in this region can be due to both ball quality or a combination of ball quality and the energy that the balls are exposed to.

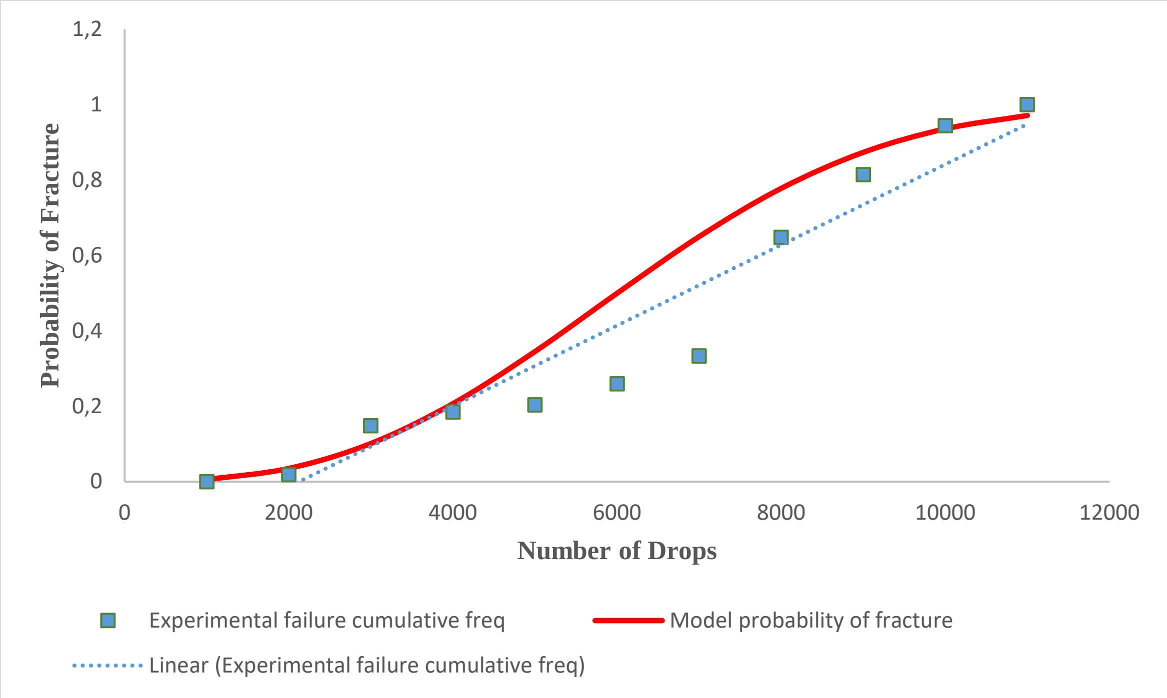

Figure 4. 8: *Failure cumulative frequency and failure model for 115mm balls*

The midsection (4000 – 9000 drops) fractures are not easily predictable. Within this region, both ball quality and energy exposure contribute to fracture.

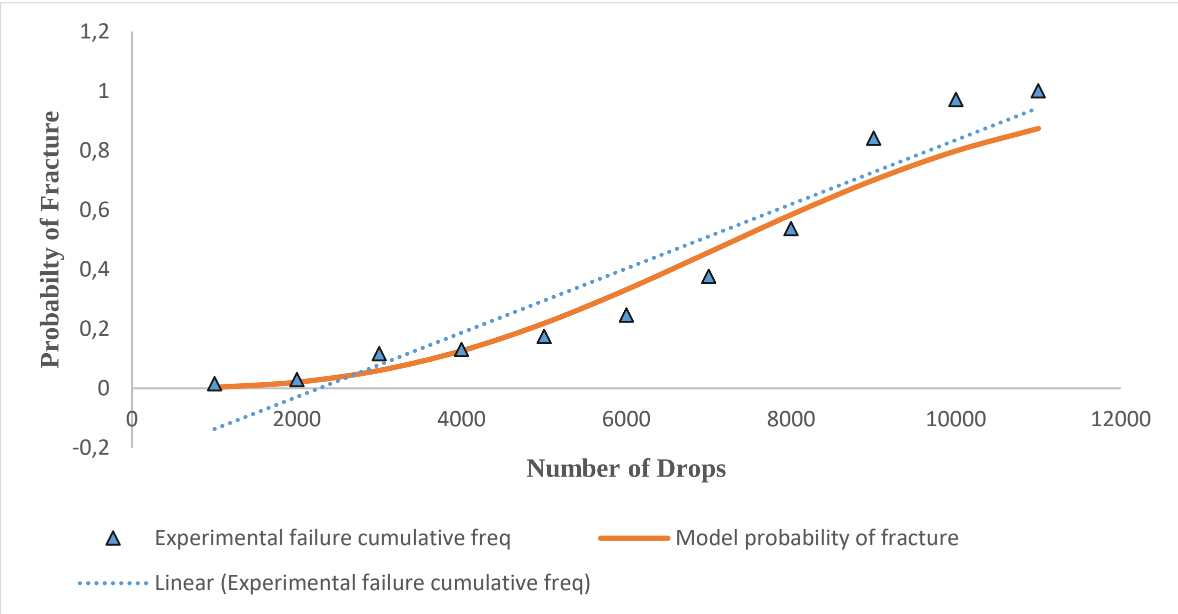

Figure 4. 9: *Failure cumulative frequency and failure model for 100mm balls*

100mm balls fracture behaviour is the most predictable in the early and midsection regions. Early ball fracture is strongly influenced by ball quality. 100mm balls have least probability of fracture in the midsection drops. This indicates that although the ball quality might aggravate fracture, 100mm ball size results in less energy exposure than 115mm and 125mm.

4.1.6. SUMMARY OF MATERIAL CHARACTERIZATION

Although the material of construction, physical and chemical properties of the balls are similar to each other, the ball's response to fracture due to impact loading differs. This suggest that the probability of ball fracture strongly depends on the energy that the balls are exposed during collisions in the DBT. This collision energy depends on the size of the ball; the larger the ball, the higher its weight and the higher the energy involved during collisions. In the succeeding sections, results of the simulation work conducted to quantify the impact energy, stress induced into the balls during collisions and an attempt to predict ball fracture in the DBT will be discussed.

4.2. DROP BALL TEST (DBT) SIMULATION WORK

A single DBT simulation was done for each of the three ball sizes under study; 125mm, 115mm and 100mm. The main sets of results for each simulation were potential, kinetic and elastic energy, energy loss and impact energy spectra. Appendix A lists all the DBT simulation input and output files.

4.2.1. POTENTIAL ENERGY (PE)

Potential energy is described as the energy that a particle possesses relative to its position. For the purpose of this work, the reference (zero) point is the position occupied by the first ball within the curved section, Figure (4.10).

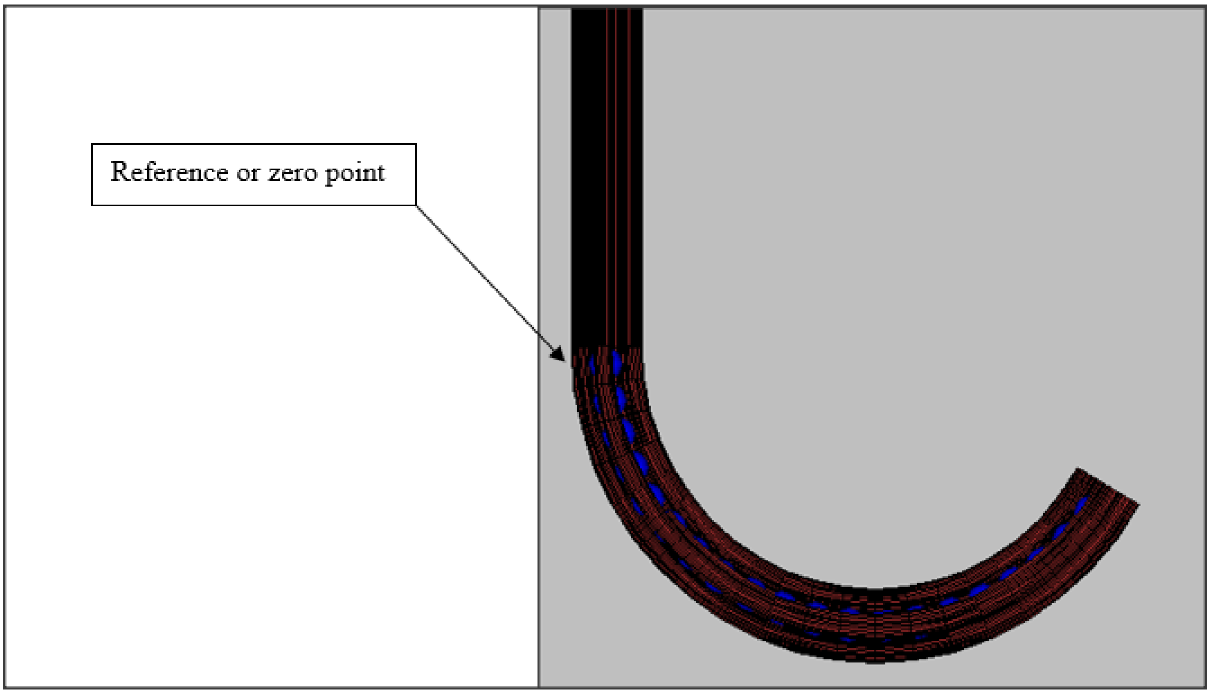

Figure 4. 10: *Potential Energy reference or zero point*

Equation (4.1) represents the mathematical calculation for potential energy. Figure (4.11) shows the potential energy behaviour of the various ball sizes as they are dropped-off from the top end of the vertical section during their respective DBT simulations. Each ball initially possessed its maximum potential energy prior to drop-off. As the ball falls, the potential energy gradually drops until the point of impact. After impact, the potential energy starts to rise again indicating rebound after impact.

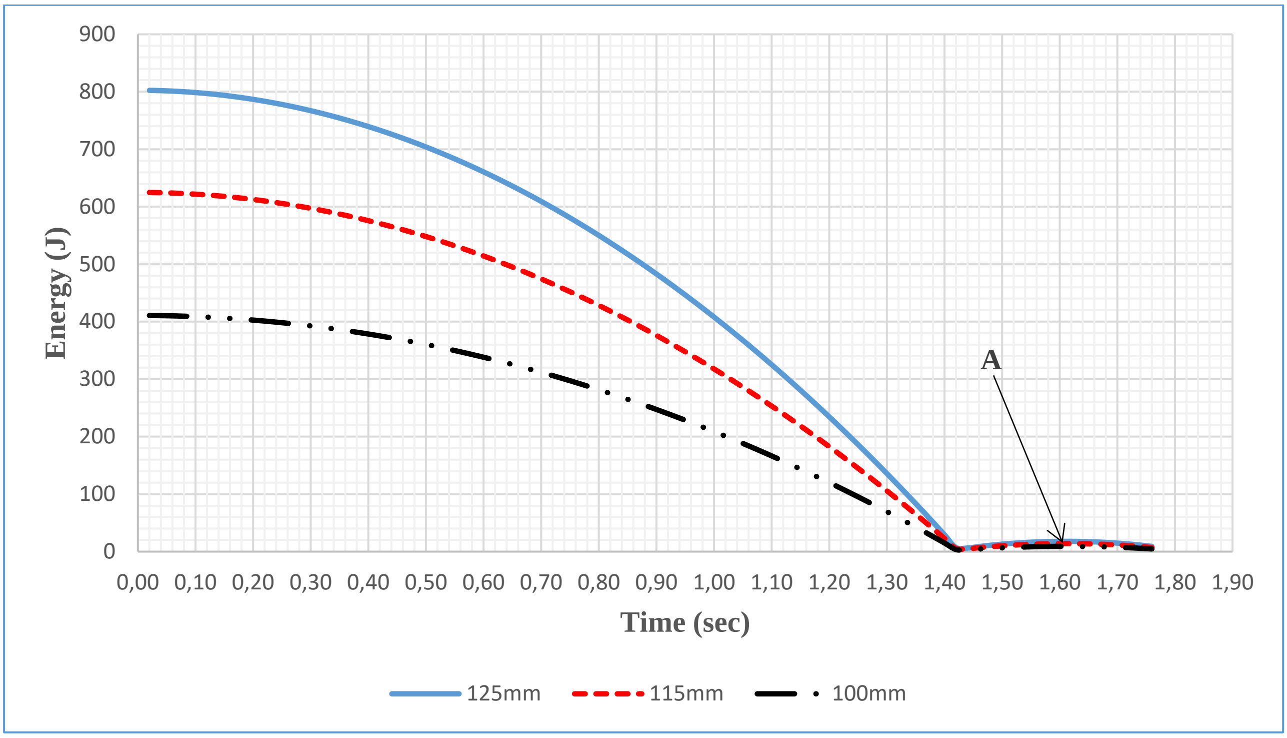

Figure 4. 11: *Potential Energy behaviour of the various ball sizes*

Of interest is the data point labelled A that represents the maximum potential energy that the ball coming from free flight reached after impact. These values were used to calculate the maximum rebound heights of each ball, Table (4.5):

Table 4. 5: *Various Ball Size rebound heights*

Ball Size (mm)	Rebound Height (m)
125	0.28
115	0.22
100	0.14

Table (4.5) shows that the rebound height is directly proportional ball size/weight. The observed trend is a result of the initial energy involved in the collision. The larger the ball size, the higher the energy on impact which gives rise to the higher rebound height.

4.2.2. KINETIC ENERGY

Kinetic energy (KE) is the energy that a particle possesses due to its motion. It is defined as the work needed to accelerate a particle of given mass from rest to a specific velocity. Mathematically, kinetic energy is calculated using Equation (4.1). For a body dropping from a specific height (free fall), its velocity increases linearly until the point of impact. Ideally, the KE that a particle possesses just before impact after being dropped from a certain height is equivalent to its potential energy before being dropped off. Velocity of the free falling ball is given by;

$$v = \sqrt{2gh} \qquad (4.7)$$

Of interest from the simulation data are the kinetic energies of the balls at the moment just after impact, Figure (4.12).

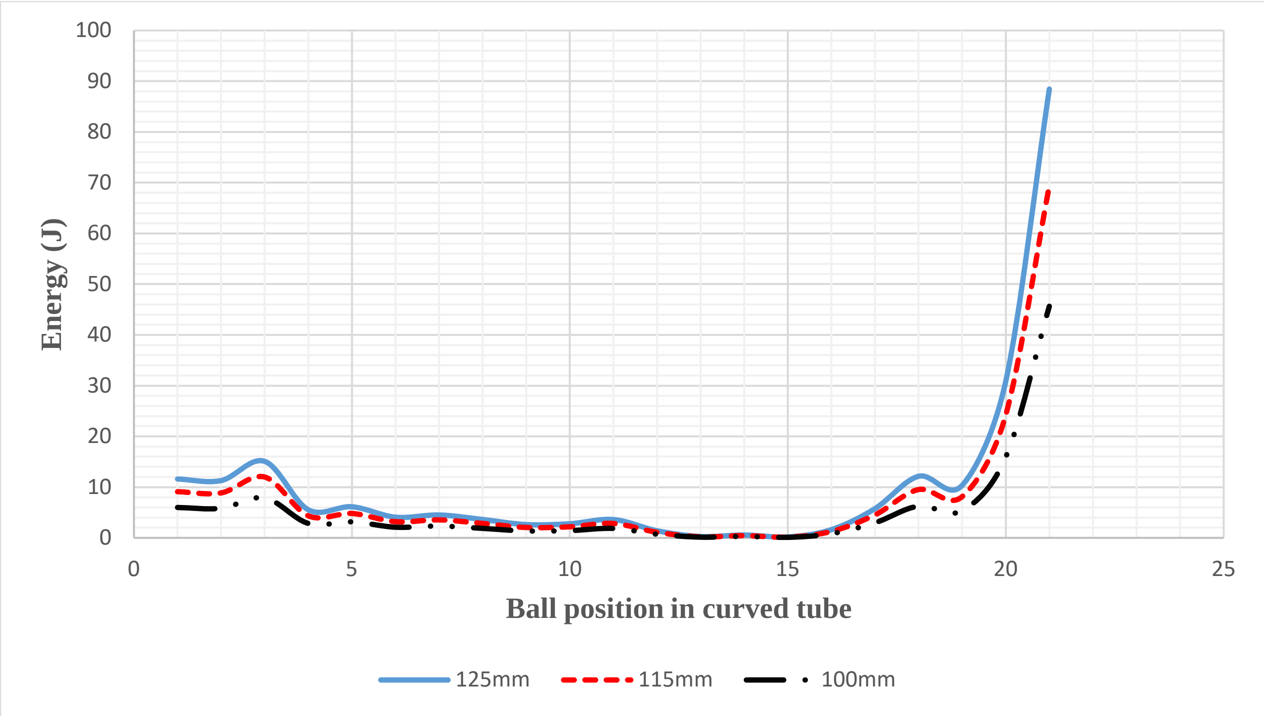

Figure 4. 12: *KE distribution after impact for the various ball sizes*

Figure (4.12) indicates that much of the movement of the balls within the curved section were at both the impact and exit ends of the curved section. The change in velocity of all the ball sizes as they respectively drop from the top end of the vertical section are the same. At the impact end, B1 rebounds after impact. This supports the rebound discussion in section 4.2. For each simulation, B21 possesses the highest kinetic energy as it is projected out. The exit kinetic energy of 125mm balls is highest. This emanates from high energy initially involved in the collision at the impact end.

The balls sitting in positions 13 – 15 barely move. This is partly because positions 13 – 15 are the central positions and represent the centre of mass of the curved section. The cumulative weight of the balls from either sides of B13 – B15 is centralised at these positions

4.2.3. ELASTIC ENERGY

For the purpose of this study, elastic energy is defined as the potential-mechanical energy that a ball is exposed to. This energy can be stored within the ball, or consumed when the ball shape is deformed or some of it is given off (energy transferred) from one ball to the other from the moment of impact until the last ball is projected out.

Among the data extracted from the DBT simulation is the impact energy of the colliding balls. Of importance is the energy recorded when the ball falling from free flight collides with the ball sitting on top of the curved section for each ball size simulation. This energy is converted to various forms although most of it is transferred to the next ball and some of it is lost through minor losses such as heat, sound and friction. Table (4.6) shows the energy transferred between Ball 1 (B1) and Ball 2 (B2) during the collisions in the various ball size simulations.

Table 4. 6: *Energy transfer after collision for the various ball sizes*

Ball Size	125mm	115mm	100mm
Collision Energy (J)	795,37	623,96	410,42
Energy Transferred (J)	413,5	367	256,5
% Energy Transfer	52	59	62

Table (4.6) shows that more than half of the energy involved in each simulation is transferred to the next ball. However, 125mm balls have the highest energy transferred to the next ball while 100mm transfer the least energy. The observed trend is partly due to the following:

a. 125mm balls have the highest mass of the three ball sizes hence, they have the highest energy involved during collision. Much of this energy is stored in the ball and builds up as stress leading to ball fracture. This observation is also supplemented by the ball failure trend during the DBT discussed in section 4.1.5 where the 125mm have the highest failures more than any other ball size after any given number of drops.

b. The smaller ball size, 100mm balls, are exposed to the least energy upon impact compared to the other two sizes. Furthermore, they have the highest surface area of contact hence, much of the energy is transferred to the next ball during collision.

The overall effect of the observed energy transfer trend is that the large balls transfer the least energy to the next ball than smaller ball sizes. This means that much of the energy is absorbed by the ball which builds up stress in the ball as stored energy. The stored energy will continue to accumulate until a certain point where it is released i.e. point of fracture.

Table (4.7) shows the kinetic energies at which the last ball sitting in the curved section of each ball size simulation was projected at.

Table 4. 7: *Kinetic energy at ejection for the various ball sizes*

Ball Size	125mm	115mm	100mm
Collision Energy (J)	795,37	623,96	410,42
KE at Ejection (J)	81,45	91,27	96,68
% of Collision Energy	10	14	24

The smallest ball size, 100mm, was ejected with the highest KE. This indicates that most of the energy involved in the initial collision was transferred throughout the balls sitting in the curved section. 125mm represents the lowest KE. This is partially because the balls are heavier hence, their movement is not as free as 115mm and 100mm balls that are much lighter. Furthermore, 125mm absorb more energy (stored energy) than 115mm and 100mm balls.

As the energy is transferred from the impact to the exit end, each ball is initially subjected to a certain amount of energy that is converted to various forms. The various energy conversion forms include stored energy (stress absorbed by the ball), frictional loss and energy dissipated as heat and sound. The stored energy leads to fracture whilst some of it is used up when the ball shape is deformed during the collisions. Figure (4.13) shows the elastic energy distribution of the balls sitting in the curved section for the various ball size simulations. However, part of the energy is absorbed by the ball towards plastic deformation (stored energy) whilst a significant fraction of the energy (elastic energy) is passed on to the next ball.

Figure (4.13) shows the elastic energy distribution relative to the position of the ball within the curved section of the various ball size simulations.

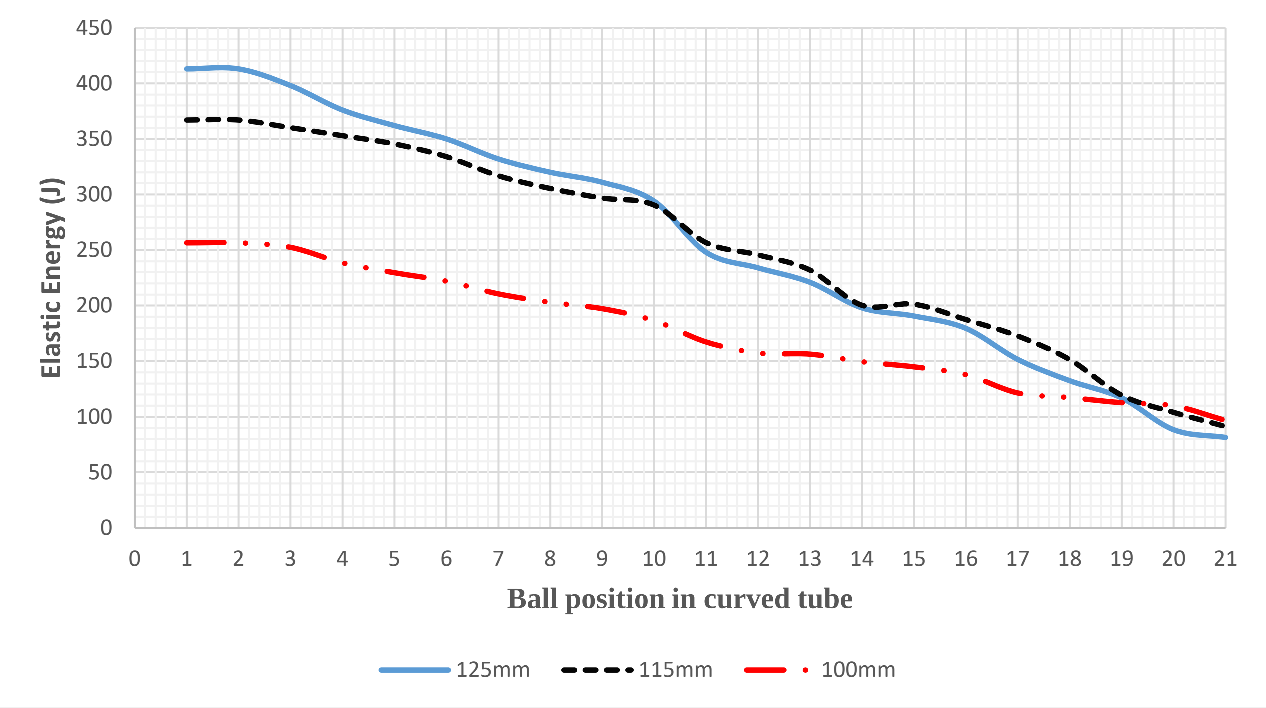

Figure 4. 13: *Elastic energy distribution after collision for the various ball sizes*

Figure (4.13) shows the successive amount of energy that was transferred from one ball to the other from the collision to the ejection end. The 125mm trend shows a steep loss in energy from the collision to the ejection end. This means that most of the stress (stored energy) induced into the 125mm balls during the DBT occurs in the first two to three positions. The 100mm ball curve is much flatter indicating that a higher percentage of energy was transferred between consecutive balls than during 125mm balls energy transfer. Overall, 125mm are more likely to be stressed than 115mm and 100mm balls.

4.2.4. DISSIPATED ENERGY AND FRICTIONAL ENERGY LOSS

Dissipated energy is defined as the total energy loss due to friction, heat, sound and other minor losses. The frictional loss is due to the rubbing action between balls in contact with each other and balls in contact with the DBT machine walls.

Figure (4.14) shows the energy dissipated behaviour for the various ball size simulations. Initially the dissipated energy is high at the first position in the curved section. This is the collision end where most of the impact energy is transferred into the curved section. Because of the high energy involved in the collision, a significant fraction is also lost i.e. dissipated energy. Between position 9 and 18 in the curved section, more energy is dissipated than any other positions. These are the positions where the least ball movement happens after collision. The centre of mass of the balls in the curved section lies within this region. Additionally, in these positions the balls are also perfectly in contact with each other and rubbing against walls of the DBT machine hence the higher dissipated energy.

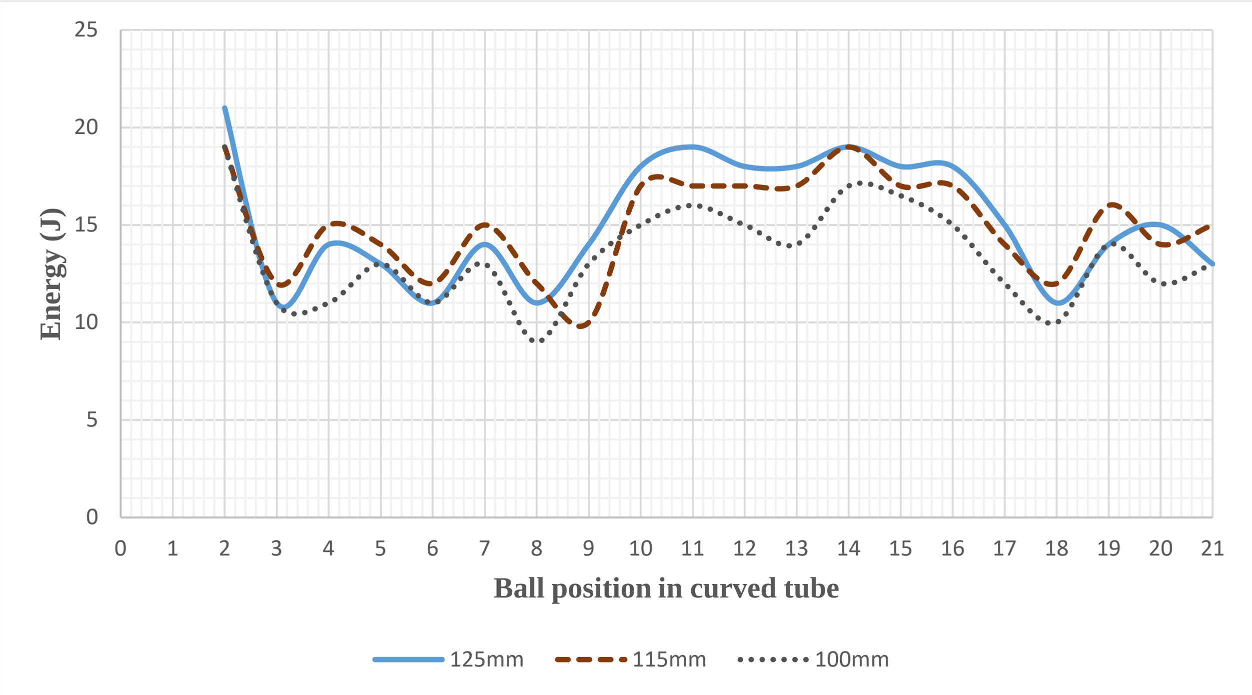

Figure 4. 14: *Dissipated energy during collision for each ball size*

The dissipated energy is largely dominated by frictional loss. Frictional loss is the energy loss due to the rubbing action of the balls against each other and the walls of the DBT machine. Figure (4.15) shows the frictional energy loss trend for each of the three ball size simulations. Figure (4.15) somewhat follows the trends of dissipated energy shown in Figure (4.14). However, the frictional loss is lowest at both the collision and exit ends of the DBT machine. At the collision end, the energy loss is largely due to sound and heat because of the impact between Ball 1 and Ball 2. At the discharge end, Ball 21 is expelled and flies out resembling projectile motion hence the frictional loss is minimal. Frictional loss is maximum at the mid sections where the balls are in contact with each other. The contacts in-between consecutive balls and balls with walls are almost perfect. Frictional loss is a function of contact area hence it reaches its maximum in the mid sections.

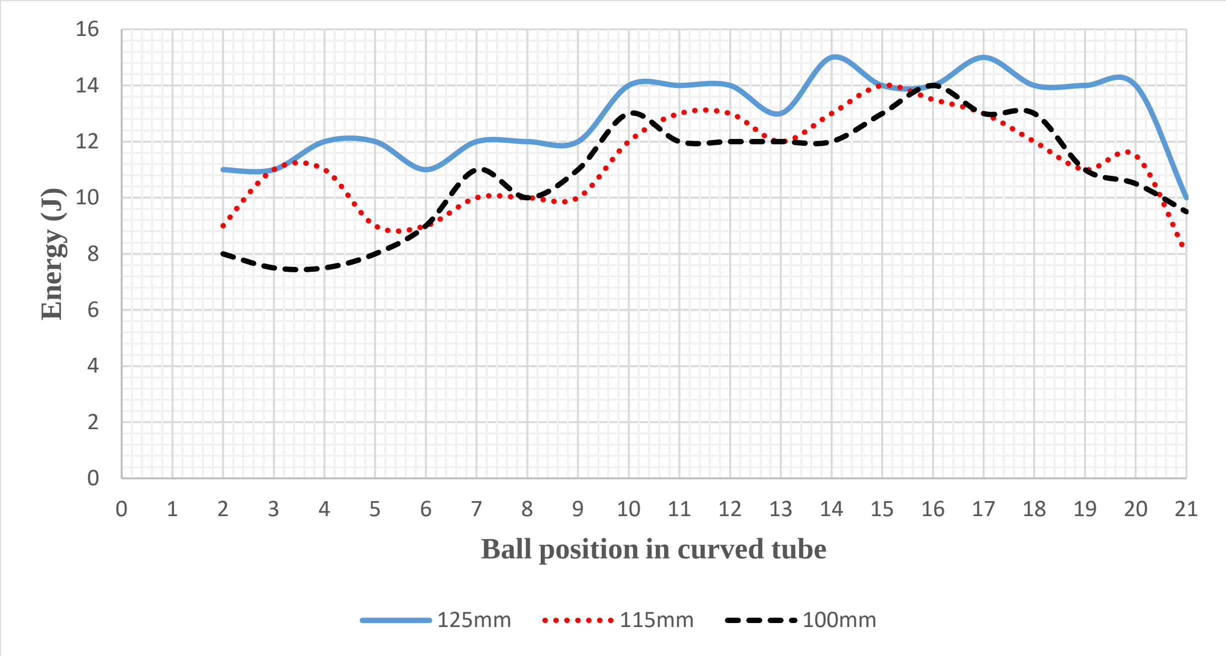

Figure 4. 15: *Frictional energy loss for each of the ball sizes*

4.2.5 ENERGY BALANCE

The purpose of studying the elastic energy balance was to; firstly, account for the usage of the energy that was initially delivered into the system and the various forms it was converted to. Secondly, to quantify the actual energy and stress that the balls are likely to be exposed to. Lastly, it was very important to compare the simulated values with the values obtained from physical calculations.

Ideally, in all simulations, all the initial potential energy that Ball 1 possessed at the top end of the vertical section should be delivered into the curved section and transferred throughout all the balls until the last ball is projected out. However, this is hardly the case because most of the energy is converted to various forms. These energy conversions are dominated by stress induced into the balls (stored energy), frictional, heat and sound energy loss.

Table 4. 8: *Energy balance of the various ball size collisions*

Ball Size	125mm	115mm	100mm
Initial Collision Energy (J)	795,37	623,96	410,42
Elastic Energy (J)	413	367	256,5
Total Dissipated (J)	204	167	116.5
Elastic + Dissipated (J)	617	534	373
Unaccounted Energy	178.37	89.96	37.42

An attempt was made to balance the energy relative to the available and measurable forms of energy collisions. Table (4.8) shows the various forms of accounted energy conversions which are described below:

a. **Initial Collision Energy –** refers to the energy that was delivered into the curved section as a result of the collision between Ball 1 coming from free flight and Ball 2 is the first ball at the beginning of the curved section.
b. **Elastic Energy –** is the energy that was transferred into Ball 2 as a result of the collisions and the energy that was transferred into the rest of the balls sitting in the curved section. This energy exponentially decays as some of it is absorbed into the balls (as stored energy) while some of it is transferred through the balls sitting in the curved section until the last ball is projected out.
c. **Total Dissipated –** is the total of the energy lost due to friction, sound heat and other unmeasurable losses.
d. **Elastic + Dissipated –** the sum of the elastic and dissipated energy.
e. **Unaccounted for Energy –** this is the difference between the initial energy in the system before dropped ball collides with first ball in the curved section and the (elastic + dissipated).

A certain fraction of the unaccounted energy, if not all, is assumed to be absorbed by the ball as stress induced into the ball (part of elastic energy). Elastic energy can also cause ball breakage if the material's elastic limit is exceeded. Fatigue is also a major contributor to ball failure, that is, repeated cyclic loading that exceeds the elastic limit. The unaccounted energy is relatively high and future auditing of the program is recommended to improve accuracy of the data.

4.2.6. EFFECT OF SIMULATION PARAMETERS

In real Drop Ball Test systems, there are imperfections that can result in deviations from process parameters. For example, balls are not perfectly spherical and such a variation affects secondary material characteristics such as stiffness and coefficient of restitution. Furthermore, in industry, the alignment of joining sections in the Drop Ball Test Machine (DBT) is not as perfect as will be in a DEM simulation. Usually before and after machine maintenance, the vertical section will not be perfectly aligned with the curved section, thus overlap by a few millimetres.

The overall effect of the above scenarios is that there will be variation in the impact energy within the colliding balls. This variation will lead to less (or more) stress induced into the balls during the test. Potentially, the quality of the results obtained from the DBT will be compromised and the downstream effect is that defective balls will pass the DBT and this might lead to significant commercial implications.

Therefore, it is fundamentally important to establish the margins under which the impact energy between Ball 1 and Ball 2 varies as a result of alteration of process parameters and material properties. The succeeding sections describe the results that were obtained after varying various material and simulation parameters. The variation in the collision energy between Ball 1 and Ball 2 was also observed and quantified.

4.2.6.1. EFFECT OF DENSITY OF MATERIAL OF CONSTRUCTION

Density of a material is its mass per unit volume. Density is calculated using Equation (4.8):

$$\rho = \frac{m}{V} \qquad (4.8)$$

where, ρ – density, m – mass and V – volume.

Equation (4.8) shows that density of a material is directly proportional to its mass hence, as the density of material is varied, its potential and kinetic energy vary in direct proportionality.

The density of steel varies between 7750g/m^3 and 8050g/m^3. Simulations were performed varying only the density whilst all other simulation parameters were kept constant. Figure (4.16) shows the variation of the impact energy between Ball 1 and Ball 2 as the density varies.

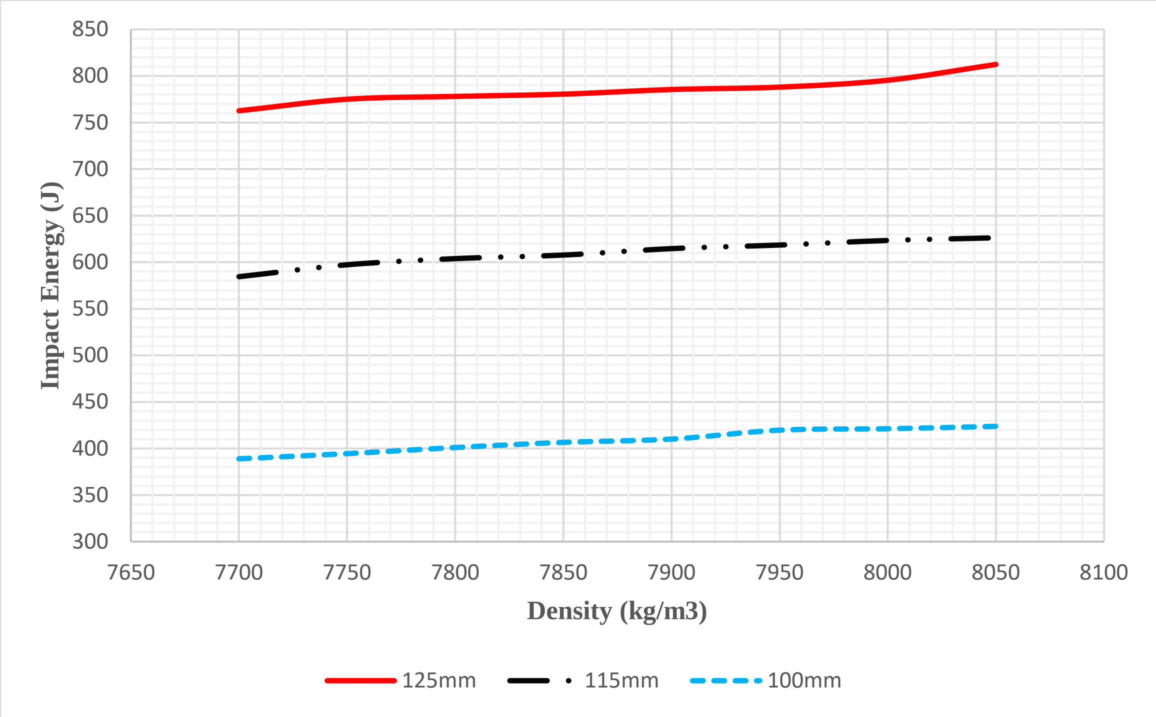

Figure 4. 16: *Variation of impact energy with density for the various ball sizes*

Figure (4.16) shows that the difference between the maximum and minimum energy values for the 125mm, 115mm and 100mm ball simulations are 49.77J, 41.75J and 34.83J respectively. Increased ball density results in higher collision energy. This extra energy is converted into various forms such as stored energy into the balls, heat, friction and sound. However, the change in density affects the large balls, 125mm, more than 115mm and 100mm.

4.2.6.2. EFFECT OF COEFFICIENT OF RESTITUTION

The coefficient of restitution (COR) is a measure of the damping property of the material. Its values ranges from 0 to 1 where 1 is a perfectly elastic collision. COR is a material property that primarily depend on the stiffness of the colliding balls. The stiffness of the ball is directly linked to its hardness. That is, the harder the ball, the stiffer it is.

In production systems, hardness of the manufactured balls vary within reasonable tolerances. The hardness depends on factors such as chemical composition of the alloy, heat treatment procedure applied and its operating parameters. All these factors affect the material stiffness and consequently the coefficient of restitution.

Effect of COR applied for the simulations and other simulation parameters does not constitute scope of this work and is recommended for future studies.

4.2.6.3. EFFECT OF STRUCTURAL MISALIGNMENT

During or after DBT machine maintenance, the vertical and curved sections might be misaligned by a few millimetres. This results in cushioning of the impact energy between the colliding balls. Simulations were conducted for the three ball sizes with a 10mm misalignment between the vertical and curved sections. This resulted in 3.2%, 3.7% and 4.3% drop in the elastic energy transferred to the next ball for 125mm, 115mm and 100mm balls respectively. Furthering the misalignment between the two sections results in more energy being cushioned. The overall result is that the DBT results obtained will not be representative of the energy that the balls are exposed and their strength under impact loading.

4.2.7. SUMMARY OF DROP BALL TEST SIMULATION WORK

The DEM is an attractive tool that has the potential of providing quantitative data on the collision behaviour of various ball types during the DBT. The flexibility of the DEM allows various aspects of the DBT to be studied in-depth to improve our understanding of the DBT machine performance, ball collision behaviour and energy involved during ball collisions. The study has shown that the energy involved during ball collision in the DBT can be quantified to form a basis of comparison with other balls sizes. However, the DBT energy quantification does not give an indication of how this energy compares to the energy that the balls are exposed to in high impact loading environments such as Semi-Autogenous Grinding (SAG) mills. The following chapter has been dedicated to SAG mill simulation using the DEM.

CHAPTER 5

SAG MILL SIMULATION WORK

5.0. INTRODUCTION

In the previous chapter, energy comparison studies for 125mm, 115mm and 100mm balls in the Drop Ball Test (DBT) were made. However, our main interest is the grinding media performance in the mill environment; both in terms of effectiveness in causing breakage as well as durability. During the grinding process, the grinding balls are subjected to stress that might lead to ball failure that manifests itself as breakage or spalling similar to ball failure modes observed in the DBT. This chapter describes the simulation work that was performed on the Semi-Autogenous (SAG) mill with parameters described in Chapter 3. An overview of the simulation results will be considered, hence mill output factors such as power draw, ball trajectories and impact energy spectra will be analysed to understand the mill load behaviour and its influence on the stress induced into the grinding media. The grinding balls' impact energy spectra provides the basis for determining the severity of the SAG environment compared to that of the DBT.

5.1. SAG MILL SIMULATION RESULTS

The results obtained from the SAG mill simulation included mill power draw and distribution, impact energy spectra and visual load behaviour. Some of the simulation results obtained were as expected. However, there were some results obtained especially on the charge dynamics, particle interactions and energy transfer that needed to revert back to literature reviewed so as to formulate logical explanations. The results are discussed below.

5.1.1. LOAD BEHAVIOUR

The key result obtained from the SAG mill DEM simulation is the information provided by the visual display of the load behaviour inside the mill. With these, the frequency of balls occupying different spaces during the simulation are visualised. The load motion pictures are given as either;

a. Stills – snapshots that show the position of particles at a given instance.
b. Particle Paths – that show the paths taken by the particles during the load motion.

Load behaviour (motion) pictures are snapshots images of particles at specified intervals during simulation. These images can be combined consecutively to produce an animation video that shows the cascading and cataracting behaviour of the mill load throughout the simulation. Figure (5.1) shows images of the load behaviour at the maximum cataracting heights.

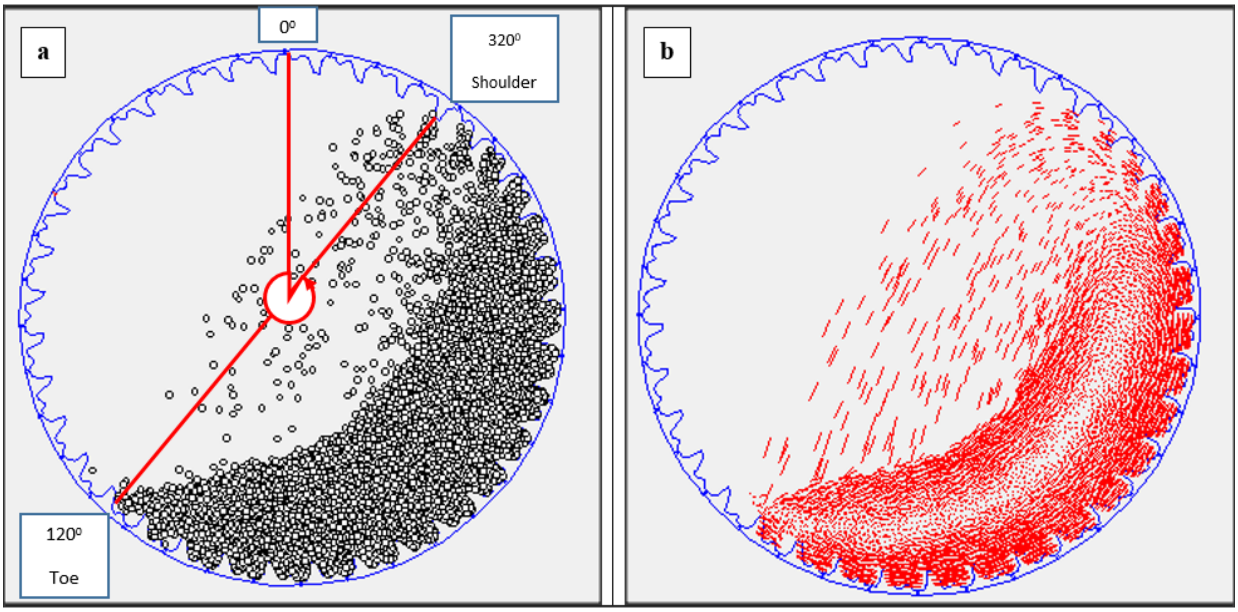

Figure 5. 1: *Load behaviour a. Stills, and b. Particle path traces*

Figure (5.1) shows a significant amount of cataracting particles. As the mill rotates in a counter-clockwise direction, the charge is carried along the perimeter of the mill by the lifters until a point of dynamic equilibrium (shoulder) where the charge falls to the bottom of the mill (toe). The shoulder and toe position of the simulations were determined to be at 120^0 and 320^0 counter-clockwise direction respectively. The highest free fall height achieved in this environment was 9.98m. This free fall height is very close to the 10m ball drop height in the DBT simulation.

5.1.2. MILL POWER DRAW

Upon completion of the simulation, a report is generated that contains the summary of the simulation including the mill power draw, impact energy spectra, number of simulated mill revolutions and total simulation time. Figure (5.2) shows a caption of the mill power draw section of the simulation report. The full simulation reports are presented in Appendix B.

Time(s)	Power(W)	Power (kW)	Totlss(W)	TotalLoss (kW)	Damplss(W)	DampLoss (kW)	Frclss(W)	FrictionLoss (kW)	Normlss(W)	NormLoss (kW)	Tanglss(W)
0,10	-911299,35	911,30	4044797,33	4044,80	2835337,29	2835,34	1209460,04	1209,46	2835337,29	2835,34	0,00
0,20	-889641,50	889,64	3987113,59	3987,11	2819263,33	2819,26	1167850,26	1167,85	2819263,33	2819,26	0,00
0,30	-901968,85	901,97	4165491,03	4165,49	2936947,07	2936,95	1228543,97	1228,54	2936947,07	2936,95	0,00
0,40	-881580,92	881,58	4167424,03	4167,42	2957002,61	2957,00	1210421,42	1210,42	2957002,61	2957,00	0,00
0,50	-900693,31	900,69	4084740,01	4084,74	2837860,99	2837,86	1246879,02	1246,88	2837860,99	2837,86	0,00
0,60	-894267,85	894,27	4511093,27	4511,09	3191105,26	3191,11	1319988,01	1319,99	3191105,26	3191,11	0,00
0,70	-909354,39	909,35	4346050,86	4346,05	3046729,18	3046,73	1299321,68	1299,32	3046729,18	3046,73	0,00
0,80	-908262,74	908,26	4171289,20	4171,29	2923251,27	2923,25	1248037,92	1248,04	2923251,27	2923,25	0,00
0,90	-895744,66	895,74	3884614,14	3884,61	2729421,96	2729,42	1155192,18	1155,19	2729421,96	2729,42	0,00
1,00	-926923,22	926,92	3792011,39	3792,01	2624499,45	2624,50	1167511,94	1167,51	2624499,45	2624,50	0,00
1,10	-932886,91	932,89	3446503,20	3446,50	2393671,04	2393,67	1052832,16	1052,83	2393671,04	2393,67	0,00
1,20	-948982,94	948,98	3213464,76	3213,46	2197649,45	2197,65	1015815,31	1015,82	2197649,45	2197,65	0,00

Figure 5. 2: *Caption of the mill power draw simulation file.*

The first column gives the time periods when average power was sampled. The next column refers to power calculated by considering the torque on the mill surface as the balls tumble (power draw). To obtain the actual mill power draw about 10% increase should be considered to account for losses due to motor and other transmission inefficiencies. Total power loss, the third column, is power calculation based on the losses during ball-ball and ball-wall collisions. The loss due to friction and damp-loss are summed up to get this value. In other words, this accounts for energy dissipation and should be as close as possible to the total power draw (second column).

Figure (5.3) shows the average mill power draw scaled up to full mill from the simulated slices for various simulations. The average power draw is directly proportional to the volume of the mill charge occupied by the steel balls. This is attributed to the difference in the density between the rocks (ore) and the steel balls. In practical mineral processing circuits, the density of steel ranges between 7.75 – 8.00 g/cm^3 whilst ore ranges between 2.40 – 2.85 g/cm^3 hence the observed power draw trend. Thus increasing or reducing the ball load of the charge will increase or decrease the power accordingly.

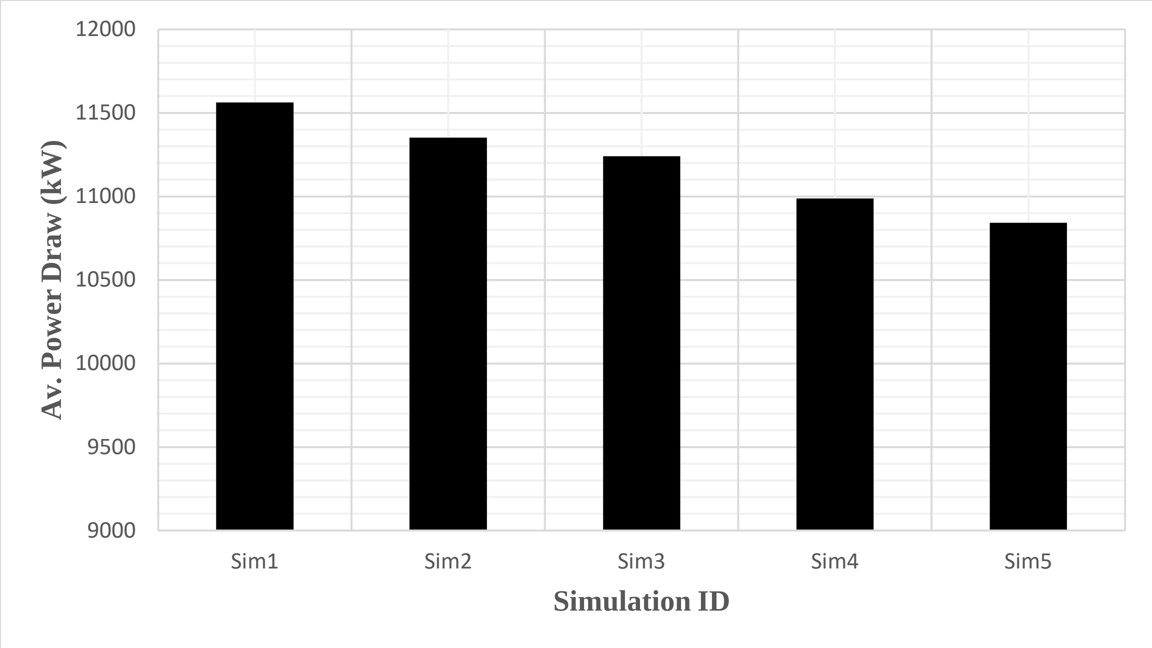

Figure 5. 3: *Average SAG mill power draw.*

The total power loss is mainly attributed to damping loss and frictional loss. Damping loss is the power loss due to both normal and tangential elastic deformation that is modelled by the dashpot in the DEM model. The frictional power loss is due to the rubbing action as sliding occurs between particle and wall surfaces. The summation of damping and frictional loss gives the total power loss hence, the load behaviour can be further studied by analysing the split between damping and frictional loss.

Figure (5.4) shows the trends of the damping and frictional power loss. The total power draw is dominated by damping loss and this indicates that the load assumed more of the cataracting behaviour than cascading. The cataracting behaviour is characterised by lifting of the charge to the mill shoulder level where it falls down in free flight to the toe of the mill. This load behaviour leads to impact breakage of the ore and stress on the grinding media.

The trend on the frictional energy loss shows an increase in the frictional power loss with an increase of ore (rocks) in the mill. As more rocks are added to the charge, they fracture easily than steel balls representing a progeny of ore particles varying in size from the largest ore particle fed into the mill to the smallest particle that can escape through the mill grate. Abrasion and attrition are the dominant forces responsible for comminution of the small ore particles. Hence, the particles break and tear through the rubbing action between ore particles and steel balls, mill walls or other ore particles. This results in more power loss due to friction than damping.

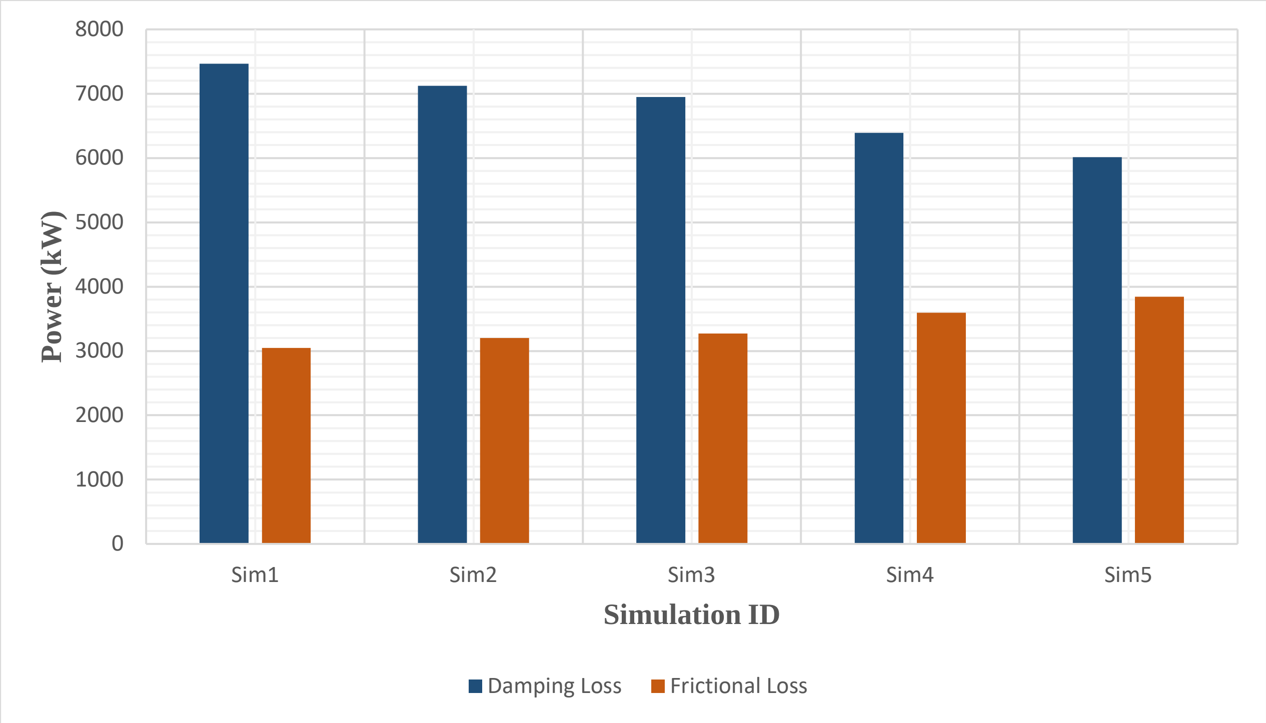

Figure 5. 4: *Total power draw split; damping and frictional loss*

There are two salient points to take note of; an increase in the cataracting fraction of the charge will increase breakage rates of the coarse particles while at the same time subject the grinding balls to significant stress due to the impact loading. On the other hand, if the cascading is dominant, the result is more power loss due to friction, finer grinds and increased wear rate of both the grinding balls and mill liners.

5.1.3. IMPACT ENERGY SPECTRA

The Impact Energy Spectra (IES) is a record of all the impact collisions that occur in the simulation period. The IES consists of number of collision events populated into fixed energy classes. The user selects the desired span of energy classes. The wider span reduces resolution of the energy spectra while a narrower span will increase the number of classes and making handling of the data impractical.

Figure (5.5) shows the impact energy spectra of the various simulations. The vertical axis of the graph was plotted on a logarithmic scale to show a clearer picture since some energy classes had over 10 million interaction events. As expected, there was a very high number of low energy events than high-energy events. These low energy events result from any low energy contact event, including mere vibration. Interestingly, the impact energy is inversely proportional to the ore (rock) fraction within the charge. That is, as the ball:ore ratio shifted from mostly steel balls to mostly ore, the number of events in low energy classes increased while high-energy collision events diminished. This observation directly results from the difference between densities of the steel balls and the rocks. Because of the low density of the rocks (2.4 – 2.85 g/cm^3), they tend to cushion some of the impact energy as the balls collide at the toe from free flight. In industrial mineral processing units, this action will cushion the balls from high-energy collisions that can potentially fracture the balls although this might cause the breakage rate of the large rocks to suffer whilst accelerating ball wear rate as the interaction between ball and ore increases.

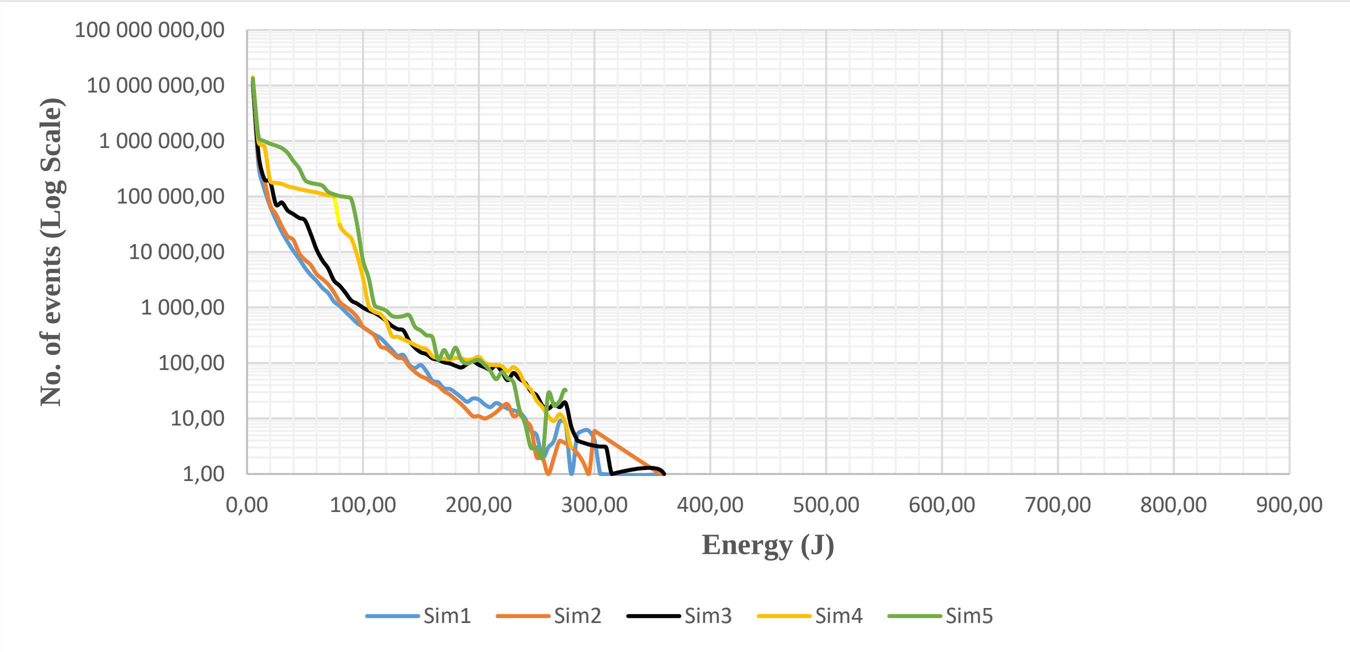

Figure 5. 5: *Impact Energy Spectra based on the charging ball:ore ratio*

SAG mills constitute a significant fraction of cataracting charge that exposes the steel balls to impact loading. The resultant collision energy between balls in the mill is determined by the cataracting trajectory height, size of the ball and type of collision particle (ball/ore). A comparison was made amongst the maximum impact energies in the various simulations as shown in Figure (5.6). To assess the influence of ball size on the collision energies, another simulation was conducted with 100mm balls only, under the same operating parameters.

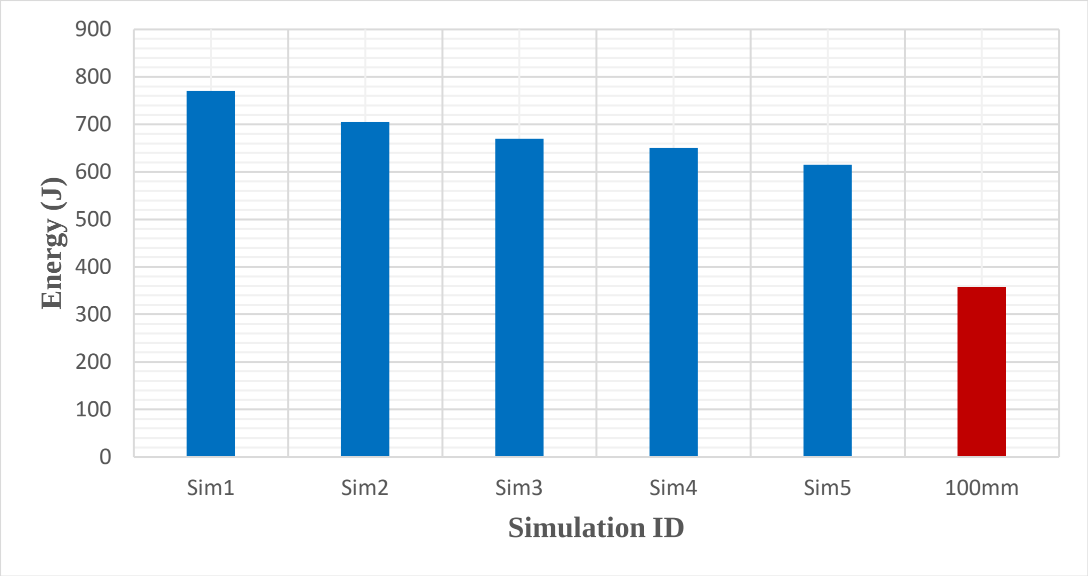

Figure 5. 6: *Maximum impact energies of the various simulations*

The first simulation shows the highest collision energy events because it was only 125mm steel balls involved in the collisions without any rocks. Thus, the ball-on-ball and ball-on-wall collisions were very aggressive and should be avoided to minimize ball fracture within the mill. As the ball:ore ratio decreases, the energy collision events correspondingly decrease due to the cushioning effect provided by the ore.

The 100mm balls simulation was performed without any ore particles. Even though the collisions were the ball on ball contacts, the highest collision energy recorded was only 387J. This value is 42% less than Sim5, which constitutes 125mm and the highest ore fraction. This implies that the use of 125mm balls that are massive will have a higher susceptibility of damage even if cushioning particles are present. The overall effect is that the large size and mass of 125mm balls exposes them to severe collisions that involve high energy, hence increasing their probability of fracture more than smaller balls sizes such as 100mm balls.

To further understand the energy that the 125mm steel balls were subjected to, an attempt was made to track the simulation history of a set of ten (10) 125mm steel balls. Each of the 10 balls' impact energy spectra was established in the same way as the previously discussed IES. That is, the number of collisions that each ball was exposed to were quantified into regular energy class intervals similar to Figure (5.5) energy classes. Figure (5.7) shows the impact energy spectra of the tracked ball sets of 10 in each simulation.

Figure (5.7) shows the average number of collisions events in each energy classes for each simulation. That is, say in the first simulation, the number of collisions in the 0 – 5J energy class was averaged for the 10 balls. This was repeated for all the other energy classes in the first simulation. This procedure was applied to all the other four simulations and plotted in Figure (5.7).

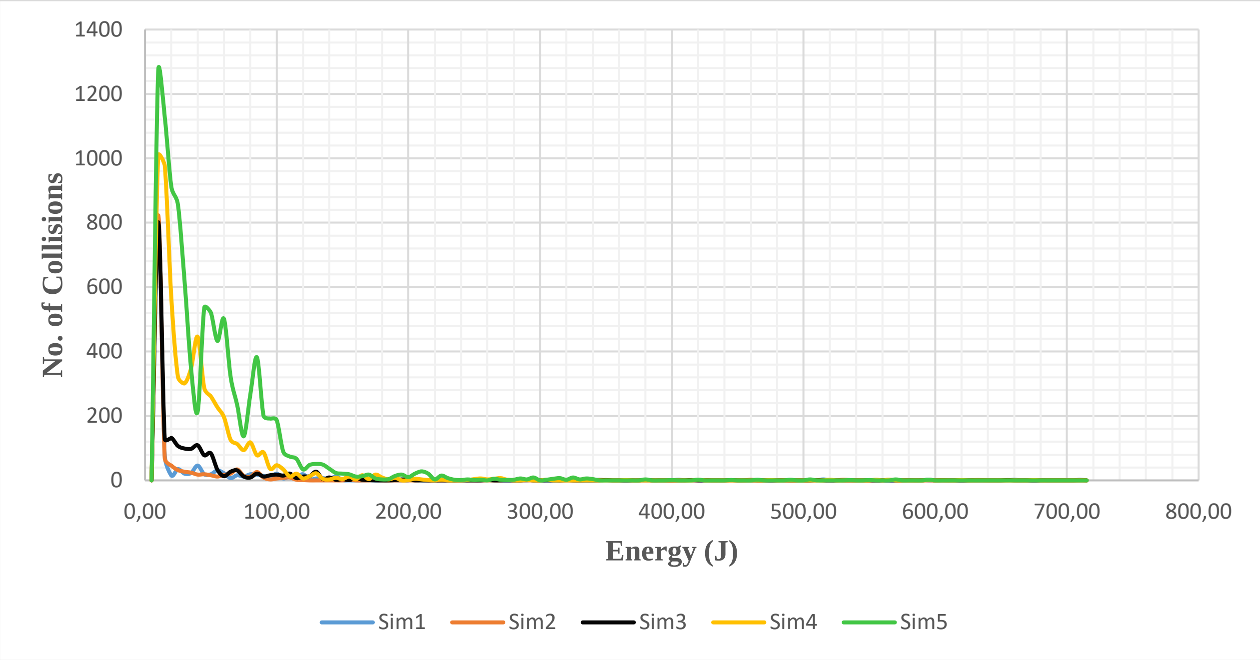

Figure 5. 7: *IES of the tracked 125mm balls*

The ball tracking quantifies the energy that the tracked balls were exposed to throughout the simulation period. The number of low energy collision events increases with an increase in the ore fraction of the charge. The first simulation containing steel balls only shows the highest energy that the balls are exposed to. Interestingly, the last simulation that contains the highest ore fraction still recorded high-energy collisions of up to 615J. This value can be regarded as an outlier. However, this also indicates that although the high ore fraction in the charge cushions the steel balls from severe ball-on-ball or ball-on-ore collisions, there is still very low probability of ball-on-ball collisions. This has been observed in industrial SAG mills with ball filling as low as 3 – 5% still showing chipped and broken balls in the discharge scats.

Figure (5.8) shows the maximum energy that the balls were exposed to during the simulation period.

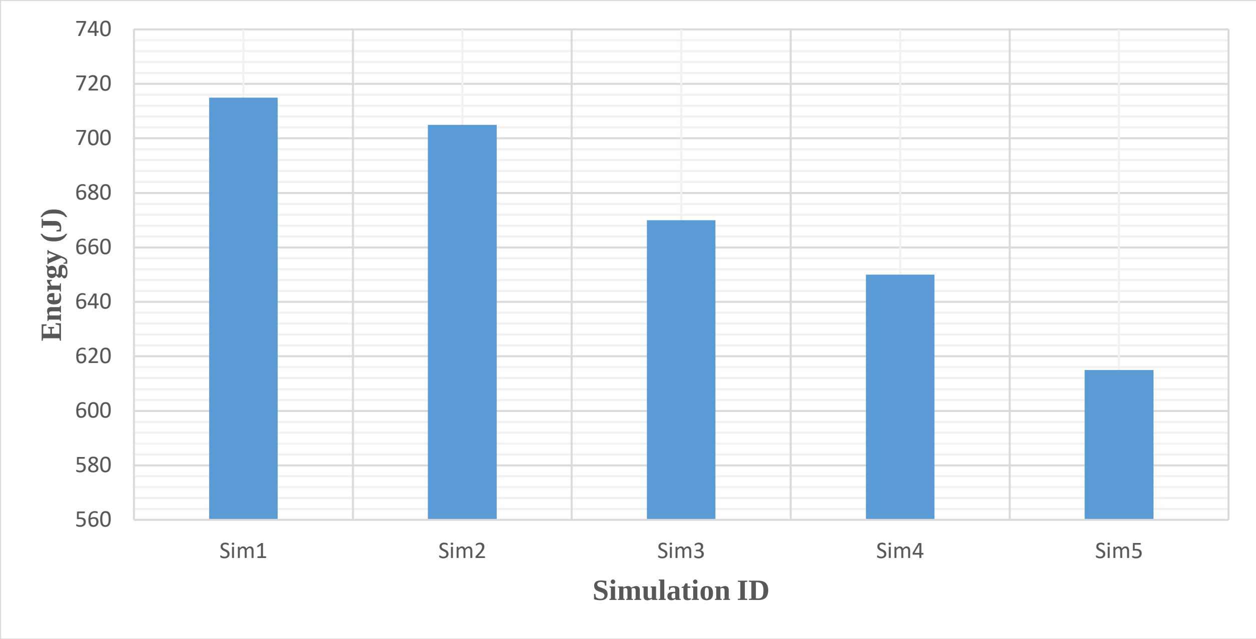

Figure 5. 8: *Maximum impact energy (125mm balls only)*

The 'Sim1' energy is the most severe ball-on-ball and ball-on-wall collisions and 'Sim5' the least severe. Thus SAG mill designers must be aware of these limits to optimize between higher breakage rates with an increase in ball:ore ratio and lower number of ball damage when the ball:ore ratio is decreased. The other solution that should be explored further is the use of smaller ball diameters, but other issues such as ore competency, which is beyond the scope of this research, should also be considered. It is desirable to achieve the required ore breakage rates at the least possible ball load because:

- Lower ball load results in more cushioning of the high-energy collisions that have the potential to fracture the balls
- A reduction in ball load results in a SAG operation that is more power effective
- Reducing ball load of the charge will significantly reduce the cost of grinding since grinding media replenishment can account for up to 45% of grinding costs.
- Using smaller ball sizes reduces ball damage probability.

5.2. SUMMARY OF THE SAG MILL SIMULATION WORK

From the analysis of the SAG mill simulation work, it has been shown that the DEM-PFC 3D is a tool that has the potential to provide quantitative data on the charge dynamics in SAG mills. The attractiveness of the tool lies in its flexibility to change mill geometry and operating parameters to understand their effect on load behaviour, power draw and energy that both the grinding media and ore particles are exposed to. This information is very important to SAG mill operators and designers because it sets the ground for improved estimation of ore breakage rates, power draw, production throughput and overall mill performance. Furthermore, this information is also important to grinding media manufacturers because if the energy that the balls are potentially exposed to in SAG mills is clearly understood, ball manufacturers will know the required mechanical properties to supply to mill operators. Both scenarios can potentially lead to significant commercial savings.

The data that was analysed from both the Drop Ball Test (DBT) and SAG mill simulation will be used to compare the severity of the DBT to SAG mills in terms of the energy that the grinding balls are exposed to. The succeeding sections are devoted to this cause.

5.3. PREDICTING STRESS INDUCED INTO THE GRINDING MEDIA

The quantitative information about the Drop Ball Test (DBT) and SAG mill available from the DEM has already been discussed in Chapter 4. In this section, a scheme that applies the impact energy spectra to quantify and compare the energy that 125mm balls are exposed to during both the DBT and SAG mills is developed. The main challenge of this scheme is estimating the number of drops required to break a ball during the DBT and number of impact collisions that has the potential to break the balls in a 11.2m diameter SAG mill under study. In the following sections, approaches to estimate the number of drops and energy required to break the balls during the DBT and SAG mills are discussed under the appropriate sub-sections.

5.3.1. PREDICTING ENERGY AND NUMBER OF DROPS REQUIRED TO BREAK A BALL DURING THE DBT

During the Drop ball Test (DBT), a single drop exposes the colliding balls and the balls sitting in the curved section to energy that is determined by the size of the ball, density of material of ball construction and drop height. Combining Equation (4.1), and Equation (5.1) gives Equation (5.2)

$$\rho = \frac{m}{V} \qquad (5.1)$$

$$E = \rho V g h \qquad (5.2)$$

Where, ρ is the material density, m is the ball mass, V is volume of the ball, h is the drop height, g is the acceleration due to gravity and E is the impact energy.

The balls are spherical in shape, with diameter d and their volume is given by Equation (5.3);

$$V = \frac{\pi d^3}{6} \tag{5.3}$$

Combining Equation (5.3) and (5.2) gives:

$$E = \frac{\rho \pi d^3}{6} gh \tag{5.4}$$

Of all the parameters described in Equation (5.4), change in drop height (h) within allowable limits has the most significant effect on the energy (stress) subjected to the balls.

For 125mm balls being dropped from a 10m height with material density 7.75 g/cm^3, the probability of fracture are shown in Figure (5.9);

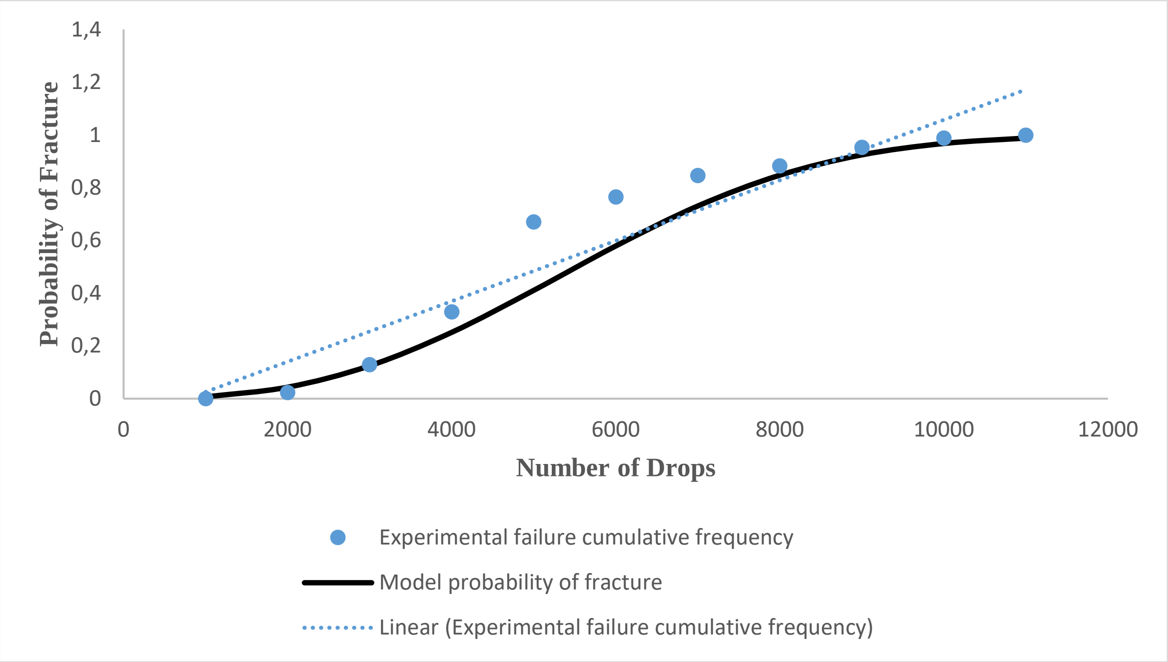

Figure 5. 9: *125mm balls probability of fracture vs number of drops*

Figure (5.9) is an extension of the physical data gathered and initially presented in Figure (4.7). The 125mm balls' probability of fracture peaks at about 6000 drops. This indicates that the failures below 6000 drops are attributed more to the quality of the ball than to the energy or number of drops that the balls are exposed to. Beyond 8000 drops, ball failures in this region are attributed to both the quality of the ball and the number of drops (energy) that the balls are exposed to. If the number of drops exceeds 9000, any failures beyond that are mainly attributed to fatigue failure that eventually takes its toll.

Assuming that the energy that can cause significant damage to the ball exists in the first 3 positions. The energy that the ball is exposed to during the first 3 positions can be summed up from Figure (4.13), hence the total energy that has potential of damaging the ball after a single drop can also be established. Extrapolating this energy over various number of drops gives Figure (5.10).

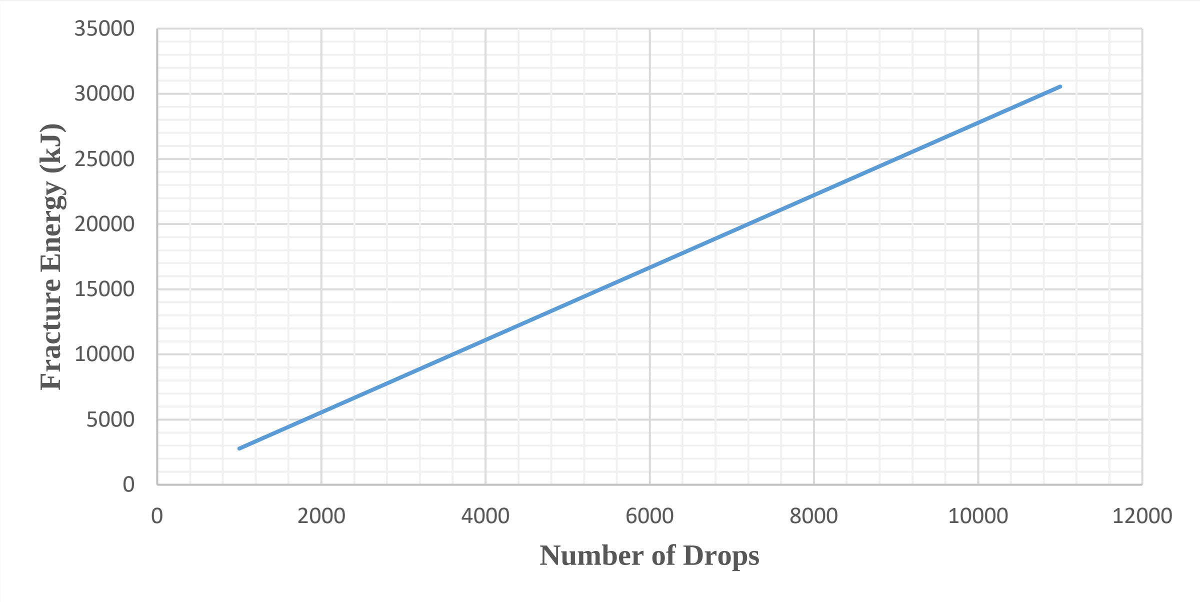

Figure 5. 10: *Fracture energy of 125mm balls*

Figure (5.10) shows the total energy that has potential of damaging the ball after a specific number of drops. The fracture energy only applies if the summed energies are within the first 3 positions (or any other number of positions yet to be determined) that expose the ball to energy that has potential of causing significant damage. If the ball is exposed to energy below a certain threshold, no significant damage will happen to the ball even after exposing the ball to millions of such low energy collisions. Determining this threshold energy remains to be established in future studies of the balls' specific material of construction.

5.3.2. PREDICTING THE ENERGY THAT THE BALLS ARE EXPOSED TO IN A SAG MILL

During the Semi-Autogenous-Grinding (SAG) process the mill charge (grinding balls, ore and water) is intimately mixed and may assume any of the different types of load behaviour (cataracting, cascading or surging) depending on the mill speed, lifter design and charge filling level. The SAG mill simulation work showed that the load behaviour was dominated by cataracting and cascading. Cataracting behaviour exposes both the ore and the grinding balls to impact loading that causes rock fracture. However, the high energy provided by the cataracting load behaviour also exposes the grinding balls to impact loading that stresses the grinding balls until breakage occurs. The quantification of the stress (energy) required to cause ball breakage and predicting ball failure as a result of the load behaviour within the SAG mill is the main objective of this section.

The quantification of the threshold energy (stress) that is required to break a ball was derived from the SAG mill simulation impact energy spectra. The simulation history of ten (10) 125mm balls was tracked to observe the number of events in various energy classes that each of the 10 balls were exposed to. The energies that the balls were exposed to throughout the simulation period were averaged to give the energy that each of the ten balls was exposed. The minimum energy that was summed in the SAG mill energy quantification corresponded to the minimum energy that was used for the DBT breakage energy quantification. This was very important to provide a basis for comparison between the DBT and the SAG mill.

The minimum energy that was summed in the SAG mill simulations was 375J, which corresponded with the 376J, considered in the DBT calculations. The number of events in each class multiplied each energy class. The total energy was summed for each simulation. This energy represents the total amount of energy captured during the simulation that has potential of damaging the ball. The total energies were averaged to get 6708J that a 125mm ball was exposed during a mill simulation time of 2.48 revolutions.

The mill speed was 9 revs/min hence, each ball was exposed to:

$$\frac{6708}{2.48} \times 9 = 24\ 343\text{J per minute}$$

After 1000 drops in the DBT, a single ball is exposed to 2 777 000,74J. The equivalent number of DBT drops that a ball is exposed to in a single mill revolution is:

$$\frac{24\ 343}{2\ 777\ 000.74} \times 1000 = 8{,}77 \text{ drops/mill rev.}$$

The energy that a ball is exposed to in a single SAG mill revolution is equivalent to 8.77 drops in the DBT.

This figure can be used to estimate severity of a certain number of drops relative to grinding time within the SAG mill. For example, 10 000 drops is equivalent to:

$$\frac{10\ 000}{8{,}77} = 1140.25 \text{ mill revolutions.}$$

For a mill running at say 9 rev/min, this will translate to:

$$\frac{1140.25\,rev}{9\,rev/min} = 126.69\,minutes\ OR\ 2\ hrs\ 7\ mins\ mill\ running\ hours$$

Using Equation (4.5), the minimum amount of energy, E_{xo}, required to cause ball fracture can be determined. Ball collisions events in the SAG mill with impact energy equal to or exceeding E_{xo} can be summed to determine probability of fracture by applying Equation (4.5) for specific number of mill revolutions.

The comparison between the DBT and SAG mill energy is dependent on the following characteristics in both processes:

- DBT – drop height, ball size, number of balls in the curved section, total number of balls in circulation and number of drops.
- SAG Mill – Mill geometry (diameter vs length), lifter design, mill speed, mill filling and ball:ore ratio.

There are some pending areas to uncover such as a more inclusive DBT energy balance, minimum energy required to cause damage for specific material of construction and further estimating the frequency of collision events above the cut-off energy in the SAG mill simulations. However, the work presented above shows that the DEM is an attractive method to study the collision behaviour in SAG mill and energy transfer within the DBT and a method to estimate the energy that the balls are exposed to has been demonstrated.

CHAPTER 6

CONCLUSION AND RECOMMENDATIONS

6.1. GENERAL REMARKS

The Discrete Element Method (DEM) was applied to model the collision behaviour of various ball sizes within the Drop Ball Test (DBT) and load behaviour and charge interactions with the SAG mill. Using the impact energy spectra generated from the simulation of both processes, it was possible to estimate the energy that 125mm balls are exposed to during both processes. This provided a basis of comparing the severity of the DBT to a SAG mill environment in terms of the energy exposed to the balls.

Although the method developed to compare the severity of the DBT and SAG mill is very simplified, a foundation has been laid for future research to further uncover the particle interactions and energy transfer in both scenarios. Furthermore, an insight has been initiated on how useful the DBT is as a quality control procedure in SAG mill grinding media manufacturing units.

This work has not only shown how the DEM can be used to compare the severity of the DBT to the SAG mill but has revealed other possibilities and attractiveness of the DEM as a tool to further understand collision behaviour, forces and particles that are exposed to certain energy levels in both the DBT and SAG mills. The DEM has also revealed insights into the high impact loading SAG mill environments and measures that can be taken to achieve minimal ball damage for a reasonably performing SAG mill.

6.2. IMPROVING QUALITY AND ACCURACY OF THE SIMULATION DATA

The requirements for evaluating more accurate energy transfer and collisions between particles in both the DBT and SAG mill are:

- Use of a lower time step to allow more accurate energy calculations
- Determination of experimental and more representative simulation parameters for both the DBT and SAG mill simulations.
- More simulation time for SAG mill to allow for more mill revolutions. This will widen the sample size and improve the quality of the data.
- Allowing more mill revolutions before sampling begins in SAG mill simulations. This will ensure that the charge is homogenously mixed.

6.3. RECOMMENDATIONS FOR FUTURE WORK

The following areas have been identified for future research work:

6.3.1. MATERIAL OF BALL CONSTRUCTION

The damping behaviour and energy transfer of the balls depends on the properties of the ball's material of construction. In practical grinding media manufacturing units, the toughness (damping property) of the ball is designed according to application. Some balls are manufactured to achieve excellent wear (hard balls) while others are manufactured to have good impact toughness. In both cases, the material of construction behaves differently during impact loading. Further studies on the material of ball construction will also enable more accurate determination of simulation parameters.

6.3.2. SIMULATION PARAMETERS

The simulation parameters that affect the quality of the data generated are material stiffness, coefficient of restitution and coefficient of friction.

- **Material Stiffness** has an effect on the distribution of the collision energy. During the DBT simulations, energy is transferred from one ball to the other and the amount of energy absorbed by each ball and transferred to the next ball depends on the stiffness of the ball. Hence, accurate determination of this parameter for specific ball material of construction is recommended.
- **Coefficient of Restitution** also determines the energy absorbed by each ball during collisions as well as rebound height. This property is material specific and its experimentally determination will improve the quality of the data.
- **Coefficient of Friction** is mainly applicable to the particles in the cascading region of the mill. Hence, for determination of grinding rates of the ore and ball wear, accurate determination of this property will improve the quality of the data generated.

6.3.3. ADDRESSING EFFECT OF WEAR ON THE BALLS

As the mill rotates, the grinding balls are subjected to both impact loading due the cataracting behaviour and wear due to abrasion and attrition in the cascading and toe regions of the mill. The probability of ball fracture is directly proportional to the ball size. Hence, as the ball is worn off, its chances of surviving fracture failure further increase. This is primarily because of two reasons. Firstly, as the ball wears off, it reduces in size and its surface area per unit mass of contact increases and as discussed in Chapter 2 smaller particles have lower breakage rates than large particles. Secondly, as the ball wears off, the inner softer part of the ball is exposed. The softer the ball, the tougher is the ball. Further studies will enlighten the ball size ranges which are most vulnerable to fracture under specific impact loading conditions.

6.3.4. BALL SHAPE

As the balls wear off, they expose the inner and softer parts of the ball. In the presence of severe impact loading, the ball shape becomes distorted taking various shapes such as cuboids and the pancake shape. Using advanced DEM versions, particle shapes can be modified to be more representative of practical SAG mill charge. This approach can potentially reveal the effect of particle shape on grinding media wear, fracture behaviour and ore grinding rates.

6.4. FINAL REMARKS

The attractiveness of the DEM as a tool to study collision behaviour and evaluate the energy that participating balls are subjected to in the Drop Ball Test (DBT) and Semi Autogenous Grinding (SAG) mills has been shown. Whilst this study has focused on comparing the severity of the energy that the balls are exposed to, both grinding media manufacturers and SAG mill operators and designers can gather more information that is useful from the program at a higher resolution such as:

- The effect of misalignment of joining sections in the DBT on the collision energy experienced by the balls.
- The effect of changes in material properties such as density, hardness and stiffness on the energy transfer, stress induced into the grinding balls and quality of the data gathered from the DBT.
- The effect of particle shape on the stress induced into the grinding media during the SAG process

Furthermore, the flexibility of the tool enables the design of the simulated, DBT or SAG mill, to be more accurately defined and tailored to the user’s satisfaction. Hence, the author views this work as a prospect that might evolve into future work that is more exciting.

REFERENCES

Ahmad, Z. (2006) *Principles of Corrosion Engineering and Corrosion Control*. 1st edn. Oxford, UK: Butterworth-Heinemann.

Aldrich, C. (2013) ‘Consumption of steel grinding media in mills – A review’, *Minerals Engineering*. Elsevier Ltd, 49, pp. 77–91.

Basquin, O. . (2010) ‘The exponential law of endurance test’, *Proceedings of ASTM*, 10(II), pp. 625–630.

Bhat, S. and Patibandla, R. (2011) ‘Metal Fatigue and Basic Theoretical Models: A Review’, in Dr. Eduardo Valencia Morales (ed.) *Alloy Steel - Properties and Use*. Dr. Eduard. India: Vellor Institute of Technology, pp. 203–233.

Bond, F. C. (1961) ‘Crushing and Grinding calculations Part 1’, *Brazilian Journal of Chemical Engineering*, 6(No.6), pp. 378–385.

Bwalya, M. M. (2005) *Using the Discrete Element Method to guide modelling of semi and fully autogenous milling*. University of the Witwatersrand, Johannesburg.

Bwalya, M. M. (2006) ‘Manual on the use of DEMSIM’, *University of the Witwatersrand, Johannesburg*, Unpublishe.

Bwalya, M. M. (2018) ‘Revisiting the dropweight model for predicting particle breakage probability’.

Bwalya, M. M., Moys, M. H. and Hinden, A. L. (2001) ‘The use of the Discrete Element Method and fracture mechanics to improve grinding rate prediction’, *Minerals Engineering*, 14(6), pp. 565–573.

Callister, W. (2007) *Materials Science and Engineering: An Introduction*. 7th edn. Edited by D. . Rethwisch. New York: John Wiley & Sons Inc.

Cleary, P. W. and Sinnott, M. D. (2015) ‘Simulation of particle flows and breakage in crushers using DEM : Part 1 – Compression crushers’, *Minerals Engineering*. Elsevier Ltd, 74, pp. 178–197.

Etter, J. (2012) ‘Tutorial report on Hertzian Contact Stress Theory’. Tuscan: University of

Arizona, pp. 1–5.

Gupta, A. and Yan, D. . (2006) *Mineral Process Design and Operations: An Introduction*. first. Amsterdam: Elsevier B.V.

Itasca Consulting Group (2014) ‘Itasca DEM Framework’, p. 2014.

Jonsén, P., Pålsson, B. I. and Häggblad, H. Å. (2012) ‘A novel method for full-body modelling of grinding charges in tumbling mills’, *Minerals Engineering*, 33, pp. 2–12.

Karl, K. (2012) *Probabilistic modeling of fatigue failures*. Royal Institute of Technology, Stockholm.

Kiangi, K. K. (2011) *Effect of particle filling and size on the behaviour of the ball load and power in a dry mill*. University of the Witwatersrand, Johannesburg.

Louthan, M. . J. (2008) ‘Hydrogen embrittlement of metals: A prime for the failure analyst’. Aiken: Savannah River Laboratory, pp. 2–39.

Mishra, B. K. and Rajamani, R. K. (1992) ‘The discrete element method for the simulation of ball mills’, *Applied Mathematical Modelling*, 16(9), pp. 598–604.

Moema, J., Papo M., Stumpf, W. and Slabbert D., (2010) ‘The role of retained austenite on performance of grinding media’, in Papo, M. . (ed.) *Second International Tribology Symposium*. Rio de Janeiro: Mintek, South Africa, pp. 2–18.

Moema, J., Papo M., Slabbert D. and Zimba J., (2009) ‘Grinding media quality assurance for the comminution of gold ores’, in *World Gold Conference*. Johannesburg: South African Institute of Mining and Metallurgy, pp. 27–34.

Muzambi, R. T. (2014) *Development of High Chromium White Cast Iron (HCWCI) as Grinding Balls by Recycling Scrap Metal*. University of Zimbabwe, Harare.

Napier-Munn, T., Morrell S., Morrison R., (1999) *Mineral Comminution Circuits Their Operation and Optimisation*. 2nd edn. Edited by T. . Napier-Munn. Queensland, Australia: Julius Kruttschnitt Mineral Research Center.

Newage Testing Instruments (2010) ‘Rockwell Hardness Testing System: Identron NI-300 Series’, *Operator’s Manual*. Haryana, India: Newage Testing Instruments, Inc, pp. 2–34.

Owen, P. and Cleary, P. W. (2015) ‘The relationship between charge shape characteristics and fill level and lifter height for a SAG mill’, *Minerals Engineering*. Elsevier Ltd, 83, pp. 19–32.

Polycarpou, A. A. (2005) ‘Measurement and Modeling of Normal Contact Stiffness and Contact Damping at the Meso’, *Journal of Vibration and Acoustics*, 127(59), pp. 52–60.

Powell, M., Smit I., Radziszweski P., Cleary P., Rattray B., Goran-Klas E., and Schaeffer E., (2006) ‘The selection and design of mill liners’, *Advances in Comminution*. Colorado: Society of mining, metallurgy and exploration, pp. 331–376.

Powell, M. S. (1991) ‘The effect of liner design on the motion of the outer grinding elements in a rotary mill’, *International Journal of Mineral Processing*, 31(3–4), pp. 163–193.

Royston, D. (2007) ‘Semi-autogenous grinding (SAG) mill liner design and development’, *Society of mining, metallurgy and exploration*, 23(3), pp. 121–132.

Stevenson, A. N. J. and Hutchings, I. M. (1996) ‘Development of the dry sand/rubber wheel abrasion test’, *Wear*. Elsevier Ltd, 195(1), pp. 232–240.

Sun, Y. I., Dong M., Mao Y. and Fan D., (2009) ‘Analysis on Grinding media Motion in Ball Mill by Discrete Element Method’, in Khashman, A. (ed.) *1st International Conference on Manufacturing Engineering, Quality and Production Systems*. Brasov, Romania: WSEAS Press, pp. 227–231.

Tönshoff, H. K., Peters J., Inasaki I. and Paul T., (1992) ‘Modelling and Simulation of Grinding Processes’, *CIRP Annals - Manufacturing Technology*, 41(2), pp. 677–688.

Tylczak, H. (1989) ‘Evaluation of commercial US grinding balls by laboratory impact and abrasion tests’, *Minerals & Metallurgical Processing*, 13(May), pp. 88–653.

Weerasekara, N. S. Powell M., Cleary P., Tavares L., Evertsson M., Morrison D., Quist J. and Carvalho R., (2013) ‘The contribution of DEM to the science of comminution’, *Powder Technology*. Elsevier B.V., 248(2013), pp. 3–24.

Wills, B. and Napier-Munn, T. . (2006) *Wills’ Mineral Processing Technology*. 7th edn. Edited by T. . Napier-Munn. Oxford, UK: Butterworth-Heinemann.

Zhu, X. (2012) ‘Tutorial on Hertz Contact Stress’. Tuscan: University of Arizona, pp. 1–8.

APPENDIX A – DROP BALL TEST (DBT) SIMULATION FILES

A similar program to the mill simulation script file was created in order to model the collision behaviour during the DBT. The program contains a script file that can be edited to define the geometry of the DBT machine and the mill simulation parameters. The script file can be created on any word editor such as MS Word or Notepad. Figure A1 shows the DBT input script file.

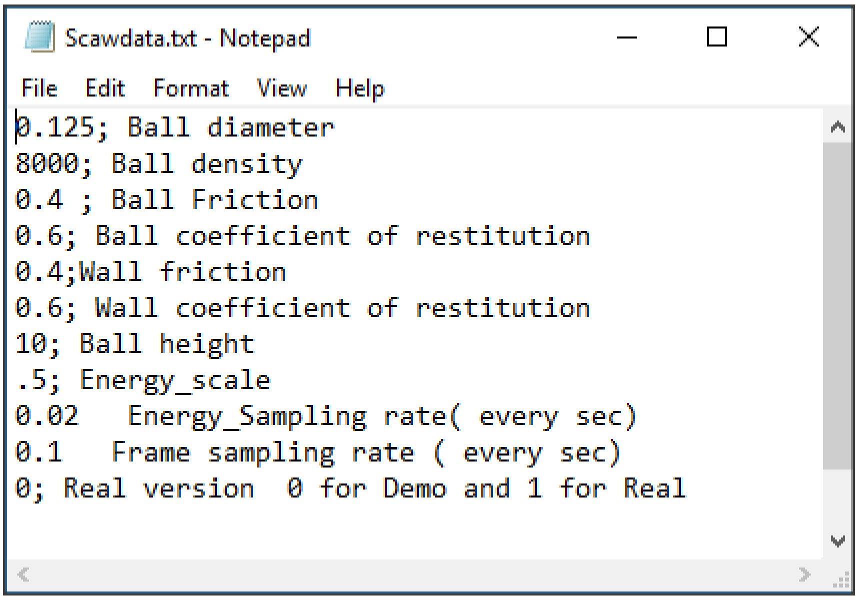

Figure A 1: *DBT input script file*

Most of the parameters shown in Figure A1 are self-explanatory. The energy-sampling rate is the frequency of sampling energy readings. Frame sampling rate defines frequency of capturing frames used for creating the animation video.

After the simulation is completed, the following output files are generated:

- **Generic Simulation Report** that lists the total number of collisions classified into regular energy classes
- **Detailed Output File** that lists the various collision events that each ball was exposed to classified into regular energy classes as defined in the script file, Figure A1.
- **Energy Output File** that defines the various kinetic and potential energy of each ball throughout the simulation period.

The data obtained from the output files can be imported to MS Excel or any spreadsheet for analysis. The data imported into spreadsheet for each DBT output report is shown in Figure A2 – A4.

```
File   Edit   Format   View   Help
joules ,Events
0,0
5.00000000000e-001,1288,1511,1511
1.00000000000e+000,85,0,0
1.50000000000e+000,42,0,0
2.00000000000e+000,32,0,0
2.50000000000e+000,22,0,0
3.00000000000e+000,6,0,0
3.50000000000e+000,3,0,0
4.00000000000e+000,2,0,0
4.50000000000e+000,6,0,0
5.00000000000e+000,4,0,0
5.50000000000e+000,1,0,0
6.00000000000e+000,0,0,0
6.50000000000e+000,0,0,0
.
.
.
4.09000000000e+002,0,0,0
4.09500000000e+002,0,0,0
4.10000000000e+002,0,0,0
4.10500000000e+002,0,0,0
4.11000000000e+002,0,0,0
4.11500000000e+002,0,0,0
4.12000000000e+002,0,0,0
4.12500000000e+002,0,0,0
4.13000000000e+002,0,0,0
4.13500000000e+002,1,0,0
4.14000000000e+002,0,0,0
```

Figure A 2: *DBT simulation generic file.*

Figure A2 shows the generic simulation file showing the energy class and number events. The dotted part of the file shows some energy classes that were excluded to fit the long file into the dissertation.

```
File  Edit  Format  View  Help
Ball number,1
 ,P_E,K_E,Rot_E
1,8.02422062955e+002,1.55566085932e-001,0.00000000000e+000
2,8.01949752692e+002,6.26749117284e-001,0.00000000000e+000
3,8.01161817431e+002,1.41355714571e+000,0.00000000000e+000
4,8.00058257174e+002,2.51599017122e+000,0.00000000000e+000
5,7.98639071919e+002,3.93404819380e+000,0.00000000000e+000
6,7.96904261667e+002,5.66773121347e+000,0.00000000000e+000
7,7.94853826418e+002,7.71703923021e+000,0.00000000000e+000
8,7.92487766172e+002,1.00819722440e+001,0.00000000000e+000
9,7.89806080929e+002,1.27625302549e+001,0.00000000000e+000
10,7.86808770689e+002,1.57587132629e+001,0.00000000000e+000
11,7.83495835452e+002,1.90705212679e+001,0.00000000000e+000
12,7.79867275218e+002,2.26979542701e+001,0.00000000000e+000
13,7.75923089986e+002,2.66410122693e+001,0.00000000000e+000
14,7.71663279758e+002,3.08996952656e+001,0.00000000000e+000
15,7.67087844533e+002,3.54740032589e+001,0.00000000000e+000
16,7.62196784310e+002,4.03639362494e+001,0.00000000000e+000
17,7.56990099090e+002,4.55694942369e+001,0.00000000000e+000
18,7.51467788874e+002,5.10906772215e+001,0.00000000000e+000
19,7.45629853660e+002,5.69274852031e+001,0.00000000000e+000
20,7.39476293449e+002,6.30799181819e+001,0.00000000000e+000
21,7.33007108241e+002,6.95479761577e+001,0.00000000000e+000
22,7.26222298036e+002,7.63316591306e+001,0.00000000000e+000
23,7.19121862834e+002,8.34309671006e+001,0.00000000000e+000
24,7.11705802635e+002,9.08459000677e+001,0.00000000000e+000
25,7.03974117438e+002,9.85764580318e+001,0.00000000000e+000
26,6.95926807245e+002,1.06622640993e+002,0.00000000000e+000
27,6.87563872055e+002,1.14984448951e+002,0.00000000000e+000
28,6.78885311867e+002,1.23661881907e+002,0.00000000000e+000
29,6.69891126682e+002,1.32654939859e+002,0.00000000000e+000
30,6.60581316501e+002,1.41963622809e+002,0.00000000000e+000
31,6.50955881322e+002,1.51587930755e+002,0.00000000000e+000
32,6.41014821146e+002,1.61527863699e+002,0.00000000000e+000
33,6.30758135973e+002,1.71783421640e+002,0.00000000000e+000
34,6.20185825803e+002,1.82354604578e+002,0.00000000000e+000
35,6.09297890636e+002,1.93241412512e+002,0.00000000000e+000
```

Figure A 3: *PE and KE output file.*

Figure A3 shows the Potential (PE) and Kinetic Energy (KE) change simulation output file. The first column shows the time intervals. Each time interval corresponds with the sampling interval described in the input script file described in Figure A1. For example, the 12th time interval represents:

$12 \times 0.02 = 0.24$ seconds after Ball 1 has been dropped off from the top end of the DBT.

The second, third and fourth columns represents the PE, KE and Rotational energy of the ball at that time interval respectively. For example, at the 12^{th} interval, 0.24 seconds after Ball 1 has been dropped off, its PE and KE were 779.86J and 22.69J respectively. This procedure is the same for all the other 20 balls in the curved section.

The detailed output file records all the collisions that each ball was involved in, classified into regular energy classes.

```
File  Edit  Format  View  Help
Detailed tracking report ,All
Time interval: 1
0,1,1,1,2,2,2,3,3,3,4,4,4,5,5,5,6,6,6,7,7,7,8,8,8,9,9,9,10,10,10,11,11,11,12,12,12,13,13,13,14,14,14,15,15,15,16,16,16,17,17,17,18,18,18,19,19,19,20,20,20,21,21,21
5.00000000000e-001,0,0,0,1,0,0,5,6,6,4,5,5,4,5,5,9,10,10,10,11,11,9,11,11,4,6,6,4,5,5,8,9,9,9,10,10,4,6,6,4,5,5,6,6,6,8,10,10,6,6,6,4,6,6,8,9,9,4,5,5,0,0,0
1.00000000000e+000,0,0,0,0,0,0,0,0,0,0,0,0,0,0,0,0,0,0,0,0,0,0,0,0,0,0,0,0,0,0,0,0,0,0,0,0,0,0,0,0,0,0,0,0,0,0,0,0,0,0,0,0,0,0,0,0,0,0,0,0,0,0,0
1.50000000000e+000,0,0,0,0,0,0,0,0,0,0,0,0,0,0,0,0,0,0,0,0,0,0,0,0,0,0,0,0,0,0,0,0,0,0,0,0,0,0,0,0,0,0,0,0,0,0,0,0,0,0,0,0,0,0,0,0,0,0,0,0,0,0,0
2.00000000000e+000,0,0,0,0,0,0,0,0,0,0,0,0,0,0,0,0,0,0,0,0,0,0,0,0,0,0,0,0,0,0,0,0,0,0,0,0,0,0,0,0,0,0,0,0,0,0,0,0,0,0,0,0,0,0,0,0,0,0,0,0,0,0,0
2.50000000000e+000,0,0,0,0,0,0,0,0,0,0,0,0,0,0,0,0,0,0,0,0,0,0,0,0,0,0,0,0,0,0,0,0,0,0,0,0,0,0,0,0,0,0,0,0,0,0,0,0,0,0,0,0,0,0,0,0,0,0,0,0,0,0,0
3.00000000000e+000,0,0,0,0,0,0,0,0,0,0,0,0,0,0,0,0,0,0,0,0,0,0,0,0,0,0,0,0,0,0,0,0,0,0,0,0,0,0,0,0,0,0,0,0,0,0,0,0,0,0,0,0,0,0,0,0,0,0,0,0,0,0,0
3.50000000000e+000,0,0,0,0,0,0,0,0,0,0,0,0,0,0,0,0,0,0,0,0,0,0,0,0,0,0,0,0,0,0,0,0,0,0,0,0,0,0,0,0,0,0,0,0,0,0,0,0,0,0,0,0,0,0,0,0,0,0,0,0,0,0,0
4.00000000000e+000,0,0,0,0,0,0,0,0,0,0,0,0,0,0,0,0,0,0,0,0,0,0,0,0,0,0,0,0,0,0,0,0,0,0,0,0,0,0,0,0,0,0,0,0,0,0,0,0,0,0,0,0,0,0,0,0,0,0,0,0,0,0,0
4.50000000000e+000,0,0,0,0,0,0,0,0,0,0,0,0,0,0,0,0,0,0,0,0,0,0,0,0,0,0,0,0,0,0,0,0,0,0,0,0,0,0,0,0,0,0,0,0,0,0,0,0,0,0,0,0,0,0,0,0,0,0,0,0,0,0,0
5.00000000000e+000,0,0,0,0,0,0,0,0,0,0,0,0,0,0,0,0,0,0,0,0,0,0,0,0,0,0,0,0,0,0,0,0,0,0,0,0,0,0,0,0,0,0,0,0,0,0,0,0,0,0,0,0,0,0,0,0,0,0,0,0,0,0,0
5.50000000000e+000,0,0,0,0,0,0,0,0,0,0,0,0,0,0,0,0,0,0,0,0,0,0,0,0,0,0,0,0,0,0,0,0,0,0,0,0,0,0,0,0,0,0,0,0,0,0,0,0,0,0,0,0,0,0,0,0,0,0,0,0,0,0,0
6.00000000000e+000,0,0,0,0,0,0,0,0,0,0,0,0,0,0,0,0,0,0,0,0,0,0,0,0,0,0,0,0,0,0,0,0,0,0,0,0,0,0,0,0,0,0,0,0,0,0,0,0,0,0,0,0,0,0,0,0,0,0,0,0,0,0,0
6.50000000000e+000,0,0,0,0,0,0,0,0,0,0,0,0,0,0,0,0,0,0,0,0,0,0,0,0,0,0,0,0,0,0,0,0,0,0,0,0,0,0,0,0,0,0,0,0,0,0,0,0,0,0,0,0,0,0,0,0,0,0,0,0,0,0,0
7.00000000000e+000,0,0,0,0,0,0,0,0,0,0,0,0,0,0,0,0,0,0,0,0,0,0,0,0,0,0,0,0,0,0,0,0,0,0,0,0,0,0,0,0,0,0,0,0,0,0,0,0,0,0,0,0,0,0,0,0,0,0,0,0,0,0,0
7.50000000000e+000,0,0,0,0,0,0,0,0,0,0,0,0,0,0,0,0,0,0,0,0,0,0,0,0,0,0,0,0,0,0,0,0,0,0,0,0,0,0,0,0,0,0,0,0,0,0,0,0,0,0,0,0,0,0,0,0,0,0,0,0,0,0,0
8.00000000000e+000,0,0,0,0,0,0,0,0,0,0,0,0,0,0,0,0,0,0,0,0,0,0,0,0,0,0,0,0,0,0,0,0,0,0,0,0,0,0,0,0,0,0,0,0,0,0,0,0,0,0,0,0,0,0,0,0,0,0,0,0,0,0,0
8.50000000000e+000,0,0,0,0,0,0,0,0,0,0,0,0,0,0,0,0,0,0,0,0,0,0,0,0,0,0,0,0,0,0,0,0,0,0,0,0,0,0,0,0,0,0,0,0,0,0,0,0,0,0,0,0,0,0,0,0,0,0,0,0,0,0,0
9.00000000000e+000,0,0,0,0,0,0,0,0,0,0,0,0,0,0,0,0,0,0,0,0,0,0,0,0,0,0,0,0,0,0,0,0,0,0,0,0,0,0,0,0,0,0,0,0,0,0,0,0,0,0,0,0,0,0,0,0,0,0,0,0,0,0,0
9.50000000000e+000,0,0,0,0,0,0,0,0,0,0,0,0,0,0,0,0,0,0,0,0,0,0,0,0,0,0,0,0,0,0,0,0,0,0,0,0,0,0,0,0,0,0,0,0,0,0,0,0,0,0,0,0,0,0,0,0,0,0,0,0,0,0,0
1.00000000000e+001,0,0,0,0,0,0,0,0,0,0,0,0,0,0,0,0,0,0,0,0,0,0,0,0,0,0,0,0,0,0,0,0,0,0,0,0,0,0,0,0,0,0,0,0,0,0,0,0,0,0,0,0,0,0,0,0,0,0,0,0,0,0,0
1.05000000000e+001,0,0,0,0,0,0,0,0,0,0,0,0,0,0,0,0,0,0,0,0,0,0,0,0,0,0,0,0,0,0,0,0,0,0,0,0,0,0,0,0,0,0,0,0,0,0,0,0,0,0,0,0,0,0,0,0,0,0,0,0,0,0,0
1.10000000000e+001,0,0,0,0,0,0,0,0,0,0,0,0,0,0,0,0,0,0,0,0,0,0,0,0,0,0,0,0,0,0,0,0,0,0,0,0,0,0,0,0,0,0,0,0,0,0,0,0,0,0,0,0,0,0,0,0,0,0,0,0,0,0,0
1.15000000000e+001,0,0,0,0,0,0,0,0,0,0,0,0,0,0,0,0,0,0,0,0,0,0,0,0,0,0,0,0,0,0,0,0,0,0,0,0,0,0,0,0,0,0,0,0,0,0,0,0,0,0,0,0,0,0,0,0,0,0,0,0,0,0,0
1.20000000000e+001,0,0,0,0,0,0,0,0,0,0,0,0,0,0,0,0,0,0,0,0,0,0,0,0,0,0,0,0,0,0,0,0,0,0,0,0,0,0,0,0,0,0,0,0,0,0,0,0,0,0,0,0,0,0,0,0,0,0,0,0,0,0,0
1.25000000000e+001,0,0,0,0,0,0,0,0,0,0,0,0,0,0,0,0,0,0,0,0,0,0,0,0,0,0,0,0,0,0,0,0,0,0,0,0,0,0,0,0,0,0,0,0,0,0,0,0,0,0,0,0,0,0,0,0,0,0,0,0,0,0,0
1.30000000000e+001,0,0,0,0,0,0,0,0,0,0,0,0,0,0,0,0,0,0,0,0,0,0,0,0,0,0,0,0,0,0,0,0,0,0,0,0,0,0,0,0,0,0,0,0,0,0,0,0,0,0,0,0,0,0,0,0,0,0,0,0,0,0,0
1.35000000000e+001,0,0,0,0,0,0,0,0,0,0,0,0,0,0,0,0,0,0,0,0,0,0,0,0,0,0,0,0,0,0,0,0,0,0,0,0,0,0,0,0,0,0,0,0,0,0,0,0,0,0,0,0,0,0,0,0,0,0,0,0,0,0,0
1.40000000000e+001,0,0,0,0,0,0,0,0,0,0,0,0,0,0,0,0,0,0,0,0,0,0,0,0,0,0,0,0,0,0,0,0,0,0,0,0,0,0,0,0,0,0,0,0,0,0,0,0,0,0,0,0,0,0,0,0,0,0,0,0,0,0,0
1.45000000000e+001,0,0,0,0,0,0,0,0,0,0,0,0,0,0,0,0,0,0,0,0,0,0,0,0,0,0,0,0,0,0,0,0,0,0,0,0,0,0,0,0,0,0,0,0,0,0,0,0,0,0,0,0,0,0,0,0,0,0,0,0,0,0,0
1.50000000000e+001,0,0,0,0,0,0,0,0,0,0,0,0,0,0,0,0,0,0,0,0,0,0,0,0,0,0,0,0,0,0,0,0,0,0,0,0,0,0,0,0,0,0,0,0,0,0,0,0,0,0,0,0,0,0,0,0,0,0,0,0,0,0,0
```

Figure A 4: *Detailed output file.*

Figure A4 shows the elastic, dissipation and frictional energy state of each ball after a specific time interval. This file is important in describing the energy distribution (state) after a specific time interval.

APPENDIX B – SAG MILL SIMULATION FILES

The SAG mill simulation program is very similar to the DBT simulation code. Prior to initiating the actual simulation, the mill properties and simulation parameters are set using an external script file. Figure B1 shows part of an input script file for Sim1 reflecting the relevant information.

```
File  Edit  Format  View  Help
Clumpdia= 14582
Ballreq= ' 14582 '
Sections = 1
SectionLength (1) =0.5
Lifters (1) =36
Lifterwalls(1) =24
Lx(1) =' 0 9.112931 -90.54332 -117.1264 -143.7095 -171.9494 -167.8557 -259.2032 -291.5854 -323.9677 -464.2664 -485.8545 -519.0652 -638.6526 -665.2357 -701.7845 -730.024
Ly(1) =' 0 -109.6219 -117.9064 -160.2542 -202.6021 -225.0186 -515.6786 -503.2034 -475.7919 -448.3804 -209.1811 -190.9068 -153.5296 -163.471 -205.8189 -248.9951 -271.411
FeedEndSections = 0
DischargeEndSections = 0
lifterx = 36
MillLength = 0.5
Ballprop='prop dens  = 7800.00 kn 4000000 ks 3000000  fric 0.40'
Wallprop=' kn 4000000 ks 3000000  fric 0.20'
fname = 'ScawSim1'
mspeed = 8.991154
Frames = 1800
E_range = 5
Prevs = 1
Revs = 5
Thissim = 1
FinalSpeed = -0.9415514
Pdpreq = 1
GenClumps = 0
Gnum = 0
Pltreq = 1
SimU = 1
Timefactor = 10
forcereq = 0
End
mycycle
def spinstart
command
 Wall id =  3 x =5.8 z =5.8 yspin= FinalSpeed
 Wall id =  4 x =5.8 z =5.8 yspin= FinalSpeed
 Wall id =  5 x =5.8 z =5.8 yspin= FinalSpeed
 Wall id =  6 x =5.8 z =5.8 yspin= FinalSpeed
```

Figure B 1: *SAG mill simulation input file.*

The input file for a specific mill is exported to the Particle Flow Code (PFC) in a format that can be read by the DEM simulation software. The input file is saved with its family name as the prefix and ".dat" as the suffix. For example, the input file for Sim1 reads: "Sim1.dat".

At the end of the simulation, a number of files are generated as requested by the user. The simulation output files include:

- **Summary File** – this file is identified by the sum.txt suffix. For example if the input file was "Sim1.dat", the summary file will be "Sim1sum.txt. The file summarises the simulation set-up and also contain the mill geometry, operating parameters, simulation parameters as initially requested by the user in the script file. This file also contains the impact energy spectra and the mill power behaviour throughout the simulation. Figure B2 shows the "sum.txt" file generated.

```
FILE FAMILY NAME: Sim1

Posn and Vel plot in: Sim1plt.fil



____________________        MILL  DATA  _________________________


Dia. = 11.60   Mill_speed = 9.0    % Mill fill = 24.00

WN_stiff = 4000000  WS_stiffs = 3000000  WFric = 0.2  WRestit = 0.60


_________________    SIMULATION SET-UP  ____________________

Revs prior to sampling = 1
Simulation revs = 2.48
Simulation Frames = 534
Time for 1 rev = 6.673 secs
Total Mill running time simulated = 9.91 secs
Scale for energy (J) = 5.00000
Particle settling time    = 0Hr(s) : 7 min(s) : 24 sec(s)
Pre-sampling time period = 150Hr(s) : 57 min(s) : 26 sec(s)
Simulation time period   = -362Hr(s) : 56 min(s) : 8 sec(s)


Simulation time step used   = 1.71636463633e-004


________________      BALL DATA     ______________________

Total Number of balls  14582 Total Mass 43167.514
```

Figure B 2: *Part of the sum.txt file showing the simulation set-up*

The impact energy spectra and power behaviour are shown in figure B3 and B4.

```
File  Edit  Format  View  Help
Average millpower draw = -952669.262 Energy Gain/Loss = -1.82534019011e+005

Time(s),Power(W),Totlss(W),Damplss(W),Frclss(W),Normlss(W),Tanglss(W)
0.10,-9.11299352061e+005,4.04479732959e+006,2.83533728846e+006,1.20946004113e+006,2.83533728846e+006,0
0.20,-8.89641503998e+005,3.98711359299e+006,2.81926332820e+006,1.16785026479e+006,2.81926332820e+006,0
0.30,-9.01968852079e+005,4.16549103344e+006,2.93694706609e+006,1.22854396735e+006,2.93694706609e+006,0
0.40,-8.81580923493e+005,4.16742403167e+006,2.95700261395e+006,1.21042141772e+006,2.95700261395e+006,0
0.50,-9.00693305257e+005,4.08474000907e+006,2.83786098855e+006,1.24687902052e+006,2.83786098855e+006,0
0.60,-8.94267851563e+005,4.51109327310e+006,3.19110526302e+006,1.31998801008e+006,3.19110526302e+006,0
0.70,-9.09354387325e+005,4.34605085684e+006,3.04672918169e+006,1.29932167514e+006,3.04672918169e+006,0
0.80,-9.08262739344e+005,4.17128919680e+006,2.92325127433e+006,1.24803792247e+006,2.92325127433e+006,0
0.90,-8.95744663384e+005,3.88461413622e+006,2.72942195957e+006,1.15519217666e+006,2.72942195957e+006,0
1.00,-9.26923217929e+005,3.79201138792e+006,2.62449944684e+006,1.16751194108e+006,2.62449944684e+006,0
1.10,-9.32886913894e+005,3.44650320111e+006,2.39367104411e+006,1.05283215699e+006,2.39367104411e+006,0
1.20,-9.48982940803e+005,3.21346475838e+006,2.19764944754e+006,1.01581531083e+006,2.19764944754e+006,0
1.30,-9.56154734476e+005,3.03574141547e+006,2.06111001836e+006,9.74631397107e+005,2.06111001836e+006,0
1.40,-9.68391403393e+005,3.08190527798e+006,2.06885305149e+006,1.01305222649e+006,2.06885305149e+006,0
1.50,-9.88392547937e+005,2.55835753289e+006,1.69434341980e+006,8.64014113090e+005,1.69434341980e+006,0
1.60,-9.63658944450e+005,2.19997482183e+006,1.46046341424e+006,7.39511407597e+005,1.46046341424e+006,0
1.70,-9.91285080408e+005,2.16904430730e+006,1.42967177452e+006,7.39372532786e+005,1.42967177452e+006,0
1.80,-9.67745523418e+005,2.20533434403e+006,1.48316387646e+006,7.22170467567e+005,1.48316387646e+006,0
1.90,-9.73071391847e+005,2.27055819487e+006,1.52684988712e+006,7.43708307748e+005,1.52684988712e+006,0
2.00,-9.99212956858e+005,2.13981684534e+006,1.41070420169e+006,7.29112643654e+005,1.41070420169e+006,0
2.10,-1.01023666118e+006,2.06719320340e+006,1.39758899300e+006,6.69604210403e+005,1.39758899300e+006,0
2.20,-9.79463189929e+005,2.13484844247e+006,1.43520319229e+006,6.99645250181e+005,1.43520319229e+006,0
2.30,-9.94394313471e+005,2.31093994550e+006,1.56616826578e+006,7.44771679716e+005,1.56616826578e+006,0
2.40,-9.71183229749e+005,2.18258467974e+006,1.46834892915e+006,7.14235750582e+005,1.46834892915e+006,0
2.50,-9.71418287356e+005,2.23801787542e+006,1.52902203294e+006,7.08995842483e+005,1.52902203294e+006,0
2.60,-9.67800082830e+005,2.55524348254e+006,1.76149487971e+006,7.93748602828e+005,1.76149487971e+006,0
2.70,-9.63594396708e+005,2.69285304916e+006,1.83117633134e+006,8.61676717822e+005,1.83117633134e+006,0
2.80,-9.67478629833e+005,2.58470766352e+006,1.78445704597e+006,8.00250617546e+005,1.78445704597e+006,0
2.90,-9.28701327250e+005,2.69005419675e+006,1.85708806389e+006,8.32966132857e+005,1.85708806389e+006,0
3.00,-9.42727598934e+005,2.87549632465e+006,2.01833014348e+006,8.57166181177e+005,2.01833014348e+006,0
3.10,-9.36566720600e+005,3.14549140728e+006,2.20134979351e+006,9.44141613770e+005,2.20134979351e+006,0
3.20,-9.28552824661e+005,3.14034067251e+006,2.17387655042e+006,9.66464122087e+005,2.17387655042e+006,0
3.30,-9.25867841372e+005,2.97499601975e+006,2.08097096465e+006,8.94025055102e+005,2.08097096465e+006,0
3.40,-9.18571642905e+005,3.24907264473e+006,2.23781353022e+006,1.01125911451e+006,2.23781353022e+006,0
```

Figure B 3: *sum.txt file showing the power behaviour.*

The first column gives the time periods when average power was sampled. The second column refers to power calculated by considering the torque on the mill surface as the charge tumbles (power draw). For actual mill power draw user may consider an increase of about 10% as loss attributed to motor and other transmission inefficiencies. Total loss, the third column is power calculation that is based on the losses during ball-ball and ball-wall collisions. The loss due to friction and damp-loss is summed to get this value. In other words this accounts for energy dissipation and should as close as possible to the total power draw (second column). The other terms refer to normal or tangential loss, with tangential being mostly negligible, (Bwalya, 2006).

Figure B4 shows the Impact Energy Spectra part of the simulation report.

```
File   Edit   Format   View   Help
Lower Size,89,106,90,0,0,0
Number,14582,7234,4172,611,0,0
J,TEvents,b_b,b_b,b_b,b_b,b_b
5.00000000000e+000,9467345,5967231,0,2876679,0,413136,0,0,0,0,0
1.00000000000e+001,362510,233287,0,104802,0,13128,0,0,0,0,0
1.50000000000e+001,141812,91028,0,41043,0,5136,0,0,0,0,0
2.00000000000e+001,73101,46535,0,21592,0,2697,0,0,0,0,0
2.50000000000e+001,41761,26489,0,12461,0,1533,0,0,0,0,0
3.00000000000e+001,26540,16757,0,7959,0,969,0,0,0,0,0
3.50000000000e+001,17646,11253,0,5233,0,625,0,0,0,0,0
4.00000000000e+001,12332,7779,0,3779,0,422,0,0,0,0,0
4.50000000000e+001,8795,5614,0,2671,0,282,0,0,0,0,0
5.00000000000e+001,6502,4112,0,1939,0,266,0,0,0,0,0
5.50000000000e+001,4852,3064,0,1501,0,167,0,0,0,0,0
6.00000000000e+001,3740,2331,0,1175,0,139,0,0,0,0,0
6.50000000000e+001,2863,1780,0,906,0,108,0,0,0,0,0
7.00000000000e+001,2270,1431,0,713,0,76,0,0,0,0,0
7.50000000000e+001,1809,1113,0,577,0,63,0,0,0,0,0
8.00000000000e+001,1471,905,0,480,0,42,0,0,0,0,0
8.50000000000e+001,1143,699,0,367,0,42,0,0,0,0,0
9.00000000000e+001,965,601,0,307,0,33,0,0,0,0,0
.
.
.
5.75000000000e+002,1,1,0,0,0,0,0,0,0,0,0
5.80000000000e+002,0,0,0,0,0,0,0,0,0,0,0
5.85000000000e+002,0,0,0,0,0,0,0,0,0,0,0
5.90000000000e+002,0,0,0,0,0,0,0,0,0,0,0
5.95000000000e+002,1,1,0,0,0,0,0,0,0,0,0
6.00000000000e+002,0,0,0,0,0,0,0,0,0,0,0
6.05000000000e+002,0,0,0,0,0,0,0,0,0,0,0
6.10000000000e+002,0,0,0,0,0,0,0,0,0,0,0
6.15000000000e+002,1,1,0,0,0,0,0,0,0,0,0
6.20000000000e+002,0,0,0,0,0,0,0,0,0,0,0
6.25000000000e+002,2,1,0,0,0,1,0,0,0,0,0
6.30000000000e+002,0,0,0,0,0,0,0,0,0,0,0
```

Figure B 4: *Impact Energy Spectra part of the summary file*

The first column indicates the energy class. The second and third columns show the number of events recorded in that energy class. The third to the last column show the number of collisions recorded for a specific ball size.

- **Ball Tracking File** - shows the number of collision events classified into regular energy classes that an individual ball of specific size and material is exposed to. The program gives the flexibility to pick a set of ten balls whose individual simulation history can be tracked. Figure B5 shows the file orientation.

File Edit Format View Help

```
Class ,All
,1,2,3,4,5,6,7,8,9,10
,b_b,b_b,b_b,b_b,b_b,b_b,b_b,b_b,b_b,b_b
5.00000000000e+000,724,651,579,788,1239,588,757,745,788,1048
1.00000000000e+001,54,36,21,43,50,12,59,18,26,35
1.50000000000e+001,20,17,7,15,19,8,24,11,18,13
2.00000000000e+001,18,6,6,13,7,2,7,6,13,7
2.50000000000e+001,6,4,2,5,6,1,6,2,4,6
3.00000000000e+001,4,3,2,5,2,0,5,1,3,3
3.50000000000e+001,4,0,2,5,2,0,2,1,0,1
4.00000000000e+001,3,0,0,1,1,1,1,1,1,0
4.50000000000e+001,0,1,0,1,2,0,3,2,2,0
5.00000000000e+001,1,0,0,0,1,0,0,0,3,0
5.50000000000e+001,1,1,0,2,0,0,1,0,1,0
6.00000000000e+001,0,0,0,0,0,1,1,0,0,1
6.50000000000e+001,0,0,0,0,0,0,1,1,0,0
7.00000000000e+001,0,0,0,1,0,0,0,0,0,0
7.50000000000e+001,1,0,0,0,0,0,0,0,0,0
.
.
.
.
5.60000000000e+002,0,0,0,0,0,0,0,0,0,0
5.65000000000e+002,0,0,0,0,0,0,0,0,0,0
5.70000000000e+002,0,0,0,0,0,0,0,0,0,0
5.75000000000e+002,0,0,0,0,0,0,0,0,0,0
5.80000000000e+002,0,0,0,0,0,0,0,0,0,0
5.85000000000e+002,0,0,0,0,0,0,0,0,0,0
5.90000000000e+002,0,0,0,0,0,0,0,0,0,0
5.95000000000e+002,0,0,0,0,0,0,0,0,0,0
6.00000000000e+002,0,0,0,0,0,0,0,0,0,0
6.05000000000e+002,0,0,0,0,0,0,0,0,0,0
6.10000000000e+002,0,0,0,0,0,0,0,0,0,0
6.15000000000e+002,0,0,0,0,0,0,0,0,0,0
6.20000000000e+002,0,0,0,0,0,0,0,0,0,0
6.25000000000e+002,0,0,0,0,0,0,0,0,0,0
```

Figure B 5: *Part of the ball-tracking file*

The second row shows the ball numbers that were tracked. For the SAG mill simulations, the 125mm steel balls were generated first hence, the tracking in Figure B5 represent the simulation history of 10 individual 125mm steel balls. The first row represents the energy classes whilst all the other succeeding columns show that number of events for the corresponding ball number.